MECHANISTIC STUDY OF CATIONIC IRON(II) SANDWICH COMPLEXES AS PHOTOINITIATORS FOR POLYMERIZATION REACTIONS

by

WEI DING

(Under the direction of CHARLES KUTAL)

ABSTRACT

Light excitation of Fe(II) sandwich complex photoinitiators of the types [CpFe(η^6-arene)]Z (Cp is cyclopentadienyl and Z is the counterion), benzoyl-functionized ferrocene, and [Fe(η^6-arene)$_2$]Z_2 results in deligation of the complexes in the primary photochemical processes, leading to the formation of active but short-lived intermediates, usually in the form of the corresponding half-sandwich complex ion with added monodentate ligands. The intermediates further decompose into fully ring-deligated Fe(II) complexes in a secondary thermal process. Some of these photoproducts function as active initiating species capable of starting polymerization of monomers. Elucidation of the mechanism of initiation and polymerization of cyclohexene oxide (CHO) with [CpFebz]PF_6 (bz is benzene) has been achieved by probing the photoreaction with an on-line electrospray ionization mass spectrometry (ESI-MS) technique capable of identifying intermediates with lifetimes of 4 – 400 ms. Three initiating species responsible for the polymerization of CHO have been identified: the half-sandwich intermediate, the fully ring-deligated Fe(II) complex ion, and a non-iron monocation with m/z of 140.1. The establishment of a parent-offspring relationship between the half-sandwich intermediate and the fully ring-deligated Fe(II) complex species, and the proven nature of oligomers from the three initiating species allow for the proposal of a mechanism to describe the initiation and polymerization of CHO with the photoinitiator. Products from the photodeligation of dibenzoylferrocene (DBF) in acetonitrile (AN) are characterized using the on-line ESI-MS and ^{1}H NMR techniques. The identification of the half-sandwich species [(η^5-$C_5H_4C(O)Ph$)Fe$(AN)_3]^+$ and its decomposition product, $[Fe(AN)_6]^{2+}$, as well as 1-benzoyl-1,3-cyclopentadiene lead to a detailed mechanism for the photoreaction of DBF. The strong nucleophilic nature of the benzoylcyclopentadienide anion photoreleased from

the deligation of DBF is reflected by its fast abstraction of a proton from the solvent environment, confirming its role in initiating anionic polymerization.

INDEX WORDS: Photoinitiators, Electrospray ionization, Mass spectrometry, Initiation, Propagation, Photoinduced polymerization, Iron(II) sandwich complexes, Monomer, Mechanism

MECHANISTIC STUDY OF CATIONIC IRON(II) SANDWICH COMPLEXES AS PHOTOINITIATORS FOR POLYMERIZATION REACTIONS

by

WEI DING

B.Eng., Institute of Engineering, Wuhan University, P.R. China, 1982

M.Eng., Institute of Engineering, Wuhan University, P.R. China, 1984

A Dissertation Submitted to the Graduate Faculty of The University of Georgia in Partial Fulfillment of the Requirements for the Degree

DOCTOR OF PHILOSOPHY

ATHENS, GEORGIA

2002

MECHANISTIC STUDY OF CATIONIC IRON(II) SANDWICH COMPLEXES AS PHOTOINITIATORS FOR POLYMERIZATION REACTIONS

by

WEI DING

Approved:

Major Professor: Charles Kutal

Committee: I. Jonathan Amster
Michael K. Johnson
Thomas E. Johnson
R. Bruce King

Electronic Version Approved:

Gordhan L. Patel
Dean of the Graduate School
The University of Georgia
August 2002

DEDICATION

This work is dedicated to my wonderful parents and my lovely wife, Shili Chen. Without their love, trust, and support none of this would have happened. In memory of my loved mother.

ACKNOWLEDGEMENTS

I would like to express my appreciation to my major advisor, Dr. Charles Kutal, for his guidance and support throughout my graduate studies. It is his understanding, encouragement, and patience that have accompanied my challenging and tough research times here. Without his help, I could not reach where I want to. Dr. Kutal is my role of model for becoming a nice, decent, professional, honest, and successful person. Many thanks to Dr. R. Bruce King, Dr. Michael Johnson, Dr. Jonathan Amster, and Dr. Thomas Johnson for their serving on my advisory committee. They are always there whenever I am in needs of help and advice.

Dr. Amster is a wonderful professor who introduced me into the powerful and also colorful mass spectrometry techniques. His enthusiasm for science, solid and broad knowledge helped me so many times in his lab, and eventually made me love MS. I want to show my gratitude to Dr. Keith Johnson, Dr. Kristina Taylor, Dr. Todd Mize, Julia Johnson, Bryan Parks, and Cynthia Sanderson. These smart and nice lab buddies helped me a lot in the lab and made the life there enjoyable.

I owe appreciation to the many people who advised and assisted me in a variety of ways, including Dr. John Stickney and his group members, especially Dr. Billy Flowers and Marcus Lay, Dr. Michael Johnson's group, Dr. Richard Dluhy and his group, Dr. Michael Duncan and his group, Drs. Charles Atwood,

Quincy Teng, and Bobby Stanton. Thanks also to the Department of Chemistry for having so many nice people.

TABLE OF CONTENTS

Page

LIST OF TABLES

Page

LIST OF FIGURES

Page

CHAPTER 1

INTRODUCTION

1.1 Photoinitiated polymerization

Polymerization is a process by which macromolecular substances, termed polymers, are synthesized from simple repeating units, or monomers. Polymers may be synthesized by several types of reactions such as the self-addition of vinyl units or strained rings, and the condensation of two functional groups with the expulsion of a small molecule (e.g., water). Addition polymerizations can be initiated thermally or photochemically. In the latter process, the photoinitiator (P in Equation 1) absorbs a photon of light and reacts to form the active initiating species, IN. IN can be a radical, cation, anion, or any species capable of reacting with the monomer. Polymerization starts with the reaction of a monomer unit, M, with IN (Equation 2). Repetitive addition of monomer to the reactive site results in chain growth (i.e., propagation of polymerization, Equation 3), and at the same time regenerates the active center on the newly added monomer unit.

$$P \xrightarrow{h\nu \text{ or } \triangle} IN \qquad (1)$$

$$IN + M \longrightarrow IN\text{-}M \qquad (2)$$

$$IN\text{-}M + nM \longrightarrow IN\text{-}(M)_{n+1} \qquad (3)$$

Photoinduced polymerization has become a rapidly expanding technology and has found extensive applications in various industrial sectors. It is utilized in a variety of coatings, paints, printing inks, adhesives, composite materials and dental restorative formulations. The main advantage of using photons to initiate polymerization lies in the very high rates that can be reached under intense

irradiation, thus the phase change from liquid to solid can take place within a fraction of a second.[1,2] Another unique feature of light-induced reaction is that polymerization occurs only in illuminated areas, therefore allowing the generation of high resolution images for the production of printing plates, optical discs and microcircuits.[3,4] Most recently, its applications have covered three-dimensional stereolithography and holographic recording.[5,6] In addition to its great speed and spatial resolution, radiation curing provides several other striking advantages, specifically, ambient temperature operation, solvent free formulations,[7] and low energy consumption. These characteristics (i) allow for the wider selection of monomers, especially in the case of formulations involving monomers that are susceptible to high temperature, (ii) result in environmentally friendly performance by substantially reducing the emission of volatile organic compounds (VOCs), and (iii) facilitate energy efficient processes.

1.2 Types of photoinitiator

Since most monomers are not able to produce initiating species with sufficiently high yield when exposed to light, a photoinitiator compound has to be added to the formulation. After the initiation step in which the reaction of the initiating species with the monomer functional groups occurs, the chain growth reaction will proceed very much as in a conventional thermal polymerization, except for the much larger rate of initiation that can be reached by intense illumination and for the lower temperature. Thus, extensive research efforts devoted to radiation curing have been focused on the discovery and

development of highly efficient photoinitiators. Depending on the types of the active species, IN, in Equation 1, photoinitiators fall into two categories: radical and ionic. The ionic category can be further subdivided into cationic and anionic photoinitiators. A generalized family tree of photoinitiators is shown in Chart 1.

Chart 1

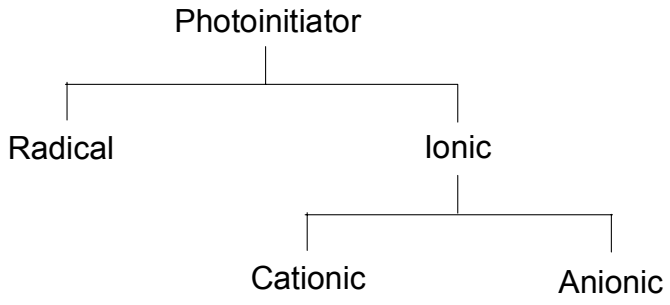

Radical polymerization is commenced by adding a monomer to a radical that is produced from a suitable initiator compound. The added radical will be the tail of the ultimately formed polymer chain, however, its nature or the nature of the initiator have minor effects on the features such as propagation rate, the selectivity, or the stereochemistry of the ensuing propagation.[8,9] All of these characteristics of radical propagation are determined mainly by the nature of the monomer and by reaction conditions, though the importance of defect groups (the end-groups in polymer structure formed in initiation and termination are the obvious examples) is recognized in recent research.[10]

Unlike radical polymerization, ionic polymerization starts with a reaction of a monomer with a species bearing an electronically charged or highly polar active group. Cationic polymerization refers to the process in which chain growth

involves positively charged or electrophilic active centers at the chain ends. An analogous description holds for anionic polymerization. One noticeable feature of ionic polymerization is that as long as the electronically charged end-groups are formed, the corresponding counter ions have to be present in the polymerization system to maintain its electric neutrality. Thus, the rate constant and the mode of ionic propagation are affected by the nature of the initiating species and its counter ion owing to the changeable character of the propagating groups (e.g., free ions and ion-pairs in equilibrium) and to the role of the counter ions that are associated with the growing active center throughout the whole course of the propagation. Moreover, in order to activate monomers by ionic initiation and propagation, the monomer structure should provide charge stabilization.

Monomers demonstrate a varying extent of selectivity with respect to the types of active center (radical, cationic, or anionic) that brings about the polymerization. Although all three types of initiators are employed in chain growth polymerization reactions, their applicability towards monomers is not indiscriminate. While many monomers will undergo polymerization with a radical initiator, those used commercially are limited to the vinyl, vinylidene, and diene monomers. On the other hand, versatile monomers, such as aldehydes, ketones, vinyl ethers, and numerous heterocyclics are only polymerized by ionic procedures.[8] It is not surprising that the polymerization of some monomers may not be started by cationic initiators while other monomers may be inert to anionic initiators if we keep in mind the selective feature of ionic initiating processes.

The selectivity for different types of initiation/propagation is summarized in Table 1, which lists the types of initiation pathways that cause the polymerization of various monomers to high molecular weight polymers.[11] The versatility of ionic polymerization stems from the polar feature of ionic or polar end-groups capable of polarizing the incoming monomer and accommodating its addition in the initiation and propagation processes, as well as from the effect of counter ions that accompany the active center and coordinate with the monomer prior to its ultimate covalent bonding to the polymer chain. These features can result in the selective polymerization of highly polarizable functionality, like the heterobonds of monomers, with which radicals interact weakly. Thus, the kinetic feasibility of polymerization is enhanced in many cases because the polarization of the monomer decreases the reaction energy barrier that otherwise would make the addition to the initiating center difficult.

Ionic polymerization, as a young technology, has not yet achieved the commercial importance comparable to the free radical process. Growing research efforts in recent years, however, have demonstrated the viability of light-induced cationic polymerization.[12] With continuing growth mainly through the introduction of new initiators along with improvements of the functional resins developed for these applications, cationic UV/Vis curing is expected[13] to reach eventually commercial significance as a complementary technology to photoinduced free radical polymerization. The present study focuses on the photochemical behavior of cationic initiators and the mechanisms of ensuing polymerization with monomers.

Table 1 Types of chain-growth polymerization undergone by various unsaturated monomers

Monomer	Type of Initiation[a]		
	Radical	Cationic	Anionic
Ethylene	+	−	+
1-Alkyl olefins (α-olefins)	−	+	−
1,1-Dialkyl olefins	−	+	−
1,3-Dienes	+	+	+
Styrene, α-methylstyrene	+	+	+
Halogenated olefins	+	−	−
Vinyl esters (CH_2=CHOCOR)	+	−	−
Acrylates, methacrylates	+	−	+
Acrylonitrile, methacrylonitrile	+	−	+
Acrylamide, methacrylamide	+	−	+
Vinyl ethers	−	+	−
N-Vinyl carbazole	+	+	−
N-Vinyl pyrrolidone	+	+	−
Aldehydes, Ketones	−	+	+

[a] + and − refer to whether or not high molecular weight products are produced.

1.3 Photochemical initiators for cationic polymerization

The cationic polymerization of vinyl and heterocyclic monomers can be started by several species including Lewis and Brønsted acids, carbonium ions, and radical cations generated from onium salts during photolysis[14] In addition to the general advantages of ionic polymerization, light-induced cationic polymerization is inert to oxygen, the inhibiting agent in a free radical polymerization process, and is ideally suited for thin film applications such as coatings, printing inks, and adhesives. Various families of cationic photoinitiators are utilized as can be seen from Table 2. All of the substances used today as cationic photoinitiators were developed within the last two decades, except diazonium salts, whose applications were discovered over ninety years ago.[13] A variety of polymers with different backbones can be used with cationic photoinitiators, providing a wide range of options when targeting chemical and physical properties for polymers obtained through monomers listed in Table 3.[7,13] From the standpoint of industrial applications, the most important monomers are epoxides, followed by vinyl ethers. Other monomers have not progressed beyond experimental studies and are waiting for either the improvement of monomer reactivity toward polymerization or the invention of new initiators with high initiation efficiency that are suited for the monomer.

There are three categories of cationic photoinitiators listed in Table 2: onium salts, non-ionic compounds, and organometallic complexes. Distinct features among them can be described in terms of their photoinitiation mechanisms and application conditions. Proton generated from the photoreaction

Table 2 Classes of cationic photoinitiators

Category	Class	Formula	Example
Onium salts	Diazonium salts	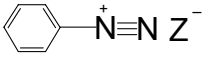	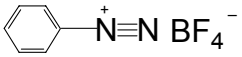
	Iodonium salts	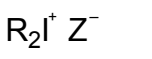	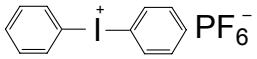
	Sulfonium salts	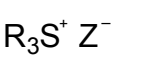	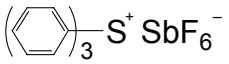
Non-ionic compounds	Silyl o-nitro-benzyl ethers	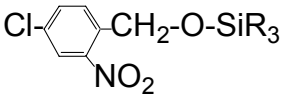	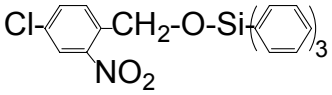
	Sulfonyloxy ketones	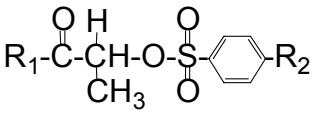	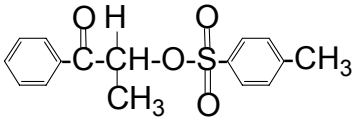
Organo-metallic complexes	Mixed-sandwich compounds	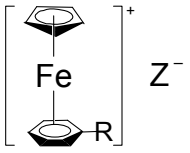	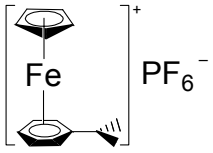
	Metal-carbonyl complexes	$[(\eta^5\text{-}C_5H_5)M(CO)_nL_m]^+Z^-$	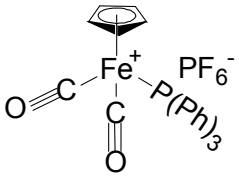

Table 3 Monomer types that can be utilized in photoinitiated cationic polymerization

Monomer	Structure	Backbone of Polymer
Epoxides	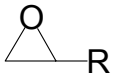	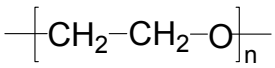
Cyclic sulfides	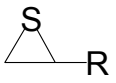	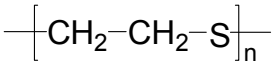
Vinyl ethers	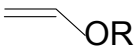	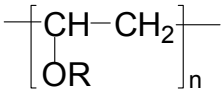
α-Olefins	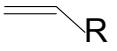	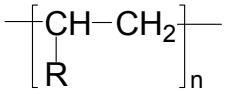
Oxazolines	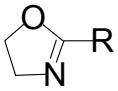	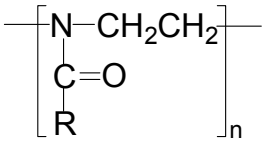
Cyclic ethers		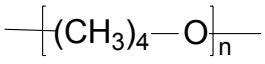
Siloxanes	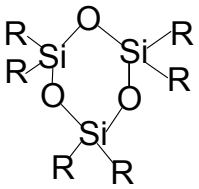	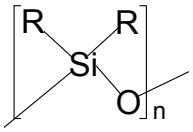
Lactones	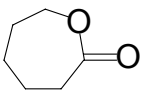	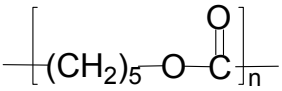
Trioxane	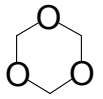	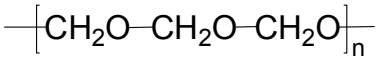

of the first two categories characterizes their Brønsted acid initiation of monomers, while Lewis acid photoproduced from organometallic complexes is the key feature of their initiation mechanism.

For onium salts of general type $[X\text{-}Y]^+Z^-$, the cation undergoes bond cleavage upon photoexcitation (Equation 4). A radical cation $X^{+\bullet}$generated in the photolysis may abstract a hydrogen from a surrounding molecule RH in the reaction system (Equation 5). The acidic XH^+ formed in the hydrogen transfer will undergo further dissociation and release H^+ along with a stable compound X (Equation 6).

$$(X\text{-}Y)^+ \xrightarrow{h\nu} X^{+\bullet} + Y^{\bullet} \quad (4)$$

$$X^{+\bullet} + RH \longrightarrow XH^+ + R^{\bullet} \quad (5)$$

$$XH^+ \longrightarrow X + H^+ \quad (6)$$

The proton produced in this step as well as the radical cation initially formed act as the potential initiating species in the presence of a monomer substrate. Onium salt photoinitiators containing simple aryl moieties generally show a principal absorption band in the short wavelength range (220 nm – 310 nm) of the UV spectrum. No significant band shift toward wavelengths beyond the middle of the UV spectrum is achieved by substituting appropriate chromophores onto the aromatic rings of these compounds.[15] Thus, applications of onium salts as photoinitiators without other reagents are limited to the UV range of illumination.

For those onium salts that do not posses absorption bands at wavelengths $\lambda > 300$ nm, a photosensitizer (PS) that strongly absorbs light at $\lambda > 300$ nm is needed to extend the wavelength sensitivity of the photoinitiated polymerization reaction.[12,16] In this case, the sensitizer is excited upon irradiation (Equation 7), and interaction of the excited photosensitizer (PS^*) with the onium salt results in the formation of radical $[X\text{-}Y]^\bullet$ and radical cation $PS^{+\bullet}$ via an electron exchange reaction (Equation 8). A salt / sensitizer system provides more routes of initiation in the cationic polymerization of monomer. For example, the spontaneous fragmentation of radical (Equation 9) will yield a radical $Y^\bullet$ that may combine with the radical cation $PS^{+\bullet}$ to generate an initiating species $Y\text{-}PS^+$ (Equation 10). At the same time, $PS^{+\bullet}$ may initiate polymerization directly or via a reaction with a surrounding molecule RH to form a strong initiating species H^+ (Equations 11, 12). Typical salt / sensitizer systems include diaryliodonium, triarylsulfonium, and

$$PS \xrightarrow{h\nu} PS^* \quad (7)$$

$$(X\text{-}Y)^+ + PS^* \longrightarrow PS^{+\bullet} + [X\text{-}Y]^\bullet \quad (8)$$

$$[X\text{-}Y]^\bullet \longrightarrow X + Y^\bullet \quad (9)$$

$$Y^\bullet + PS^{+\bullet} \longrightarrow Y\text{-}PS^+ \quad (10)$$

$$PS^{+\bullet} + RH \longrightarrow PSH^+ + R^\bullet \quad (11)$$

$$PSH^+ \longrightarrow PS + H^+ \quad (12)$$

N-alkoxy pyridium in conjunction with sensitizers such as anthracene, perylene, and phenothioazine. With onium salts photoinitiators and electron-transfer

photosensitizers, the flexibility in the application of cationic polymerization is enhanced. However, the number of sensitizers available for the operation in the long-wavelength UV and visible regions is very limited and environmental issues may arise owing to the toxicity of the sensitizers and limited solubility in various monomers.

In addition to direct photolysis and sensitized photolysis of initiators, free radical mediated methods involving the photogenerated free radicals in systems containing onium salts have been recently developed. A procedure referred to as free radical-promoted cationic polymerization is based on the oxidation of a free radical by an onium ion (Equation 13). It takes advantage of commercially

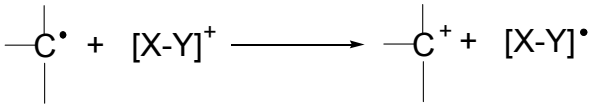

(13)

available free radical photoinitiators that upon irradiation yield carbon-centered electron-donating free radicals. The carbocation from the oxidation of the carbon-centered free radical by the onium salt becomes the reactive species capable of initiating cationic polymerization.[17] Moreover, a radical-induced fragmentation reaction has been used to generate an active radical cation.[18-20] It is an addition-fragmentation type reaction that uses a free radical initiator in conjunction with pyridinium, or phosphonium, or sulfonium salts bearing an allylic group. The addition of a free radical to the C-C double bond on the allylic moiety of the onium ion can promote the cleavage of the formed radical cation, and thus leaves behind fragments of an inert compound and a reactive radical cation

(Equation 14). The radical cation will induce initiation, or yield other initiating species similarly through equations 5, 6, or equations 11, 12. [21]

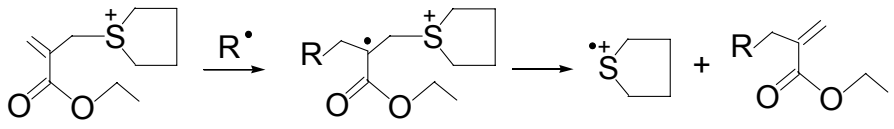

(14)

In marked contrast to the diversified pathways proposed in the investigations on the initiation of cationic polymerization with onium salts, much less mechanistic elucidation has been made on another category of photoinitiators, organometallic complexes. Instead of a radical cation or Brønsted acid from the reaction of radical cation in case of onium salts, a general feature of a photogenerated Lewis acid in the form of coordinatively unsaturated metal complexes is recognized or proposed for the photolysis of organometallic complexes. The development of new initiators within this category is hindered due to the lack of progress in mechanistic studies. For the metal-carbonyl compound class, it has been verified by infrared studies that upon exposure to light in the UV absorption region, one carbonyl group is lost. The coordinatively unsaturated species, a Lewis acid, formed in the photolysis process (Scheme 1) will take the role of initiating polymerization in the following reaction with monomer. The metal-carbonyl class of photoinitiators allows for further adjusting of reactivity either by substituting the ancillary ligands in the coordination sphere of the metal or by changing the counterion. A profound effect on epoxy cure rate was demonstrated when tuning the nucleophilicity of counterion and the acidity of Lewis acid at the metal center by the ancillary ligand, which remains bound to the

Scheme 1

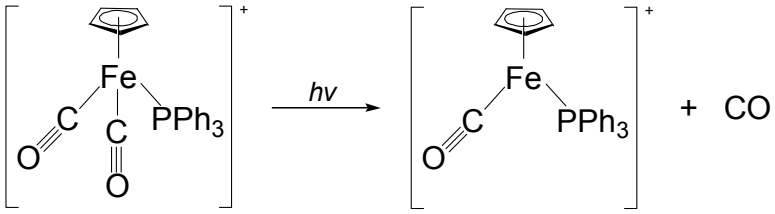

metal after photolysis. These effects suggested, to some extent, the possible role of the coordinatively unsaturated complex, or an intermediate, in the initiation mechanism of cationic polymerization. Since the identity of the active species is uncertain, the following hypothesis (Scheme 2) was tentatively used to describe the action of the active species in the case of an epoxy substrate. Excitation of metal-carbonyl photoinitiators occurs within the UV region of the spectrum and sensitized photolysis has not been reported. This class of compound has not been commercialized, possibly partially owing to the release of toxic carbon monoxide in the initiation / polymerization processes.

Scheme 2

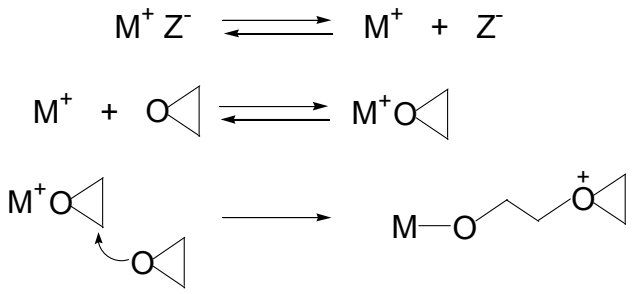

Of particular interest to research efforts and industrial applications is the family of iron-arene complexes, e.g., [(η^5-cyclopentadienyl)Fe(η^6-arene)]$^+Z^-$. They are relatively easy to synthesize and air-stable, two important features when considering potential applications in industrial processes. A few of them, namely, (η^5-cyclopentadienyl) (η^6-toluene)-iron(II) hexafluorophosphate (Irgacure 264, Ciba-Geigy), (η^5-cyclopentadienyl) (η^6-naphthalene)-iron(II) hexafluorophosphate (Complex KM 1144, Ciba-Geigy), and (η^5-cyclopentadienyl) (η^6-isopropylbenzene)-iron(II) hexafluorophosphate (Irgacure 261, Ciba-Geigy), are commercially available for cationic polymerizations.[13,22] Despite the success of the compounds in industrial applications, the mechanism of the initiation process has remained uncertain. Based on the verified loss of arene from the complex upon irradiation and on the formation of cyclic polyethers from ethylene oxide monomer, a photolysis/initiation mechanism via the generation of a Lewis acid, a coordinatively unsaturated complex $CpFe^+$, was proposed (Scheme 3).[23-26] However, there has been no evidence or direct observation to support this mechanism. Other than $CpFe^+$, an Fe^{2+} species was suggested as another

Scheme 3

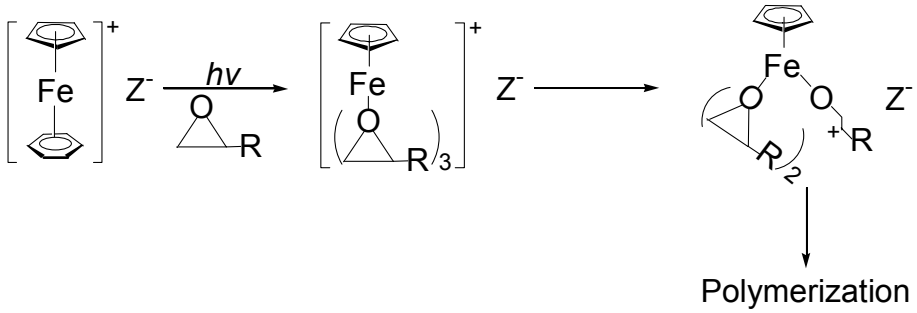

possible Lewis acid candidate in the initiation of epoxy substrates,[27] but no further report of its involvement has been found in the literature.

1.4 Iron-arene complex photoinitiators

In a broadened definition, metal arene complex photoinitiators in the present study include mixed sandwich compounds [(η^5-cyclopentadienyl)Fe(η^6-arene)]$^+Z^-$, bis-arene sandwich compounds of the type [Fe(η^6-arene)$_2$]$^{2+}$(Z^-)$_2$, and benzoyl-functionized ferrocenes. The photostability of these complexes is determined by the structural features of their ligands and the combination of ligands in the complexes. However, when considered as potential photoinitiators for cationic and anionic polymerization processes, the chemical characteristics of the products, or in some cases the intermediates, from the primary photoreactions determine the routes by which the initiation/propagation mechanism proceeds. In this section, the literature background for the three subclasses of photoinitiators will be covered with particular emphasis given to the mechanistic aspects of the corresponding photoinitiation/polymerization reactions.

1.4.1 Mixed-ligand iron sandwich complexes

Studies on the photodearylation behavior of mixed-ligand iron(II) sandwich complexes of the type [CpFe(η^6-arene)]$^+Z^-$ (Cp is cyclopentadienyl) have been the focus of research efforts since Gill and Mann reported the photochemical arene replacement reaction.[28] In their efforts to explore new synthetic routes to cyclopentadienyl iron complexes that may be difficult to prepare by other means,

they observed the formation of $[CpFe(L)_3]^+$ and $[CpFeL'_3]^+$ in the presence of a suitable monodentate ligand L (L = CO, C_6H_5CN, $P(OCH_3)_3$) and a tridentate ligand L'_3 (L'_3 = $C_6(CH_3)_6$, C_7H_8), respectively, upon visible-light photolysis of the parent complexes in a variety of solvents (Equations 15, 16). The same strategy was employed in the photochemical displacement of chlorobenzene from

$$CpFe(\eta^6\text{-p-xylene})PF_6 \xrightarrow[3L,\ solvent]{h\nu} (CpFeL_3)PF_6 + \text{p-xylene} \quad (15)$$

$$CpFe(\eta^6\text{-p-xylene})PF_6 \xrightarrow[L_3',\ solvent]{h\nu} CpFe(\eta^6\text{-}L_3')PF_6 + \text{p-xylene} \quad (16)$$

$[CpFe(\eta^6\text{-chlorobenzene})]^+$ with more basic arenes such as 2-phenylethyl tosylate, thiophene, 2-methylthiophene, 3-methylthiophene, and 2,5-dimethylthiophene.[29] When the study was extended to Ru(II) analogues, a relatively stable intermediate $[CpRu(CH_3CN)_3]^+$ from the photolysis of $[CpRu(\eta^6\text{-benzene})]PF_6$ was isolated. Starting with this intermediate, one, two, or three of the acetonitrile molecules can be selectively replaced under varied reaction conditions (temperature and solvent) by incoming ligands ($P(OCH_3)_3$, hexamethylbenzene, p-dichlorobenzene, etc.).[30] The photodecomposition reaction (Equation 17)[31] was reinvestigated to determine if there is an intermediate of the type $[CpFe(CH_3CN)_3]^+$. This species was observed as a

$$2[CpFe(\eta^6\text{-benzene})]BF_4 \xrightarrow[THF]{h\nu} Cp_2Fe + 2\text{benzene} + Fe(BF_4)_2 \quad (17)$$

stable purple complex during the photolysis of $[CpFe(\eta^6\text{-p-xylene})]PF_6$ in acetonitrile solution at -40 °C, and was characterized by low temperature proton

NMR, electronic spectroscopy, and cyclic voltammetry with a rotating photoelectrode. On the basis of the accumulated evidence, a mechanism (Scheme 4) was proposed to explain the photochemistry of [CpFe(η^6-p-xylene)]$^+$.[32,33]

Scheme 4

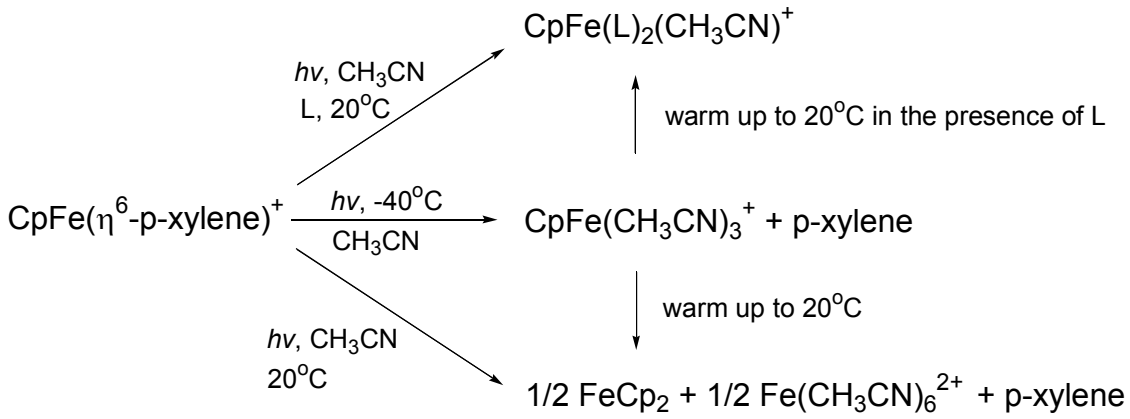

In a series of systematic studies conducted at 436 nm, the quantum yield of arene release was measured and found to be dependent on the polarity of the solvent and the nucleophilicity of the counterion.[34] A high yield in the arene replacement reaction would be facilitated by more polar solvents and more nucleophilic anions. The quantum efficiency was affected by the nature of the arene, substituents on the Cp ring, and reaction temperature for Ru(II) and Fe(II) complexes. For instance, in the case of the metal arene complex with pentamethylcyclopentadienyl, the steric blocking from the five methyl groups contributes to the very large decrease of quantum yield.[35] In a later report, the

quantum yield of photochemical arene release from [CpFe(η^6-arene)]$^+$ was found variable by a factor of 10^5 by changing the steric hindrance of the arene group, the polarity of the solvent, and the nucleophilicity of the counterion.[36] Furthermore, the lowest-lying ligand field triplet state was identified as the photoactive excited state in complexes of both metals from sensitization studies with triplet sensitizers. Temperature dependence studies indicated that the Fe-arene bond was weaker in the triplet excited state with respect to that in the singlet ground state, which causes the breaking of the Fe-arene bond in the triplet state.[37]

A significant advance in the mechanistic study of photochemical arene release from iron-arene complexes was the proposal by Schuster and co-workers[38] of different pathways (Figure 1) for ion-paired and freely solvated species. In less polar solvents the complex exists as the ion pair {[CpFe(η^6-arene)]$^+$Z$^-$}, while in relatively polar solvents freely solvated ions are formed. Upon irradiation into the ligand field excited singlet states of either species, intersystem crossing (ISC) occurs quickly to the corresponding triplet. Thereafter, a labilized arene ligand undergoes ring slippage from η^6 to η^4, thus making a coordination site on the iron available to other ligands in the system. For the ion pair a neutral intermediate containing the slipped η^4–arene ring and the counterion bound to the vacant coordination site on iron is formed. For the solvated ion, the assigned intermediate remains coordinatively unsaturated with the η^4–arene ring. Further nucleophilic attack by a molecule like a nitrile-containing ligand in a thermal reaction step forms [CpFe(η^4–arene)L]$^+$ from both

Figure 1

Ion-pair and free ion routes proposed for the photochemical reaction of [CpFe(η^6-arene)]$^+$. Nu stands for nucleophile in the system.

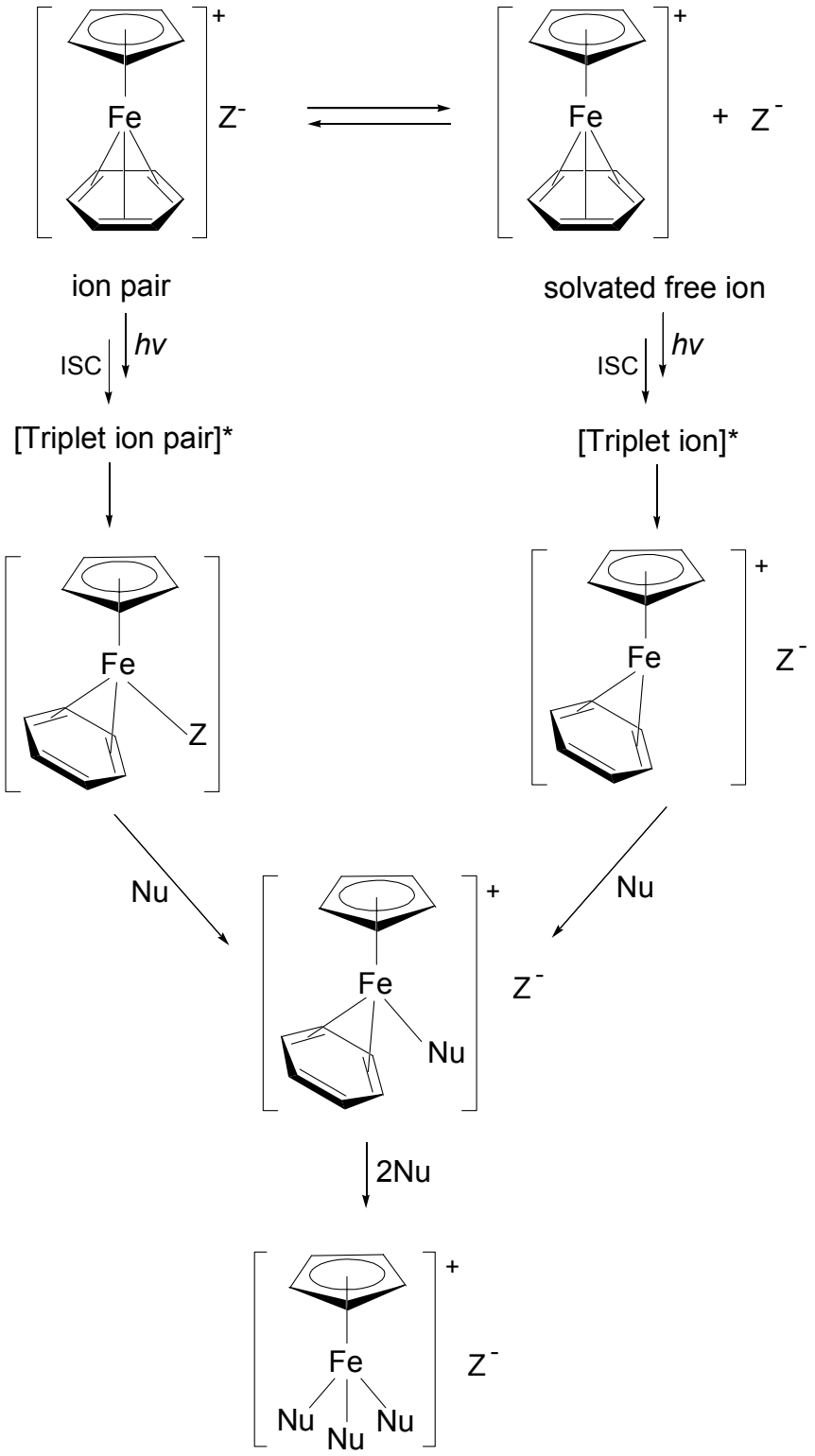
Fe
Z-
+
+ Z-
ion pair
solvated free ion
ISC
hv
ISC
hv
[Triplet ion pair]*
[Triplet ion]*
Fe
Z
Fe
Z-
Nu
Nu
Fe
Nu
Z-
2Nu
Fe
Nu
Nu
Nu
Z-

pathways. Finally, displacement of the labile arene by two more incoming L ligands yields the ligand exchange product $[CpFeL_3]^+$. The lifetime of the excited triplets were estimated to be less than 1.5 ns, while the subsequent arene lose and ligand change are relatively slow in the thermal processes with rate constants of $10^5 – 10^8$ $M^{-1}s^{-1}$.

Visible fluorescence at 520 nm from several $[CpFe(\eta^6\text{-arene})]^+$ complexes following 430 nm excitation into the lowest-lying singlet ligand field absorption band was detected by Roman et. al. at room temperature.[39] The luminescence quantum efficiency measured upon irradiation of the molecules increases with the number of methylated sites on the arene ligand. Interestingly, in the presence of hexamethylbenzene, the observed quantum efficiency for fluorescence was found to increase, and at higher concentration of hexamethylbenzene, the efficiency values approached that found for $[CpFe(\eta^6\text{-hexamethylbenzene})]^+$. This behavior led to the proposal that arene exchange may occur on the singlet excited state without significant deactivation of the complex. Most recently, Jakúbek and Lees studied the photochemical behavior of the commercialized photoinitiator, $[CpFe(\eta^6\text{-isopropylbenzene})]PF_6$, by quantitatively measuring the quantum efficiency when irradiating into UV and visible regions covering both singlet and triplet ligand field manifolds (355 nm – 683 nm).[40,41] The strong excitation wavelength dependence of arene dissociation in different solvent systems demonstrates that the arene release reaction does not solely derive from the triplet state. The finding led to the proposal of other photoreactive pathways via direct excitation into the singlet state from which an intermediate

16-electron iron complex cation with slipped (η^4-arene) ligand was formed. Direct nucleophilic attack of L on the intermediate then yielded $[CpFeL_3]^+$. This study illustrates that the photochemistry of arene dissociation from $[CpFe(\eta^6\text{-arene})]^+$ compounds can be efficiently performed throughout the ligand field spectrum, from either triplet or singlet excited state manifolds, to reach the $[CpFeL_3]^+$ reaction product.

As visible light-sensitive photoinitiators in cationic polymerization, $[CpFe(\eta^6\text{-isopropylbenzene})]PF_6$ and other members of the $[CpFe(\eta^6\text{-arene})]^+Z^-$ family have been used for initiating polymerization of a variety of monomers including epoxides,[3,23,26,42-46] dicyanate ester,[47] pyrroles,[48,49] acrylates,[50] styrene,[51] and dioxolenes.[52] However, there is little characterization of the mechanism of the initiation and propagation of polyethers except for the identified structure of bis(1,4,7,10-tetraoxacyclododecane)iron(II)-dihexafluorophosphate from the photopolymerization of ethylene oxide in a solution of methylene chloride containing $[CpFe(\eta^6\text{-arene})]^+$.[24] Moreover, results that do not support the proposal of the active initiating species in the form of $[CpFe(monomer)_3]^+$ have been reported. For instance, Rabek and co-workers found that the polymerization reaction of pyrrole photoinitiated by $[CpFe(\eta^6\text{-isopropylbenzene})]PF_6$ and $[CpFe(\eta^6\text{-naphthalene})]PF_6$ occurred only in the presence of oxygen.[48,49] Iron (III) species showed up in the Mössbauer spectra of the polypyrrole and the complete inhibition of the polymerization by addition of 1,10-phenanthroline made them assume that the polymerization is caused by Fe(III), which is the product of the oxidization of Fe(II) produced from the

photolysis of photoinitiators. A similar conclusion was reached by Bowser and Davidson.[43]

In case of the polymerization of aromatic dicyanate ester, negligible counterion dependence on the rate of polymerization was observed. It was proposed that the [CpFe(η^6-arene)]$^+$ compounds acted as catalysts that, upon illumination, provided a site for the interaction of three ligands, namely, the cyanate functionalities.[47] In the subsequent thermal curing, the formation of the triazine ring started the polymerization. When the polymerization of cyclohexene oxide (CHO) was photoinduced with iron-arene complexes, the concentration of the active propagation center, P^*, was found to vary among the initiators investigated and depend on the irradiation time and the polymerization temperature.[45] P^* was determined by a spectroscopic method[53] that introduced a phenyl ether group at the polymer chain end by the quantitative reaction of the propagating species with excess sodium phenoxide. In the plot of P^* concentration vs. polymerization temperature, a peak showed up at about 35 ^oC in the investigated temperature range from 7 ^oC to 50 ^oC. To account for the results an assumption based on the plurality of mechanism (Scheme 3) was made. It was assumed that low temperatures favor the complexation of iron and CHO, while high temperatures facilitate ring-opening but destabilize the ligand sphere in the iron cation. Unfortunately, there was no clue about the identity of the P^* or the propagating species.

In brief, previous investigations of the polymerization started by [CpFe(η^6-arene)]Z photoinitiators (Figure 2) have been focused on the photophysical

Figure 2

Processes during photochemically initiated cationic polymerization. P, IN, and M stand for the photoinitiator, the active initiating species generated in the photoreaction from P, and the monomer to be polymerized.

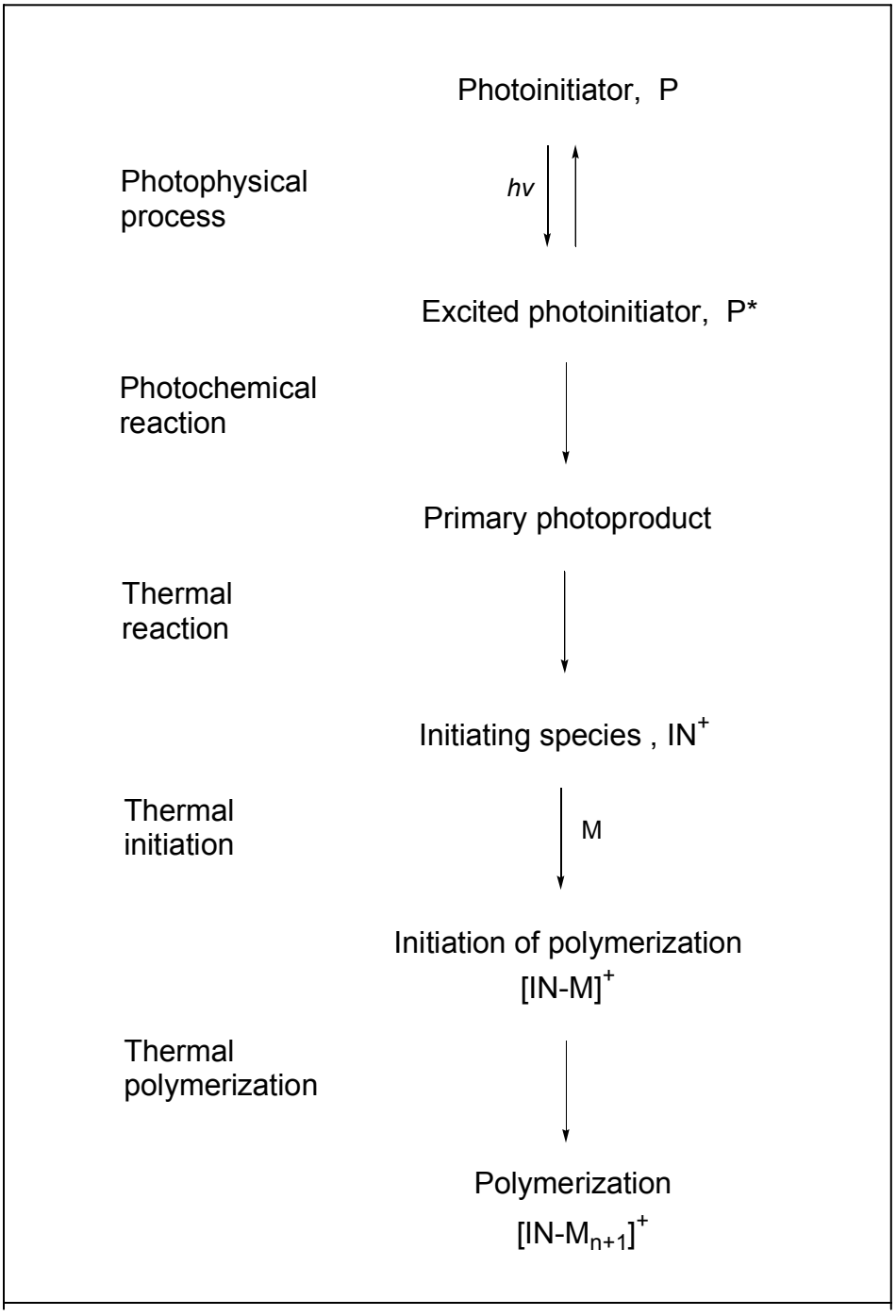
Photoinitiator, P
Photophysical process
hv
Excited photoinitiator, P*
Photochemical reaction
Primary photoproduct
Thermal reaction
Initiating species , IN+
Thermal initiation
M
Initiation of polymerization
[IN-M]+
Thermal polymerization
Polymerization
[IN-Mn+1]+

process, the photochemical reaction, and the thermal polymerization. No successful attempts have been reported in the mechanistic studies of the middle steps in the mechanism, namely, the thermal reaction between primary photoproduct and the monomer, the initiating reaction, and the first few steps of propagation before the bulk polymerization.

Looking over the situation, one has to recall the two well-recognized principles that lie at the heart of chemistry: the dependence on variables cannot be understood until the reaction mechanism is established, and a reaction mechanism cannot be fully defined when the reaction products are unknown.[10] Hence the crucial issues are that the identity of photogenerated species actually responsible for initiating the polymerization with $[CpFe(\eta^6\text{-arene})]^+$ is uncertain and that $[CpFe(monomer)_3]^+$ was postulated to play the role of actual initiating species. However, neither it nor any polymer products containing the CpFe unit have been observed. Therefore in order to elucidate the initiation mechanism, probing and identifying the initiating species, or intermediates in some cases, become key factors to the successful understanding of the polymerization study.

1.4.2 Dibenzoylferrocene and bis(arene)iron(II) complexes

Beside the mixed arene-cyclopentadienyl iron derivatives, $[CpFe(\eta^6\text{-arene})]^+$, ferrocene and its substituted cyclopentadienyl analogues along with bis(arene)iron(II) salts, $[Fe(\eta^6\text{-arene})_2]^{2+}$, are the other two main classes of iron sandwich compounds that have received research attention for their photochemical behavior. The similarity in their structures makes these three

classes the subjects for comparisons of chemical bonding properties,[54,55] electronic structure features,[56] and photoreactivity.[57,58]

Ferrocene is well known for its inertness towards photodecomposition in most solvents except halocarbon ones, in which a charge-transfer-to-solvent intermolecular process leads to a photoredox reaction that yields the ferricenium cation and radical anion of the solvent as the primary products.[59] However, the presence of electron-drawing acyl substituents on the cyclopentadienyl ring dramatically enhances the susceptibility of the substituted ferrocene compounds to photosubstitution in a variety of solvents. Benzoylferrocene and 1,1'-dibenzoylferrocene (DBF) have been the subject of mechanistic studies. Benzoylferrocene was reported to undergo photoaquation (λ>280 nm) in wet solvents (pyridine, dimethylsulfoxide, and dimethylformamide) at room temperature, which resulted in a cyclopentadienyliron salt of benzoate.[60] The identities of the photoproducts were deduced from spectroscopic observations (NMR, IR, and UV-Vis). A mechanism (Equation 18) for the primary photoreaction was proposed with the assignment of the intermediate as $[CpFe(S)_n]^+PhCO_2^-$, though it was not stable enough to be isolated. The same pattern of photochemical changes was observed for DBF. A reaction sequence of

$$\begin{array}{l} [CpFe(\eta^5\text{-}C_5H_4C(O)Ph] \\ \quad + \\ \quad H_2O \end{array} \xrightarrow[S = DMSO, etc.]{h\nu\ (\lambda > 280\ nm)} \begin{array}{l} [CpFe(S)_n]^+PhCO_2^- \\ \quad + \\ \quad \text{  } \end{array} \qquad (18)$$

photoaquation on the carbonyl moiety followed by both the iron-ring and ring-carbonyl cleavages was suggested, because no photodecomposition reaction occurred with rigorously dried solvents and the reactivity depended on the amount of water added into the system. More recent work by Che and co-workers, however, found that a small amount of water played no role in the reaction and had no effect on the products formed.[61] The presence of the strongly chelating ligand 1,10-phenanthroline (phen) in the photolysis of DBF solution irradiated with visible light at 0°C yielded a stable product, $[Fe(phen)_3]^{2+}$ (Equation 19). A charge transfer from metal to cyclopentadienyl ring under photo-

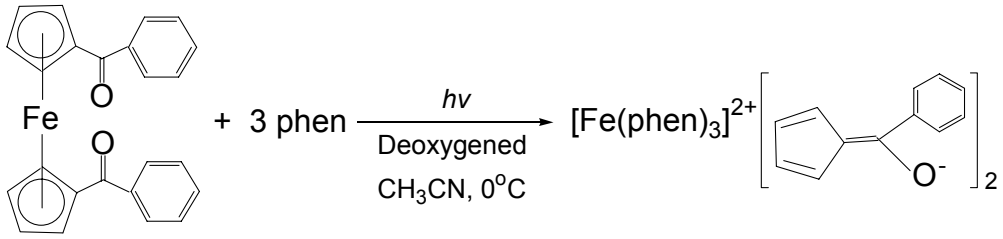

(19)

excitation was thought responsible for the cleavage of Fe-benzoylcyclopentadienyl and the generation of the $C_5H_4C(O)Ph^-$ anion. According to the structural features of the anion determined by X-ray crystallography, a tautometric equilibrium (Equation 20) was proposed and the enolate was believed to be the dominant form in the equilibrium.

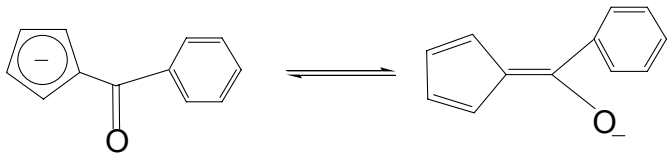

(20)

In an effort to explore the photoreaction mechanism of benzoyl-functionized ferrocene complexes and to search for new classes of anionic photoinitiators, Kutal and co-workers systematically investigated ten mono- and di-benzoyl ferrocene compounds with a variety of functionalities on the phenyl rings.[62] The electronic properties and quantum yields upon irradiation at 546 nm in several solvents were determined. The identification of a protonated benzoylcyclopentadiene and cationic iron(II) complex $[(\eta^5C_5H_4C(O)Ph)Fe(AN)_3]^+$ (AN = CH_3CN) by GC-MS from the photolyte of a DBF solution in acetonitrile led to a proposal that the primary photoreaction (Equation 21) yielded a half-sandwich iron complex ion and an intact benzoylcyclopentadienide anion. A

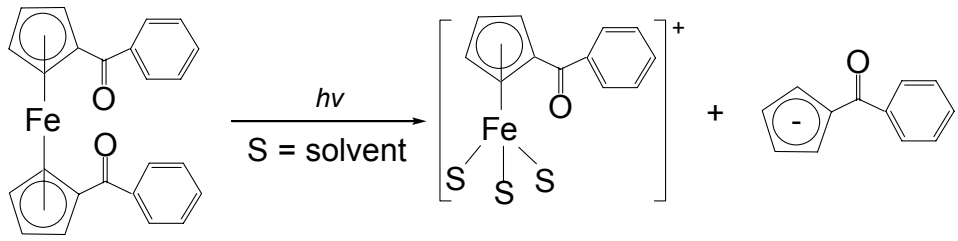

(21)

radical mediated mechanism in the system with methanol solvent was excluded on the grounds that the quantum yield of the photodecomposition reaction was not influenced by O_2, an effective radical scavenger.[63] In a subsequent study, the benzoyl substituted ferrocenes were established as a new class of anionic photoinitiators for monomers like ethyl α-cyanoacrylate[64-67], and the polymerization reaction was proposed to be initiated by the anion photoreleased from the acylferrocenes such as DBF (see Equation 21).

In contrast to the $[CpFe(\eta^6\text{-arene})]^+$ and acylferrocene compounds, relatively little information is available concerning the photodeligation mechanism

of bis(arene) iron(II) complexes. The analysis of products from the photolyte of an acetonitrile solution of $[Fe(\eta^6\text{-mes})_2](PF_6)_2$ (mes = mesitylene) confirmed a 1:2 stoichiometric ratio of $[Fe(CH_3CN)_6]^{2+}$ to mes, which supported an overall pathway for the decomposition reaction (Equation 22), while a laser flash photolysis study revealed short-lived intermediates with an estimated reaction time frame of a few microseconds for the arene deligation.[57] Different pathways

$$[Fe(\eta^6\text{-mes})_2]^{2+} \xrightarrow[CH_3CN]{h\nu} [Fe(CH_3CN)_6]^{2+} + 2\ \text{mes} \qquad (22)$$

were operative depending on the type of excited state populated. Weakened Fe-mes bonding in the ligand field excited state with respect to the ground state caused the facile substitution of mesitylene by acetonitrile. When $[Fe(\eta^6\text{-mes})_2]^{2+}$ was excited to a mesitylene → Fe charge transfer state, an intermediate iron(I) complex containing mesitylene and the mesitylene radical cation as ligands was formed. The rapid ligand loss followed by a back-electron transfer step yielded the arene deligation product $[Fe(CH_3CN)_6]^{2+}$ in acetonitrile medium (see Scheme 5). Charge transfer intermediates from bis(arene) iron(II) were characterized in the reactions where external electron donors were available.[58,68,69]

Scheme 5

$$[Fe(\eta^6\text{-mes})_2]^{2+} \xrightarrow{h\nu} [(\eta^6\text{-mes})Fe^{+}(\eta^6\text{-mes}^{\bullet+})]$$

$$\downarrow$$

$$[Fe(CH_3CN)_6]^{2+} + 2\text{mes} \xleftarrow[CH_3CN]{} [\text{mes}\cdots Fe^{+}\cdots \text{mes}^{\bullet+}]$$

The ready release of a cationic Lewis acid by photoinduced arene loss led to the exploratory test of $[Fe(\eta^6\text{-mes})_2]^{2+}$ as a photoinitiator for the polymerization of epoxides.[70] Though limited thermal stability of the complex presents a barrier for its practical application, a mechanistic study on its initiation of polymerization reaction is beneficial to the future development of photoinitiators from the $[Fe(\eta^6\text{-arene})_2]^{2+}$ family.

1.5 Probing polymerization reactions

Analysis by NMR and IR spectroscopies is commonly used to decipher the structures of polymers or oligomers, and then to deduce the plausible mechanisms for initiation and propagation based on the initiator employed in the system. However, owing to their very small mole fraction in the polymer or oligomer molecules, end-groups can be difficult to identify in some cases. Fortunately, the last two decades have witnessed the development of increasingly powerful mass spectrometry (MS) techniques that allow for the direct polymer analysis including the measurement of molecular weights of synthetic macromolecules.[71] In addition to the rapid determination of the average molecular weight and polydispersity for polymers, high resolution mass spectrometry can pin down the mass of the end-group.[72-75] Furthermore, tandem mass spectrometric techniques help identify the structure of the end-group that can be vital to understanding chemical structures of the polymers and the mechanism of the process.[76-80]

Information about the initiation reaction steps in a polymerization process has been obtained by identifying the products in the gas phase with mass spectrometry when initiating species react with the first few monomer molecules. Reaction of the fullerene dication with 1,3-butadiene was followed in a quadrupole mass filter at room temperature by the identification of oligomer chains with monomer units from one through four.[81] The ion signals detected indicate that there are two primary product channels for the reaction of C_{60}^{2+} and C_4H_6: charge transfer to form $C_{60}^{\bullet+}$ and $C_4H_6^{\bullet+}$, and adduct formation to give the initiating species $C_{60}(C_4H_6)^{2+}$ that upon further attack of monomer molecules generates $C_{60}(C_4H_6)_n^{2+}$ (n= 2,3,4). The signal distribution among oligomers depended on the flow rate at which monomer was released into the quadrupole filter. No adduct products from the two radical cations $C_{60}^{\bullet+}$ and $C_4H_6^{\bullet+}$ were found. Brodbelt et al. reported the observation on the initiating and propagating processes of cyclic ethers and thioether (ethylene oxide, cyclohexene oxide, tetrahydrofuran, and ethylene sulfide) with perfluoro crown ether cations that were formed upon loss of fluoride from the neutral compounds.[82] The ion-molecule reactions in gas phase at 2-10 microtorr at 50^{o}C were conducted in a triple-quadrupole mass spectrometer. Up to five and three monomer molecules were found attached to the cation in the case of ethylene oxide and ethylene sulfide, respectively. However, there were only two monomer units attached to the cation when the less strained cyclic ethers, cyclohexene oxide (CHO) and tetrahydrofuran, were introduced. Interestingly, the formation of cationic polymerization products instead of ion/molecule clusters is supported by the

detection of ions with formulas $(M - F + CHO - n26)^+$ and $(M - F + nCHO)^+$ (M = the neutral cyclic ether molecules; n = 1,2) for the reaction of CHO with the perfluorinated substrate ions $(M - F)^+$. The loss of 26 Da, assigned as C_2H_2, indicates that the propagation step is highly exothermic and results in cleavage within the CHO unit, which is inconsistent with the formation of van der Waals clusters held by weak electrostatic interactions. Gas phase polymerization reactions initiated by alkylzirconocene cations with alkene were recently investigated by mass spectrometric methods.[83,84] In the gas phase, the same monomer insertion process as the expected Ziegler-Natta pattern in solution was revealed by characterizing the oligomers with MS and tandem MS.

Gas phase studies provide significant insights into the mechanism of condensed phase reactions by simplifying the reaction environment. For instance, an unsolvated cation species is obtainable and studies on bond formation are feasible within a relatively isolated system.[85] However, one must be cautious not to overestimate the applicability of the information to the solution systems. The effects of ancillary ligands in the zirconocene system on the reactivity of the complex cations towards initiating polymerization in the gas phase were recognized. However, the overall polymerization reactivity in solution was found dominated by the equilibrium of ion pairing and by the rates of termination,[83] and the reaction rate difference in the two phases was addressed.[84]

Ideally, directly probing the photochemical and thermal reactions occurring in solutions will provide a better understanding of the chemistry involved for the real industrial polymerization processes, which, in turn, accelerates the

development and invention of novel photoinitiators on the basis of a thorough understanding of the initiation mechanisms. For reactions conducted in the condensed phase, techniques that are able to identify the products/intermediates in a specific time frame are desirable. Moreover, if the reaction monitoring is performed on-line, direct observation of intermediates along the reaction course is possible.

Electrospray ionization mass spectrometry (ESI-MS) developed in the last decade affords a soft transfer of ions in the condensed phase into the gas phase prior to mass analysis, and has been shown to be a powerful identification method for polar and nonvolatile species from their solution samples. Being compatible with separation techniques such as capillary electrophoresis (CE) and high-performance liquid chromatography (HPLC) enables ESI-MS to be widely employed for the characterization of various species such as biomolecules,[86] synthetic oligomers and polymers,[87-90] and inorganic/organometallic complexes[91-94] in more complicated systems. Aware of the advantages in which intact ions are generated from solutions and readily detected by ESI-MS, researchers have moved forward to explore its application in monitoring chemical reactions.[95-97] On-line ESI-MS techniques have emerged in the kinetic and mechanistic studies of organic,[98,99] biochemical,[100] electrochemical,[101] and photochemical[102-107] reactions by probing intermediates produced in the corresponding reactions. In the last category of reactions, owing to the high reactivity of intermediates as primary photoproducts, the time scale within which ESI-MS is used to detect intermediates becomes an essential issue, especially

when short-lived intermediates are the analytes of interest. Coupling a quartz cell with the ESI source before the spraying capillary, Arakawa and co-workers[102-105] performed a series of photolysis studies on the photosubstitution and photooxidation of Ru(II) complexes, and successfully detected intermediates with lifetimes of more than a few minutes in the photoreaction cell. A photolysis reactor was set on-line with ESI-MS to conduct real-time monitoring and kinetics analysis for the photolysis of idoxifene.[106] This in situ probing is applicable for moderately rapid reactions if 3-5 minutes is allowed for the introduction of samples from reactor to the mass spectrometer. The photochemical behavior of pesticides, including triazines, phenylureas, and carbamates, was described by Volmer[107] in an on-line coil photoreactor coupled to HPLC-ESI-MS/MS, and an estimated resident time of 30 seconds in the photoreactor was used in conjunction with HPLC.

Obviously, probing intermediates or products with shorter lifetimes, for example less than one second, may be crucial in some reactions. In fact, in the photolysis of $[CpFe(\eta^6\text{-arene})]^+$ complexes (see Scheme 4), Ronco et al. estimated the time for the formation of ferrocene from their flash photochemical study with a dichloromethane solution of $[CpFe(\eta^6\text{-arene})]^+$ to be in the μs – ms time domain at room temperature.[108] Warming up the purple photolyzed acetonitrile solution of $CpFe(\eta^6\text{-p-xylene})^+$ from –40 ^oC to 20 ^oC destroyed the unstable intermediate that was characterized as $[CpFe(CH_3CN)_3]^+$ at low temperature by NMR and other measurements.[32,33] We have developed a new on-line ESI-MS technique capable of detecting and identifying species with

lifetimes down to a few milliseconds. This technique will allow us to probe the thermal reaction of photogenerated intermediates with monomer substrate in the mechanistic studies of polymerization processes photoinitiated by [CpFe(η^6-arene)]Z, as well as to study the pathways for the photolysis of acylferrocenes and bis(arene)iron(II) complexes by characterizing the intermediates in the photochemical reactions.

1.6 Project objectives

The purpose of the present study is to elucidate the mechanisms of photoinitiated polymerization reactions by various families of iron arene complexes in the condensed phase via the identification of intermediates and products in the course of initiation and the first few steps of propagation. An on-line ESI-MS characterization technique will be established for probing of short-lived intermediates at the millisecond level that are generated from the photodeligation and initiation processes. Comparison will be made to the photochemical reactions among the three classes of iron complexes, [CpFe(η^6-arene)]Z, [Fe(η^6-arene)$_2$]Z_2, and dibenzoylferrocene, in addition to the evaluation of the active initiating species and their influences on the corresponding initiation mechanisms.

CHAPTER 2

EXPERIMENTAL

2.1 Reagents

General

Chemicals used in synthetic work were of reagent grade or higher quality and generally employed as received from the suppliers unless otherwise noted. Acetonitrile (HPLC grade, J.T. Baker, Phillipsburg, NJ), dichloroethane (A.C.S. grade, J.T. Baker), and tetrahydrofuran (certified grade, Fisher Scientific, Fair Lawn, NJ) for the photolysis and photoinitiated polymerization reactions were dried and distilled by a procedure described below. Iron compounds that are commercially available were purified prior to use in experiments. The purity and identity of the compounds were confirmed by comparison of their melting points to literature values, elemental analysis, NMR spectra, or mass spectra.

Solvent drying / purification

Water as impurity in acetonitrile of HPLC grade was found as a ligand in the photoproducts with observable signal intensity in photolysis-MS experiments with [CpFebz]PF_6. Intensive efforts toward rigorously drying solvents followed by fractional distillation were made. Phosphorus pentoxide (97%, Aldrich, Milwaukee, WI) and calcium hydride (laboratory grade, Fisher Scientific) are the common reagents recommended for use in removing trace amounts of moisture in the last step of purification for the aforementioned solvents.[109] It turned out that calcium hydride was easier to handle than phosphorus pentoxide, though in the preliminary tests there was no noticeable difference in the purity of the distilled solvents with both of the agents. The standard 130 mm Virgreux distillation column proved inefficient to get high purity solvent (e.g., clean

background in mass spectrum) from distilling the mixture of drying agent and solvents. Extending the length of column to 210 mm improved the purity of the distillates. However, noticeable impurity peaks still showed up in the mass spectra. A general procedure described here has been developed and employed to obtain pure and highly anhydrous acetonitrile, 1,2-dichloroethane, and tetrahydrofuran after a few attempts. Two grams of CaH_2 were added per liter of the solvent, and stirring of the mixture under an argon atmosphere at room temperature was maintained for 12 to 24 hours prior to refluxing for another 5 hours. A high reflux ratio was maintained in the fractional distillation step with a 230 mm column packed with glass beads of outer diameter 5 mm. Cutting-off the first 10% to 15% and the last 30% portions of the distillate and saving the middle portion yielded purified solvents that were stored in flasks or Aldrich 1 L Seal™ bottles. All glassware was dried at 150 ^{o}C over 12 hours immediately prior to the setup of the distillation apparatus.

Purification of cyclohexene oxide (CHO)

Cyclohexene oxide (98%, bp_{760} = 129 – 130 ^{o}C) from Aldrich or Lancaster (Windham, NH) was purified by fractional distillation under reduced pressure. It was stirred with calcium hydride under argon atmosphere at room temperature and atmosphere pressure in a fractional distillation setup with a distillation column packed with glass beads for about 2 hours prior to refluxing and distillation. Under reduced pressure with controlled leaking of argon gas, one hour refluxing was carefully maintained to the extent at which the packing beads (o.d. = 5 mm) in the column (i.d. = 20 mm, L = 230 mm) were wetted while no

condensation of cyclohexene oxide occurred in the down stream condenser. The condenser was running cooling water at about 0 ^{o}C by having tap water passed through a copper-tubing exchanger that was immersed in an ice-water bath throughout the refluxing and distillation periods. The first 10% and last 30% portions were discarded in the distillation, and the middle cut with a condensation temperature at about 45 ^{o}C and in a range of less than 3 ^{o}C was collected in a round-bottom flask. The distillation was repeated if the purity of the first distillate was not satisfactory. The CHO distillate container was kept in a sealed glass bottle with Drierite and stored at 4 ^{o}C prior to use. All glassware was cleaned and dried in an oven at 150 ^{o}C before setting up the apparatus. The switch between first and second cuts was performed with a house-made multi-joint adapter without disrupting the stable vacuum distillation condition. ^{1}H NMR spectroscopy was applied to characterize and check the purity of the distillate right after purification and on a periodic basis, or in case doubt on the quality of CHO had arisen.

Purification of 1,1'-dibenzoylferrocene (DBF)

Double recrystallization of commercial 1,1'-dibenzoylferrocene (Sigma, St. Lous, MO) was performed in addition to chromatographic column purification. One liter of hexanes (95% n-hexane, HPLC grade, J.T. Baker) was used to dissolve 1 gram of DBF at 60 – 65 ^{o}C. The insoluble impurity was removed by vacuum filtration. The filtrate was cooled down to room temperature prior to placing in a refrigerator at 4 ^{o}C for 12 hours. The needle crystals were collected, rinsed with cold hexane in two portions, and dried *in vacuo* over Drierite for at

least 12 hours. The dried DBF from a second recrystallization was then dissolved in an acetonitrile/dichloromethane (5:95 v/v) solvent mixture before being introduced into a preparative chromatographic column (i.d. = 25 mm, L = 230 mm) packed with silica gel (60 Å, EM Science, Gibbstown, NJ). The loaded column was eluted with 100 mL of pure dichloromethane followed by the solvent mixture. The middle band was collected, solvent was removed by rotary evaporation, and the resulting solid was dried over phosphorus pentoxide under vacuum overnight. Purifications were performed in a dark room under red light. The purified DBF was characterized by NMR spectroscopy and elemental analysis (Atlantic Microlab, Inc. Atlanta, GA). ^{1}H NMR (Me_2SO-d_6): δ 7.76 (m, 4H, o-Ph), 7.61 (m, 2H, p-Ph), 7.49 (m, 4H, m-Ph), 4.86 (t, 4H, $H_{2,5}$), 4.71 (t, 4H, $H_{3,4}$). 1,1'-dibenzoylferrocene calculated for $C_{24}H_{18}O_2Fe$: C, 73.11%; H, 4.60%. Found: 72.98%; H, 4.59%.

Purification of [CpFe(η^6-cumene)]PF_6

Cumene cyclopentadienyl iron(II) hexafluorophosphate (98%, Aldrich) was purified by column chromatography on silica gel. A 0.55 gram sample was dissolved in an acetonitrile/dichloromethane (20:80 v/v) solvent mixture and loaded on the top of the column. The same solvent was used for elution. The eluate of a yellow band was collected, and solvent was removed by rotary evaporation. Drying the product over P_4O_{10} under vacuum yielded 0.41 gram of a yellowish light-brown solid. It was characterized by ^{1}H NMR spectroscopy and elemental analysis. ^{1}H NMR ($CDCl_3$): δ 6.34 (m, 3H, p-,o-Ph), 6.20 (m, 2H, m-Ph),

5.06 (s, 5H, C_5H_5), 3.04 (m, 1H, CH), 1.39 (s, 6H, CH_3). [CpFe(η^6-cumene)]PF_6 calculated for $C_{14}H_{17}PF_6Fe$: C, 43.55%; H, 4.44%. Found: 43.77%; H, 4.47%.

Synthesis of [CpFebz]PF_6

Initial batches of [CpFebz]PF_6 were prepared using the conventional procedure.[110] A mixture of 2.097 grams (11 mmole) of sublimed ferrocene(mp = 173.2 – 174.0 ^oC, literature mp = 173 – 174 ^oC), 0.286 gram (11 mmole) of aluminum powder (particle size ~20μm, Aldrich), and 2.810 grams (21 mmole) of aluminum chloride (99.99%, Aldrich) in 80 mL of benzene (GR grade, EM Science, Gibbstown, NJ) was heated with continuous magnetic stirring to reflux under a nitrogen atmosphere for 6 hours before being cooled down to room temperature and then to 0 ^oC in an ice-water bath. Thereafter, 120 mL of cold water pre-bubbled with nitrogen were added slowly to hydrolyze the extra $AlCl_3$, and then 40 mL more water was added under vacuum at 0 ^oC. When water was dropped into the brown mixture, a cloudy yellow aqueous phase resulted. The mixture was allowed to stir for another 4 hours in an ice-water bath and then filtered with qualitative filter paper. A lot of ferrocene crystals were collected on the filter paper and a cloudy light-green and yellow filtrate was obtained. Refiltration of the cloudy filtrate with ashless filter paper took several hours. An aqueous solution containing excess NH_4PF_6 (99.99%, Aldrich) was added to the second filtrate. The process proved not successful as no significant amount of desired water-insoluble [CpFebz]PF_6 was precipitated with NH_4PF_6 from the filtrate solution.

A few attempts at preparing the complex used a new technique, microwave dielectric heating.[111,112] In a typical trial batch of the synthesis, 0.93 gram (5 mmole) of sublimed ferrocene, 0.13 gram (5 mmole) of aluminum powder, and 1.33 grams (10 mmole) of aluminum chloride were ground together in a mortar. To the solid mixture was added 5 mL (56 mmole) of benzene with stirring with a glass rod. The pasty mixture was then rapidly transferred into a modified 250 mL beaker as reaction vessel. A 150 mL beaker with 2 cm flanged lip was placed in the vessel as its cover. Solid carbon dioxide chunks were put inside of the cover beaker. The carbon dioxide has no dipole moment and is thus transparent to microwaves. It served as a coolant to prevent the reaction system from overheating. A 100 mL beaker containing 60 mL of water was placed alongside the reaction vessel to absorb extra microwave irradiation. After several trial-and-error experiments with a house-kitchen microwave oven (EM-P671W, Sanyo), optimized settings were 3.5-minute heating at Power level 4. In the succeeding work-up with 100 mL of cold water, the dark-green muddy mixture yielded a green-yellow solution with dark oily precipitate. This mixture was filtered, and the resulting filtrate was treated with a saturated NH_4PF_6 aqueous solution (3.7 grams in 5 mL), which resulted in yellow and off-white large particles. Chromatography on an 80 mm column containing Al_2O_3 with dichloromethane as eluant was employed to remove impurities from the desired product according to the literature procedure.[37] Light yellow crystals were obtained in a yield of 17% with a melting point of 304 – 305 ^oC. Comparison of the electronic spectrum from a dichloromethane solution of the product with

respect to that reported in literature revealed a band shift and absorbance enhancement in UV region: 368 nm (ε = 186 $M^{-1}cm^{-1}$), 455 nm (ε = 71 $M^{-1}cm^{-1}$) vs literature values of 382 nm (ε = 88 $M^{-1}cm^{-1}$), 452 nm (ε = 61 $M^{-1}cm^{-1}$). Thin layer chromatography (TLC) experiments on a 60 Å silica gel plate with acetonitrile-dichloromethane developing reagent showed a moving light-yellow spot and an immobile spot at the origin when solvents ranging from 0:100 to 50:50 for the ratio of acetonitrile to dichloromethane (v/v) were tested. This behavior indicates the presence of a strong polar impurity that could not be isolated by Al_2O_3 chromatographic column.

Later batches of [CpFebz]PF_6 were successfully prepared by combining microwave dielectric heating with benzene extraction of the filtrate after aqueous work-up[113] and an alternative silica gel chromatographic isolation. Sublimed ferrocene that was pre-ground and aluminum powder were dried over P_4O_{10} in a vacuum desiccator at room temperature with continuous pumping by a mechanical vacuum pump for over 12 hours. Then 3.5 grams (19 mmole) of ferrocene and 0.501 gram (19 mmole) of aluminum powder were ground together in a ceramic mortar with a pestle prior to being transferred to the 250 mL glass reaction vessel. To the mixture was added 5 grams (38 mmole) of $AlCl_3$ with rapid stirring with a glass rod, and then 6 mL (67 mmole) of benzene were added with fast stirring. The reaction vessel containing the brownish mixture was covered with the flanged 150 mL beaker containing dry ice chunks. The reaction apparatus along with a 100 mL beaker containing 60 mL of water at room temperature were put in the microwave oven at Power 4 and heating for 3.5

minutes. After heating, the reaction apparatus with the dark-green mixture in it was allowed to cool down to room temperature and then to 0 ^{o}C in an ice-water bath. Then 150 mL of cold water (0 ^{o}C) was added dropwise to the mixture at such a rate that the extra benzene was kept below its boiling point by the exothermic reaction. The resulting green solution and sticky black solid were stirred for one hour before gravity filtration. The 150 mL of filtrate was extracted three times in a separatory funnel by adding 10 mL of fresh benzene each time. The washed aqueous layer was filtered by gravity directly into 20 mL of an aqueous solution containing 3 grams of ammonium hexafluorophosphate. A yellow-greenish precipitate formed immediately. After standing for one hour, the solid product was collected and dried in vacuum over phosphorus pentoxide overnight to give 2.86 grams (44% yield) of yellow crystalline [CpFebz]PF_6. The dried crude product was dissolved in a minimum amount of solvent mixture of acetonitrile and dichloromethane in a ratio of 5 to 95 (v/v), and loaded on the top of a preparative column containing 150 g of 60 Å silica gel. Sequential eluting from a solvent ratio of 5:95 to 20:80 for acetonitrile and dichloromethane produced 1000 mL of eluant containing the yellow-brown middle band. The crystals resulting from evaporating the eluate were dissolved in a solvent mixture containing acetonitrile and dichloromethane (20:80, v/v), and run through a fresh silica gel column a second time. When solvent was removed by rotary evaporation, the resulting crystalline product was dried over P_4O_{10} under vacuum overnight. At this point, the polar component originally observed on TLC plate had disappeared. The final product, obtained in an overall yield of 1.77 grams

(27%), was characterized by ^{1}H NMR spectroscopy and elemental analysis. ^{1}H NMR [$CD_3C(O)CD_3$]: δ 6.22 (s, 6H, C_6H_6), 5.02 (s, 5H, C_5H_5). [CpFebz]PF_6 calculated for $C_{11}H_{11}F_6P_1Fe_1$: C, 38.40%; H, 3.22%. Found: C, 38.11%; H, 3.24%.

Synthesis of [CpFe(η^6-C_6D_6)]PF_6

A similar procedure as for [CpFebz]PF_6 was employed for the synthesis of [CpFe(η^6-C_6D_6)]PF_6 except that the scale was cut down to half and the arene extraction of the filtrate from aqueous work-up was not included owing to a concern of possible adverse effect on the deuterated benzene in the complex. The preparation started with heating a mixture of 1.74 grams (9.3 mmole) of sublimed and pre-dried ferrocene, 0.25 gram (9.3 mmole) of aluminum powder, 2.44 grams (18.3 mmole) of $AlCl_3$, and 3 mL (34 mmole) benzene-d_6 (99.5% D, Aldrich) in the microwave oven at Power 4 for 3 minutes. A green-black solution was obtained upon adding 100 mL of cold water to the heated mixture. The filtrate from a subsequent gravity filtration was directly introduced into a saturated aqueous solution of 3 grams NH_4PF_6, generating a yellow and light-green precipitate that was filtered and dried to yield 0.92 gram (28% yield). A narrow yellow band from the eluate by silica gel column yielded a single spot on the TLC test, resulting in 0.181 gram of final product [CpFe(η^6-C_6D_6)]PF_6. Reduced scale and the skipping of extraction isolation together contribute to the low overall yield.

Synthesis of [(η^5-C_5D_5)Febz]PF_6

Perdeuteration of protons on the Cp ring of [CpFe(η^6-arene)]PF_6 (arene represents a benzene derivative) was successful for the π ligands hexamethyl-

benzene, mesitylene, and toluene by a multi-step procedure starting with [CpFe(η^6-arene)]PF_6.[114] When the number of methyl substituents is reduced from six to one, the yields decrease from 73% to 8% with deuterium incorporation around 90% owing to the side reaction of the deprotonated intermediate generated in the procedure. Without methyl substituents on the arene ring as in the case of benzene, this direct perdeuteration route seems unlikely. Thus, an alternative preparation for [(η^5-C_5D_5)Febz]PF_6 was designed, using the same procedure as for [CpFebz]PF_6 but starting with perdeuterated ferrocene. Perdeuterating ferrocene was accomplished in a direct deuterium exchange reaction with D_2O catalyzed by trifluoroacetic anhydride (TFAA).[115] Two grams of pre-dried and sublimed ferrocene were transferred into a 100 mL house-made ampule. To the ampule was then added 35 mL of p-dioxane (A.C.S. grade, J.T. Baker) pre-dried by passing through a short column of 5 Å molecular sieve, which had been heated at 230 ^oC for 24 hours prior to use. Twenty-one mL of TFAA (99$^+$%, Aldrich) were quickly added to the mixture in the ampule that was immersed in a cyclohexane-dry ice bath at 6 ^oC. Two minutes later 2.6 mL of D_2O (99.9% D, Aldrich) was added dropwise to the ampule, resulting in a brown mixture. Afterwards, the ampule was kept in the bath for 5 more minutes before being flame sealed. The H / D exchange proceeded at 100 ^oC in an oil bath (100 ± 1^oC) for 24 hours. After the heating period, the ampule was removed from the oil bath, wrapped with aluminum foil, and cooled to room temperature. Pouring the dark-brown solution from the ampule to a separatory funnel containing 100 mL of ice water resulted in immediate precipitation of yellow-green particles.

Extraction of the solid product by 200 mL of diethyl ether (anhydrous, A.C.S. reagent, J.T. Baker) gave a brown-black organic layer and a light-blue aqueous layer. The organic phase was neutralized with 100 mL of an aqueous solution containing 30.19 grams of K_2CO_3, washed with four portions of water (4×100 mL), and dried over anhydrous $MgSO_4$. Rotary evaporation brought the organic solution to dryness and left behind a brown-black residue that was further purified by chromatography on a short silica gel column with 10:1 (v/v) n-hexane:ethyl acetate as eluant. The 1.51 grams of partially deuterated product were recovered by removing solvent and drying over P_4O_{10}. The same exchange procedure was repeated a second time in a corresponding scale according to the mass of the partially deuterated product from the first exchange, and yielded 0.42 gram of final product. From the ESI mass spectrum of the twice-exchanged product in a solution of acetonitrile without drying, it can be calculated that 86% of the protons had been replaced by deuterium. Starting with the deuterated ferrocene, the [(η^5-C_5D_5)Febz]PF_6 synthesis was undertaken with the identical procedure used for preparing [CpFebz]PF_6, but in a scale corresponding to the amount of deuterated ferrocene available.

Synthesis of [CpFebz]SbF_6

The same procedure as for [CpFebz]PF_6 was followed to prepare [CpFebz]SbF_6 with minor modification owing to the high solubility of the compound in water and the low solubility of the precipitating reagent in water. A mixture containing 1.7 grams (9.1 mmole) of ferrocene, 0.25 gram (9.2 mmole) of aluminum powder, 2.4 grams (18 mmole) of aluminum chloride, and 3.0 mL of

benzene (33 mmole) was heated in microwave oven for 3 minutes at Power 4. The reaction mixture was cooled to 0 ^{o}C, and 120 mL cold water (0 ^{o}C) was added dropwise over 25 minutes. Continuous stirring with a magnetic bar for an hour resulted in a greenish light-yellow solution that was extracted with three portions of benzene. To the washed aqueous solution was added 100 mL of a solution containing 1.4 grams of $NaSbF_6$, which did not give a precipitate. Adding 0.6 gram additional $NaSbF_6$ solid to the solution yielded a yellow precipitate immediately. A total of 1 gram more solid $NaSbF_6$ was added in two portions until there was no new precipitation. The mixture was placed in a refrigerator for 11 hours at 4 ^{o}C. After filtering off the light-yellow crystals, two grams of solid $NaSbF_6$ were added to the filtrate, which precipitated more solid product. A total of 0.90 gram of dried crude product was isolated for a yield of 24%. The crude product was purified by silica gel chromatography with a solvent mixture of acetonitrile and dichloromethane in a ratio of 20:80 (v/v) as eluant, and 0.47 gram of final product was recovered for an overall yield of 12%.

Synthesis of [CpFebz]Tf

Essentially the same preparative method as for [CpFebz]PF_6 was followed to synthesize [CpFebz]Tf (Tf is trifluoromethanesulfonate). A mixture comprising 2.02 grams of sublimed ferrocene, 0.29 gram of aluminum powder, 2.85 grams of $AlCl_3$, and 3.4 mL of benzene was heated in the microwave oven at Power 4 for 3.5 minutes. After the work-up with 100 mL of cold water and multiple benzene extractions, the aqueous layer was mixed with a solution containing 20 mL of water and 10 grams of trifluoromethanesulfonic acid (98%, Aldrich). At this point,

the dark green solution turned cloudy but without noticeable precipitate. Rotary evaporation at 50 ^{o}C removed most of the water solvent in the solution (ca. 90%), and yielded yellow crystals when the residue was cooled at 4^{o}C for two hours. The crude material was collected and dried over Drierite in a vacuum desiccator overnight. Silica gel chromatography with an acetonitrile/dichloromethane (1:1 v/v) eluting solvent was performed to isolate the yellow product from the brown impurity matrix. About 0.1 gram of final product was recovered from the purification procedure.

Synthesis of $NaC_5H_4C(O)C_6H_5 \cdot THF$*

A literature procedure[116] was followed in the synthesis of sodium benzoylcyclopentadienide. To 23 mL of 2 M sodium cyclopentadienide solution (46 mmole) in THF (Aldrich) was added 9.3 mL (65 mmole) of ethyl benzoate (99%, Aldrich) with stirring in a glove box that was flushed with argon gas passed through 4 Å molecular sieves and Drierite. After 20 minutes of stirring, a light-brown turbid solution was formed. Following transfer from the glove box to a Schlenk line, the reaction mixture was heated at reflux with stirring for 24 hours under Ar. When the solution was cooled down, about half of the solvent (THF) in the mixture was removed under reduced pressure, and 60 mL of pre-dried diethyl ether was added through a stainless steel needle. After stirring overnight under Ar, the resulting yellow precipitate was filtered in the glove box under Ar and rinsed with dried diethyl ether three times to produce the yellow-tan final product.

---

* Synthesized by Dr. Xingyong Li, University of Georgia.

Synthesis of $[Fe(\eta^6\text{-mes})_2](PF_6)_2$

$[Fe(\eta^6\text{-mes})_2](PF_6)_2$ was synthesized by modifying a literature method.[117] A mixture of 2.6 grams of anhydrous ferric chloride (Aldrich) dried over P_4O_{10} under vacuum, 50 mL of mesitylene (Aldrich) fractionally distilled from CaH_2, and 5 grams of fresh $AlCl_3$ (Aldrich) was heated in an oil bath at 80 – 82 ^oC for three hours. The mixture was allowed to cool to room temperature and then to 0 ^oC in an ice-water bath before dropwise addition of 40 mL of water at 0 ^oC. The two-phase solution was filtered into a separatory funnel and the aqueous layer was subjected to extraction with two 50 mL portions of diethyl ether. The bright pinkish aqueous layer from the second extraction was added to a saturated aqueous solution of NH_4PF_6 prepared by adding enough water just to dissolve 6.5 g of the salt, instantly precipitating fine orange particles. The crystal product was put in refrigerator at 4 ^oC overnight, and collected and dried over P_4O_{10} *in vacuo*, resulting in 3.05 grams of the crude product for a yield of 32%. The light-orange material was twice recrystallized by dissolving it in acetone and reprecipitating with diethyl ether. The final product, obtained in an overall yield of 24%, was characterized by elemental analysis. $[Fe(\eta^6\text{-mes})_2](PF_6)_2$ calculated for $C_{18}H_{24}F_{12}P_2Fe$: C, 36.88%; H, 4.13%. Found: C, 37.23%; H, 4.19%.

2.2 Instrumentation and procedures

Instrumentation

Electronic spectra were recorded on a Varian DMS 300 or Cary 300 Bio spectrophotometer at room temperature (20 $\pm$ 1 ^oC). ^1H NMR spectra were

acquired on a Bruker AC-250 or Bruker 400 spectrometer operating at 250.133 MHz or 400.134 MHz, respectively. ^{13}C NMR spectra were acquired on a Bruker AC-250 spectrometer operating at 62.895 MHz. Chemical shifts were referred to solvent peaks arising from residual protons, which were calibrated with tetramethylsilane (TMS) at 0 ppm. A 200 W high-pressure mercury arc lamp (Illumination Industries, Inc., Sunnyvale, CA) situated 40 cm from the sample was employed as light source for continuous photolysis. The light beam was cooled by passing it through a 10 cm quartz container filled with water and then through an interference filter prior to reaching the sample. An argon ion laser (INNOVA 70-5, Coherent, Palo Alto, CA) was used as light source for on-line photolysis and photoinduced polymerization experiments coupled with a mass spectrometer. It was operated in the Single–Line mode at 488.0 nm with an output of 1.5 W at open aperture position.

Mass spectra were acquired using a Mariner Biospectrometry Workstation (PerSpective Biosystems, Inc.), which combined a time-of-flight mass spectrometer with an electrospray ion source. All samples were ionized by nanoelectrospray in the positive mode with a typical spray tip potential at 1.9 kV. The sample solution was infused through a nanospray tip fabricated in the lab from fused silica capillary of 100 μm inner diameter and 300 μm outer diameter (Polymicro Technologies, Phoenix, AZ; or Supelco, Bellefonte, PA). The ca. 12 μm polyimide coating on the capillary was burned away and a fine tip was drawn to 10 – 20 μm inner diameter by heating the uncoated section of the capillary with a micro-torch (Microflame, Inc., Minnetonka, MN) while applying a constant

pulling force to the capillary. Sample solutions were pumped into the tip by a syringe pump (Model 55-111, Harvard Apparatus, South Natick, MS) at flow rate that ranged from 5 to 400 μL/h, typically from 10 to 80 μL/h. An ESI interface temperature of 90–150 ^{o}C was maintained to aid desolvation of electrosprayed ions.

Actinometry

Light intensity at 546 nm were determined by Reinecke's salt actinometry using the potassium salt, $K[Cr(NH_3)_2(NCS)_4]$.[118] It involved irradiating 3.0 mL of an ca. 20 mM Reinecke's salt aqueous solution for a given length of time to a reaction degree of ca. 3 percent of the initial complex, diluting 2.0 mL of the photolyte solution with a developing reagent, containing 0.1 M $Fe(NO_3)_3$ and 0.5 M of $HClO_4$, to a final volume of 10.0 mL, and measuring the absorbance of this sample at 450 nm. The same procedure was performed with a dark solution to obtain a background for any thermal aquation and the absorption at 450 nm from the Reinecke's salt itself. The concentration of the photoreleased NCS^- within the photolysis time was calculated using the known extinction coefficient of the resulting $[Fe(NCS)]^{2+}$ complex ion. In conjunction with the established quantum yield for $K[Cr(NH_3)_2(NCS)_4]$ at the excitation wavelength, the incident light intensity in einsteins per second was determined.

Quantum yield measurements

The extent of photolysis from a 2.3 mM DBF solution in methanol was determined spectrophotometrically by monitoring the decrease in absorbance of the long wavelength band at 486 nm in its electronic absorption spectrum.

Quantum yields were calculated at different extents of reaction corresponding to the percent of DBF decomposition by irradiating the sample for a varied length of time at 546 nm. The limiting yield was calculated from a plot of quantum yield versus percent of decomposition that was extrapolated to zero percent reaction.

Photochemical procedures

Continuous photolyses with the high-pressure mercury lamp were performed either in Thunberg quartz spectrophotometer cells of 1 cm pathlength, or in i.d. 5 mm NMR tubes (520–pp). The 546 nm line was isolated with a narrow-band-pass (10 nm at half-height) interference filter. In the case of quartz cells, magnetic bars were put in the cells to sustain stirring by a stirrer under the cell holder, while no stirring was applied for NMR tubes. Instead, the tubes were manually flipped over several times in an interval of 50 – 100 seconds during the irradiation. For the irradiation using the laser light source, 1 cm quartz cells were situated 10 cm from the output window of the light source and stirred by magnetic bars. A laser dumper was placed down stream of the cell to reflect and absorb the transmitted light beam.

On-line photochemistry-MS experiments

Figure 3 schematically illustrates the apparatus setup for the on-line photochemistry ESI-MS study. An argon laser provided the light source for the photochemical processes. The laser beam at 488 nm was introduced into the uncoated section of the nanospray tip via an optical fiber. The fiber was held at one end by a home-made fiber positioner containing a three dimensional translation stage that was mounted on the ESI chamber, and connected to the

Figure 3

Schematic diagram of the on-line photochemistry experiment with electrospray ionization mass spectrometry. Inset: orientation of the optical fiber and the nanospray tip, and the definition of distance D.

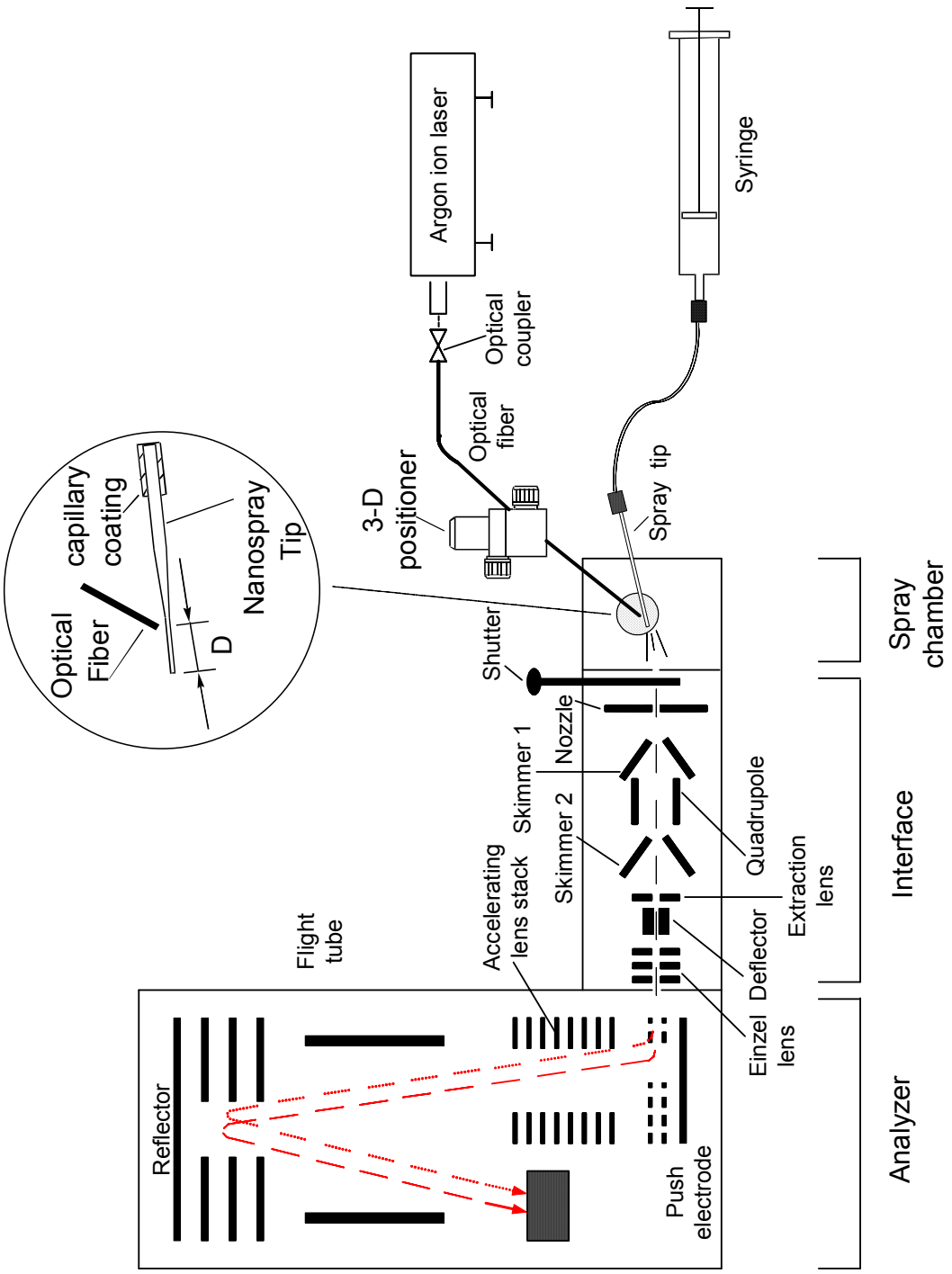
Optical Fiber
capillary coating
D
Nanospray Tip
3-D positioner
Optical fiber
Optical coupler
Argon ion laser
Syringe
Spray tip
Shutter
Nozzle
Skimmer 1
Skimmer 2
Quadrupole
Extraction lens
Deflector
Einzel lens
Accelerating lens stack
Flight tube
Reflector
Push electrode
Analyzer
Interface
Spray chamber

laser output device by a multimode fiber coupler (F-915T-DJ, Newport Co., Irvine, CA) at the other end. The positioner, with an accuracy of ±0.025 mm, enables the alignment of the optical fiber with the nanospray tip for the on-line irradiation and the adjustment of the fiber position. When the laser is off, the ESI-TOF records the mass spectrum from the original unirradiated sample, while with the laser on photoproducts or products from ensuing thermal reactions are identified by the mass spectrometry measurement. As showed in the inset of Figure 3, the distance D between the midpoint of the irradiated zone and the tip end can be varied by adjusting the position of the fiber. At a given inner diameter of the spray tip in the region with the length of D, and a constant sample flow rate, the thermal reaction time for photogenerated intermediates that have to travel to the tip end prior to spraying can be estimated. Intermediates in the system with lifetimes longer than the corresponding thermal reaction time and products formed from reactions of intermediates with substrate in the solution within the length of D can be detected and characterized by the mass spectrometer. Here the thermal reaction time corresponds to the minimum lifetime for a species to be detected by MS. The working range of D from 0.5 to 15 mm combined with the sample flow rate determines the lifetime scale within which the on-line experiments are conducted. The ESI interface also enables the performance of collision induced dissociation (CID) of the gas phase ions generated from the ESI process. Raising the skimmer 1 and / or nozzle potentials results in increasingly energetic collisions of neutral gas molecules in the relatively high pressure region in the ESI interface with the accelerated gas phase ions that are on their way to the

mass analyzer. Appropriate interface parameter settings facilitate detections both for intact ions from solution samples in normal ESI mode and for the fragments from the gas phase ions in CID mode.

CHAPTER 3

RESULTS

3.1 Exploratory studies of the ESI-MS technique

To establish an on-line mass spectrometry technique for investigating mechanisms of photoinduced polymerization reactions, the mixed sandwich complex, [CpFebz]PF_6, was employed as a model compound to verify the ESI-MS detection of intact ions in the unirradiated solution. Complications can arise from the oxidation of species at the electrospray tip and from fragmentation of electrosprayed ions by the well-known CID process. The TOF mass spectrum of a 20 μM solution of [CpFebz]PF_6 in acetonitrile, shown in Figure 4, was acquired under typical ESI nanospray conditions with spray tip potential, nozzle potential, and skimmer 1 potential at 1900 V, 120 V, and 12.2 V, respectively. The detection of the intact sample cation, $[CpFebz]^+$, at these settings can be confirmed by its monoisotopic peak at m/z = 199.0 and the isotopic pattern with peaks at 197.0, 198.0, 200.0, and 201.0 that arise from the contribution of isotopes of ^{54}Fe, ^{57}Fe, and ^{13}C. The effect of CID processes on the abundance of $[CpFebz]^+$ was explored in ESI control experiments. Figure 5 shows the mass spectra of a $[CpFebz]^+$ solution in acetonitrile with constant spray tip potential but varied nozzle and skimmer 1 potentials. As potentials increase to 250 V and 18 V for nozzle and skimmer 1, respectively, the clean background in Figure 5a acquires additional tiny fragment signals (see Figure 5b), though none of them is outstanding over the m/z range from 100 to 190. When the skimmer 1 potential is increased to 35 V while maintaining spray tip and nozzle potentials unchanged, the benzene-Fe bonds are broken in the collision between the gas phase $[CpFebz]^+$ ion and inert gas molecules in the interface region of the instrument,

Figure 4

ESI-TOF mass spectrum of 20 μM [CpFebz]PF_6 in acetonitrile. Inset: enlarged monoisotopic peak of $[CpFebz]^+$ at m/z = 199.0 and its isotopic peaks. Acquisition conditions: syringe pump flow rate, 10 μL/h; spray tip potential, 1900 V; nozzle potential, 120 V; skimmer 1 potential 12.2 V; nozzle temperature, 150^{o}C; quadrupole temperature, 150^{o}C.

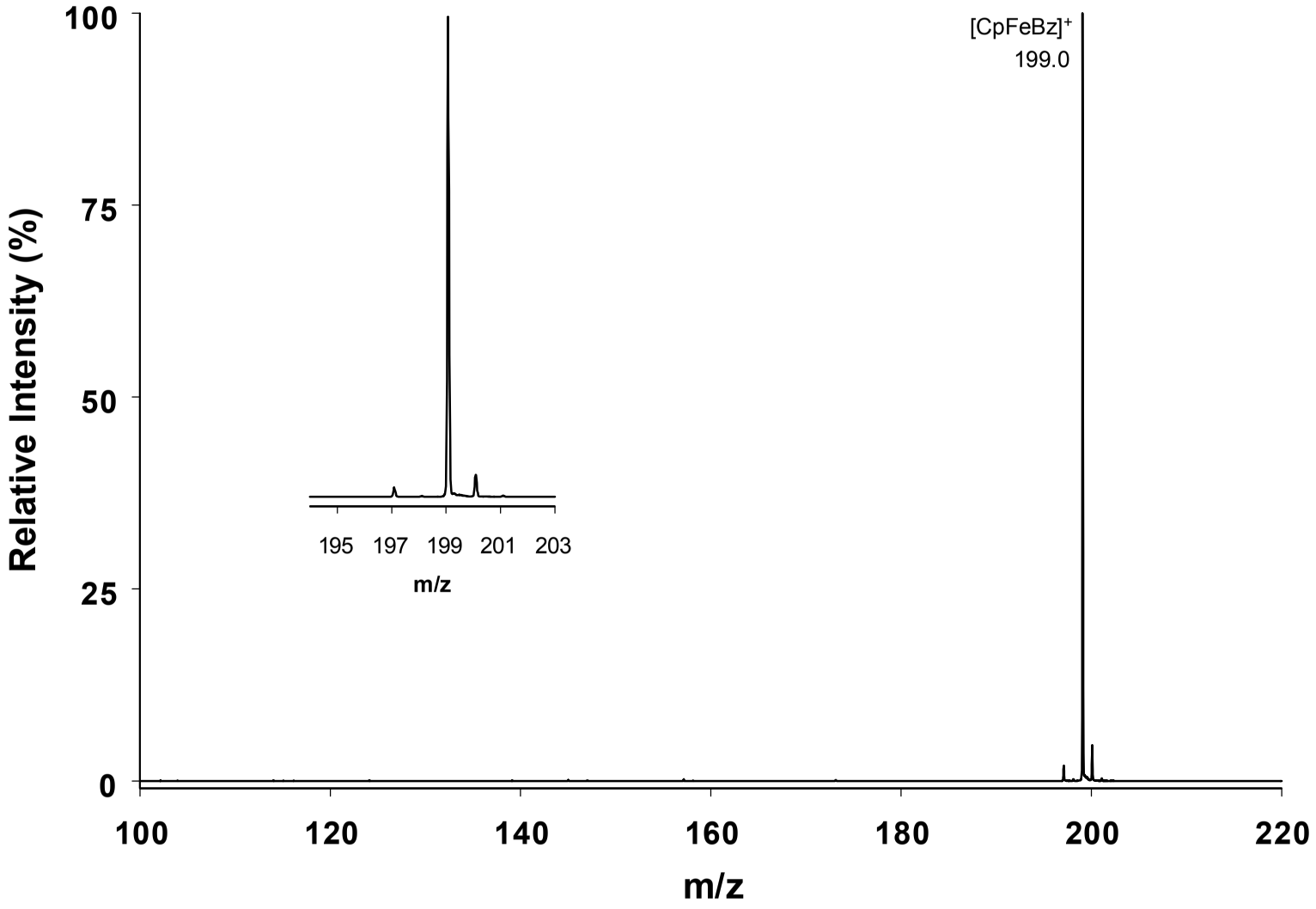
100
75
50
25
0
Relative Intensity (%)
[CpFeBz]+
199.0
195 197 199 201 203
m/z
100 120 140 160 180 200 220
m/z

Figure 5

ESI-TOF mass spectra of 20 μM [CpFebz]PF_6 in acetonitrile under different nozzle and skimmer 1 potential settings. (a) Spray tip = 1900 V, nozzle = 120 V, skimmer 1 = 12.2 V; (b) spray tip = 1900 V, nozzle = 250 V, skimmer 1 = 18 V; (c) spray tip = 1900 V, nozzle = 250 V, skimmer 1 = 35 V; (d) spray tip = 1900 V, nozzle = 260 V, skimmer 1 = 45 V.

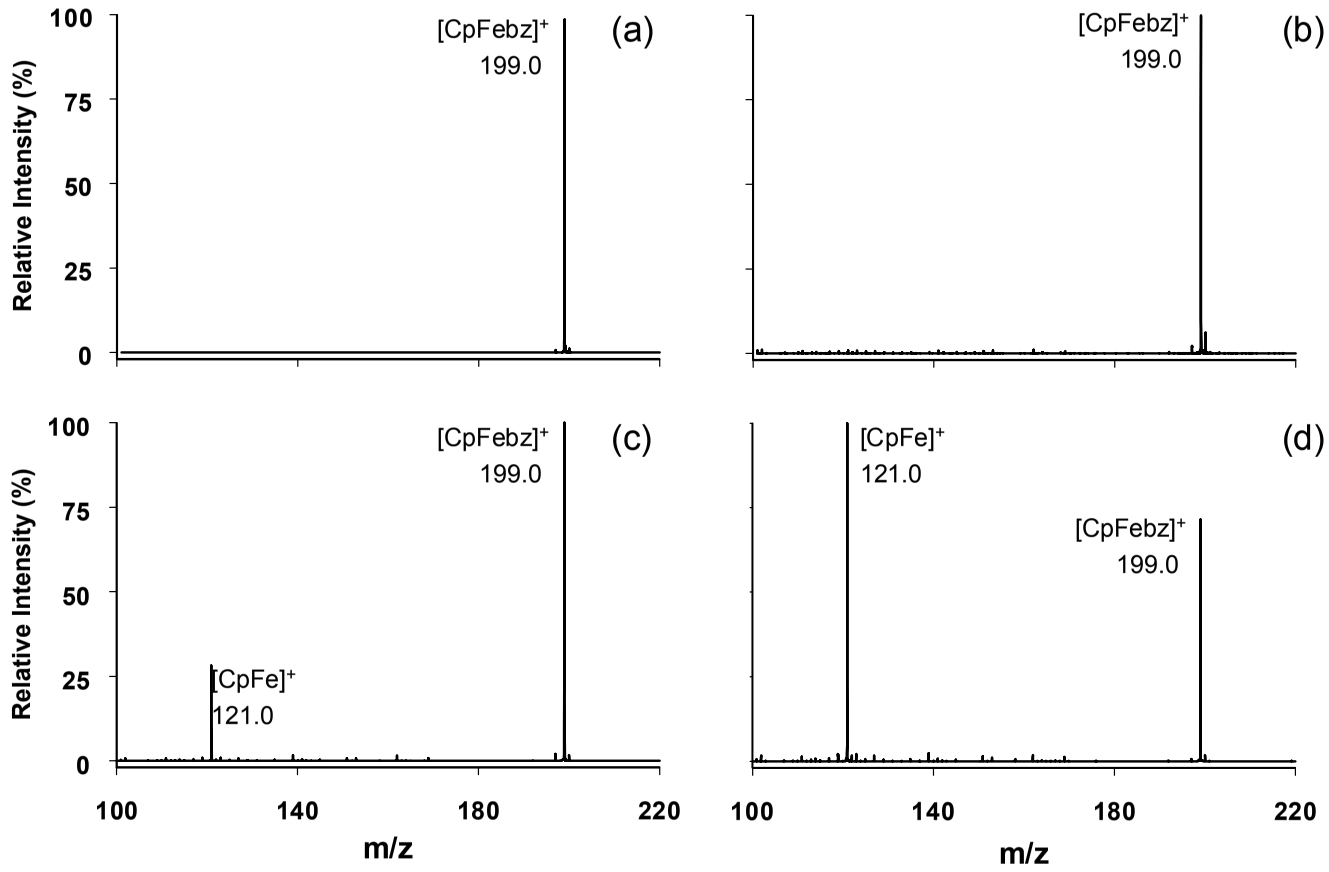
100
75
50
25
0
Relative Intensity (%)
[CpFebz]+
199.0
(a)
(b)
(c)
(d)
[CpFe]+
121.0
100
140
180
220
m/z

resulting in a $[CpFe]^+$ fragment ion with a relative intensity of 28% compared to its $[CpFebz]^+$ precursor (see Figure 5c). The further increase of both nozzle and skimmer 1 potentials to 260 V and 45 V, respectively, makes the fragment ion the prominent one in the spectrum as demonstrated in Figure 5d. Combined with other CID experiments, it turned out that the CID on $[CpFebz]^+$ can be triggered by increasing the two parameters but is more sensitive to skimmer 1 potential. Lowering both nozzle and skimmer 1 potentials from the typical nanospray ESI settings used to generate the spectrum shown in Figure 4 to 60 V and 11.5 V, respectively, also minimized fragmentation of the parent ion or other ions in the ESI-MS studies. ESI settings of 1900 V, 60 V, and 11.5 V for spray tip, nozzle, and skimmer 1 have been used throughout the photolyses and photoinduced polymerization experiments unless otherwise noted.

3.2 On-line photolysis of $[CpFebz]PF_6$ in acetonitrile

The electronic absorption spectrum of $[CpFebz]PF_6$ in acetonitrile, shown in Figure 6, exhibits two ligand field bands at 454 nm and 384 nm with fairly low molar absorptivities, reflecting the orbitally-forbidden nature of the transitions. Irradiation at 488 nm by an argon ion laser corresponds to the excitation of an electron in the a_1 (z^2) orbital to the empty e_1^* antibonding orbital, both of which are mostly metal in character. The expected products from the ligand field excitation of $[CpFebz]PF_6$ in acetonitrile (AN) at room temperature are ferrocene and $[Fe(AN)_6]^{2+}$ according to the mechanism shown in Scheme 4.[32,33] Figure 7

Figure 6

Room temperature electronic absorption spectrum of [CpFebz]PF_6 in acetonitrile

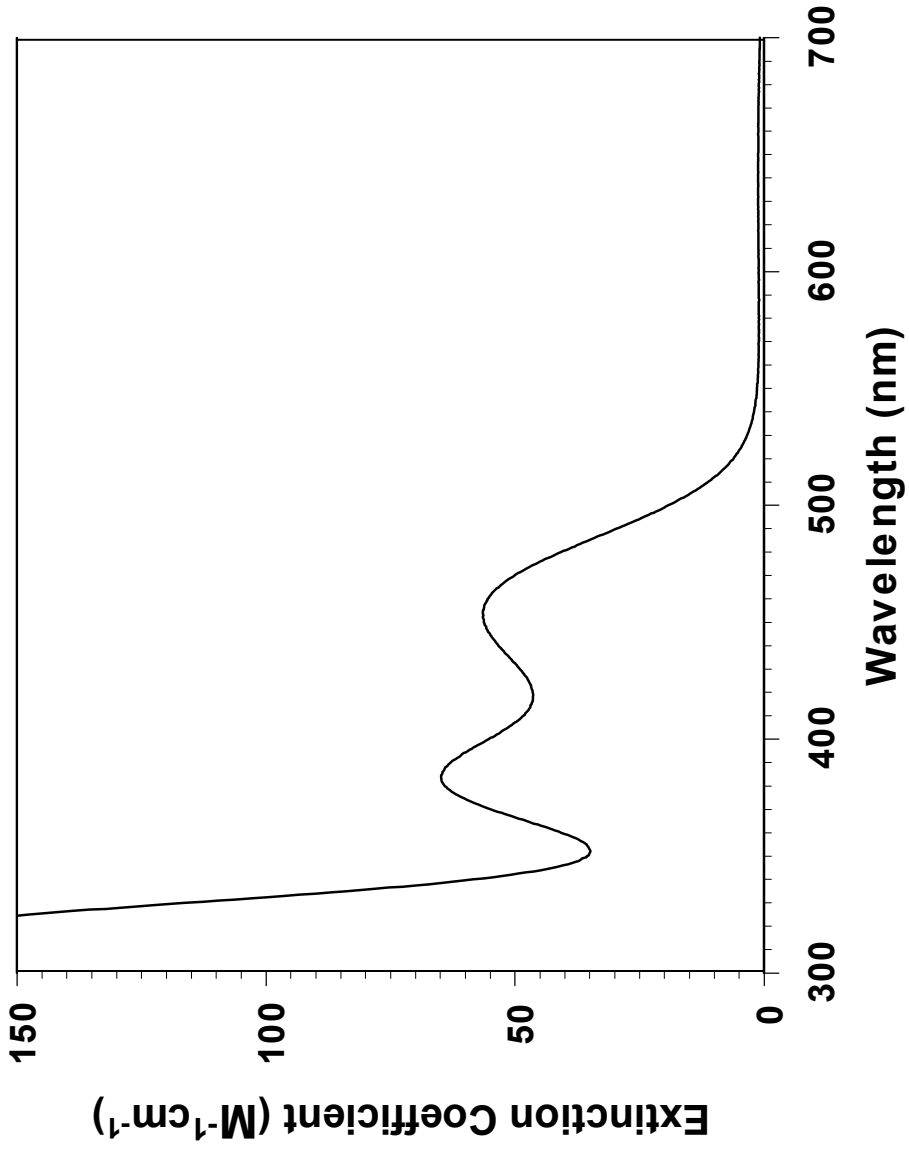
Extinction Coefficient (M-1cm-1)
150
100
50
0
300
400
500
600
700
Wavelength (nm)

Figure 7

A typical ESI-TOF mass spectrum of the photoproducts from the irradiation of a 70 μM [CpFebz]PF_6 solution in acetonitrile (AN) at 488 nm at room temperature. Acquisition conditions: spray tip potential, 1900 V; nozzle potential, 60 V; skimmer 1 potential, 11.5 V; flow rate, 40 μL/h; D, 2.0 mm. Inset: (I) blow-up of the product species, $[Fe(AN)_4]^{2+}$, at m/z = 110.0; (II) blow-up of the intermediate species, $[CpFe(AN)_2]^{+}$, at m/z = 203.0.

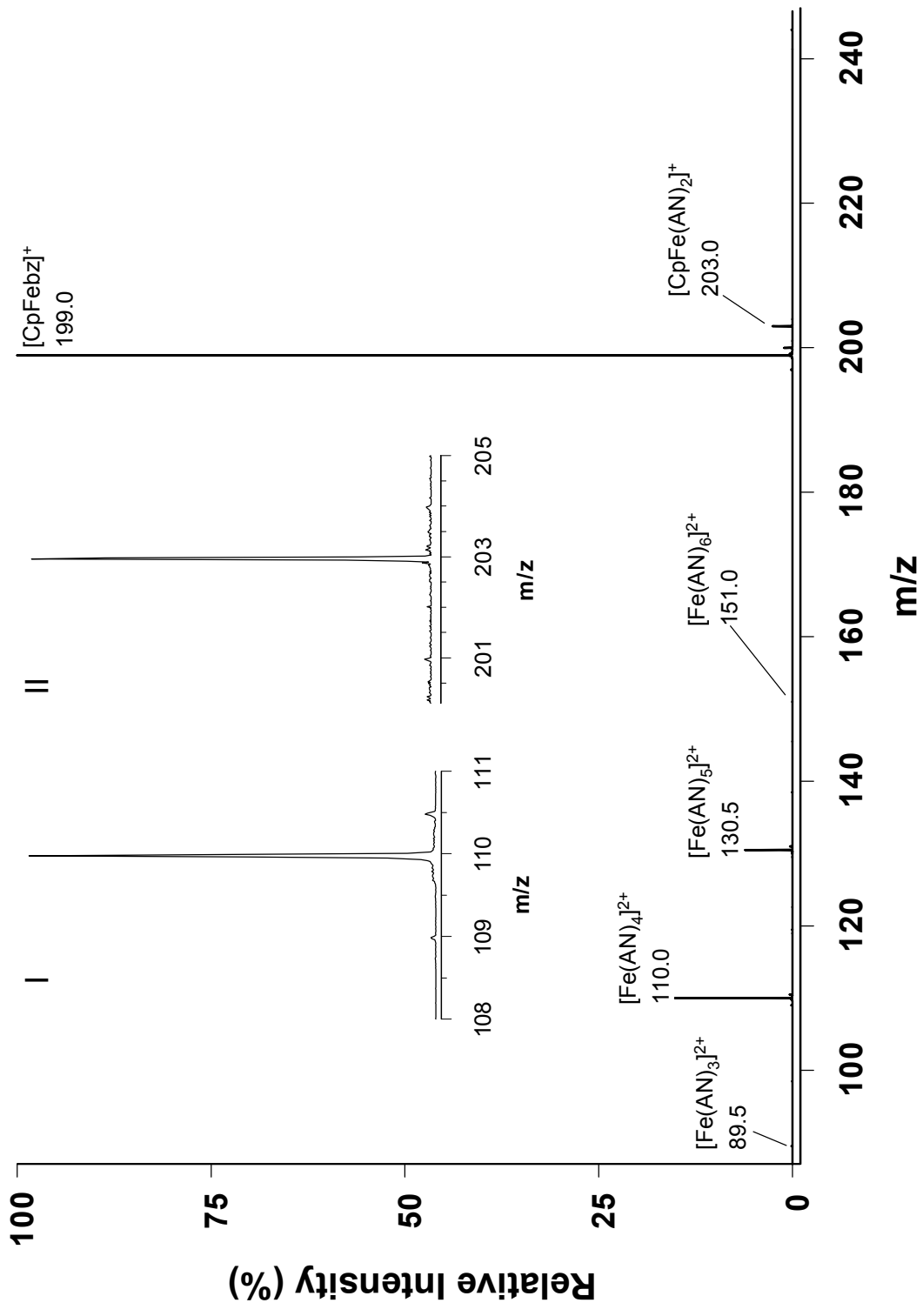
Relative Intensity (%)
100
75
50
25
0
100
120
140
160
180
200
220
240
m/z
[Fe(AN)3]2+
89.5
[Fe(AN)4]2+
110.0
[Fe(AN)5]2+
130.5
[Fe(AN)6]2+
151.0
[CpFe(AN)2]+
203.0
[CpFebz]+
199.0
I
II
108
109
110
111
m/z
201
203
205
m/z

shows the typical mass spectrum of the photolytes from the irradiation at 488 nm at the nanospray tip, which also functions as a micro flowing cell for the photochemical process. Along with product ions of $[Fe(AN)_{3-6}]^{2+}$, the half sandwich complex ion, $[CpFe(AN)_2]^+$, is also detected at m/z = 203.0. Recall the unstable nature of $[CpFe(AN)_3]^+$, which could only be characterized at -40^{o}C.[32,33] This short-lived intermediate from the on-line photochemical reaction survived traveling from the irradiation zone to the spray end, a distance D (refer to the inset of Figure 3), and was detected by the TOF mass spectrometer, because the traveling time is shorter than its lifetime in solution at room temperature. Thus, at a given tip inner diameter, value of D, and a constant volume sample flow rate, the secondary thermal reaction for the species generated in the primary photoreaction can be estimated. More generally, intermediates in the liquid phase with lifetimes longer than their corresponding thermal reaction time within the tip or products formed from these intermediates with substrates in the solution within the length D can ultimately be characterized by the mass spectrometer. It is worth noting that the time for the secondary thermal reaction, if there is any, corresponds to the minimum lifetimes for a primary photoproduct to be detected by the mass spectrometer. The working range of D, combined with practical sample flow rates for the nanospray at a known tip inner diameter, determine the lifetime range within which intermediates can be identified.

Figure 8 shows cross-section images of a working nanospray tip. An inner diameter of 14 μm at the tip end and the pulled portion was estimated from the internal standard of the 100 μm inner diameter of the original capillary that was

Figure 8

Photomicrographs of the nanospray tip. Upper-right: cross-section image of the original fused silica capillary from which nanospray tips were made. The outer diameter (o.d.) of 300 μm without coating was verified and its image size was used for calibration in the measurement of the tip end. Lower-left: cross-section image of the nanospray tip end.

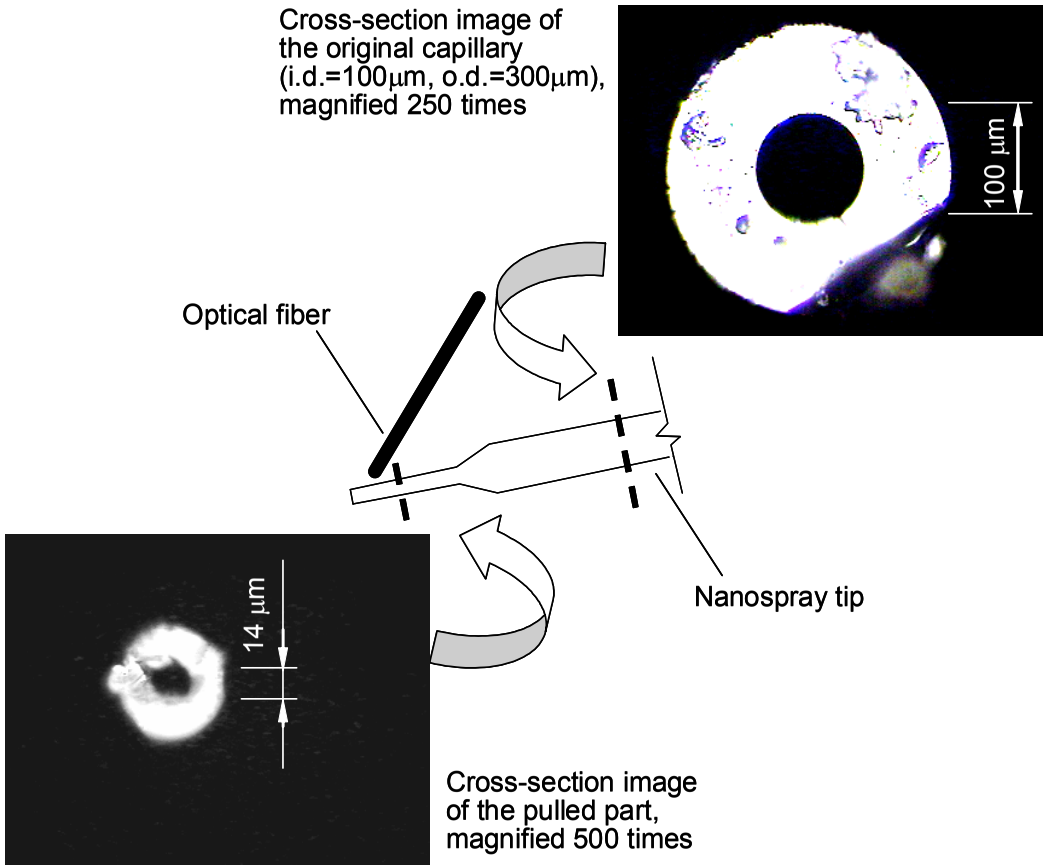
Cross-section image of the original capillary (i.d.=100μm, o.d.=300μm), magnified 250 times
100 μm
Optical fiber
Nanospray tip
14 μm
Cross-section image of the pulled part, magnified 500 times

confirmed from its image by using the 300 μm outer diameter of the fused silica capillary as a calibrating reference. Thermal reaction times of primary photoproducts in the nanospray tip with an inner diameter of 14 μm were calculated in conjunction with working sample flow rates and D values, and are reported in Table 4. Flow rates from 5 μL/h through 400 μL/h were tested in the present study, and flow rates in the shaded area in Table 4 were those used the most in the study, indicating a convenient time scale of 4 – 400 ms of lifetimes for intermediates to be determined with this on-line analysis strategy.

The nature of the intermediate $[CpFe(AN)_3]^+$ and its dependence on the thermal reaction time after its formation from the photoreaction were revealed from the photolysis experiments by setting the thermal reaction time, i.e., the traveling time through distance D in the nanospray tip, at two levels with appropriate combinations of flow rate and D values. Figure 9 shows the photoproducts probed by mass spectrometry when the thermal reaction time for intermediate $[CpFe(AN)_3]^+$ was varied from 17 ms (Figure 9a) to 50 ms (Figure 9b). At 17 ms, most species of the type $[CpFe(AN)_n]^+$ (n = 2,3) had not yet decomposed into $[Fe(AN)_m]^{2+}$ (m = 3,4,5) which shows minor intensity in the spectrum. However, half-sandwich species totally disappear after 50 ms, leaving behind only the dominant $[Fe(AN)_m]^{2+}$ family including the water substituted form, $[Fe(H_2O)(AN)_3]^{2+}$, at m/z = 98.5. Further investigation to establish the reaction mechanism at room temperature was conducted by systematically changing the distance D while keeping a constant flow rate, which sustains an identical irradiation time and flowing distribution within the micro flowing cell at each D

Table 4 Estimated thermal reaction times (milliseconds) of primary photoproduct in the nanospray tip under working sample flow rates and D values

Flow Rate (μL/h)	D (mm)											
	0.5	1	2	3	4	5	6	8	10	12	14	16
400	0.7	1.4	2.8	4.2	5.5	6.9	8.3	11	14	17	19	22
300	0.9	1.8	3.6	5.4	7.3	9.1	11	15	18	22	25	29
200	1.4	2.8	5.5	8.3	11	14	17	22	28	33	39	44
160	1.7	3.5	6.9	10	14	17	21	28	35	42	48	55
120	2.3	4.6	9.2	14	18	23	28	37	46	55	65	74
80	3.5	6.9	14	21	28	35	42	55	69	83	97	111
60	4.6	9.2	18	28	37	46	55	74	92	111	129	148
50	5.5	11	22	33	44	55	66	89	111	133	155	177
40	6.9	14	28	42	55	69	83	111	139	166	194	222
30	9.2	18	37	55	74	92	111	148	185	222	259	296
20	14	28	55	83	111	139	166	222	277	332	388	443
10	28	55	111	166	222	277	332	443	554	665	776	886
5	55	111	222	332	443	554	665	886	1108	1330	1551	1773

Figure 9

ESI-TOF mass spectra of the photoproducts from the photolysis of a 70 μM [CpFebz]PF_6 solution in acetonitrile (AN) at two thermal reaction times. (a) Flow rate, 40 μL/h; D, 1.2 mm; thermal reaction time for intermediate $[CpFe(AN)_3]^+$, 17 ms. (b) Flow rate, 80 μL/h; D, 7.2 mm; thermal reaction time for intermediate $[CpFe(AN)_3]^+$, 50 ms.

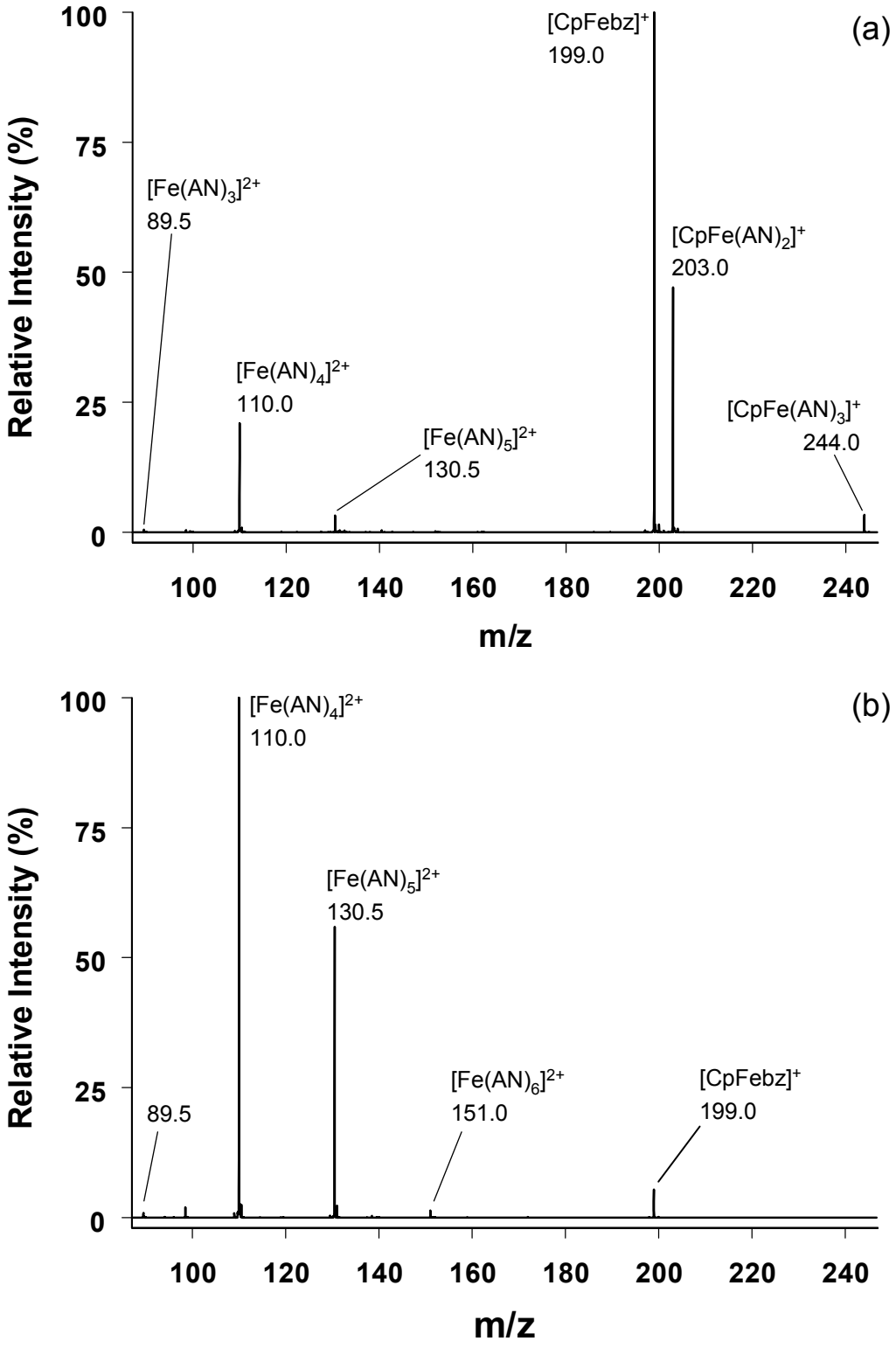
(a)
Relative Intensity (%)
100
75
50
25
0
[CpFebz]+
199.0
[Fe(AN)3]2+
89.5
[CpFe(AN)2]+
203.0
[Fe(AN)4]2+
110.0
[CpFe(AN)3]+
244.0
[Fe(AN)5]2+
130.5
100
120
140
160
180
200
220
240
m/z
(b)
Relative Intensity (%)
100
75
50
25
0
[Fe(AN)4]2+
110.0
[Fe(AN)5]2+
130.5
[Fe(AN)6]2+
151.0
[CpFebz]+
199.0
89.5
100
120
140
160
180
200
220
240
m/z

setting of the on-line characterization procedure. Figure 10 demonstrates the overall trend of product distribution for the two families, one generated from the primary photoreaction at the irradiation spot (about 0.6 mm) as an intermediate and the other from the subsequent secondary thermal decomposition of the intermediate in the solution system. As D is changed from 1.7 mm corresponding to 24 ms of thermal reaction time through 3.3 mm with 46 ms of thermal reaction time, more of the $[Fe(AN)_m]^{2+}$ family members appear at the expense of $[CpFe(AN)_n]^+$.

3.3 Photoinitiated polymerization study in acetonitrile

Photoexcitation of a photoinitiator in the presence of an appropriate monomer will bring about a photoinitiated polymerization reaction. In order to observe the initiation process and the first few steps in the propagation reaction, a $[CpFebz]PF_6$ solution in acetonitrile with monomer substrate, cyclohexene oxide (CHO), was subject to the on-line irradiation at 488 nm, and the subsequent products were probed by ESI-TOF mass spectrometry. At a ratio of 200 μM $[CpFebz]^+$ to 8 mM CHO, the photolysis in the nanospray tip yielded the same products as those from the pure initiator solution except for a strong and singlely charged species at m/z = 140.1 Da, as can be seen from Figure 11. Without irradiation, the presence of the monomer molecule in the initiator system did not alter the clean background in the mass spectrum, whereas the dominant species at m/z = 140.1 Da, designated as X^+, formed only upon the application of light. The isotopic pattern of the new product (see the inset of Figure 11) shows

Figure 10

Photolysis products from a 40 μM [CpFebz]PF_6 solution in acetonitrile (AN) recorded by ESI-TOF mass spectrometry at a flow rate of 20 μL/h and varied D values. (a) D = 1.7 mm; (b) D = 2.1 mm; (c) D = 2.5 mm; (d) D = 2.9 mm; (e) D = 3.3 mm.

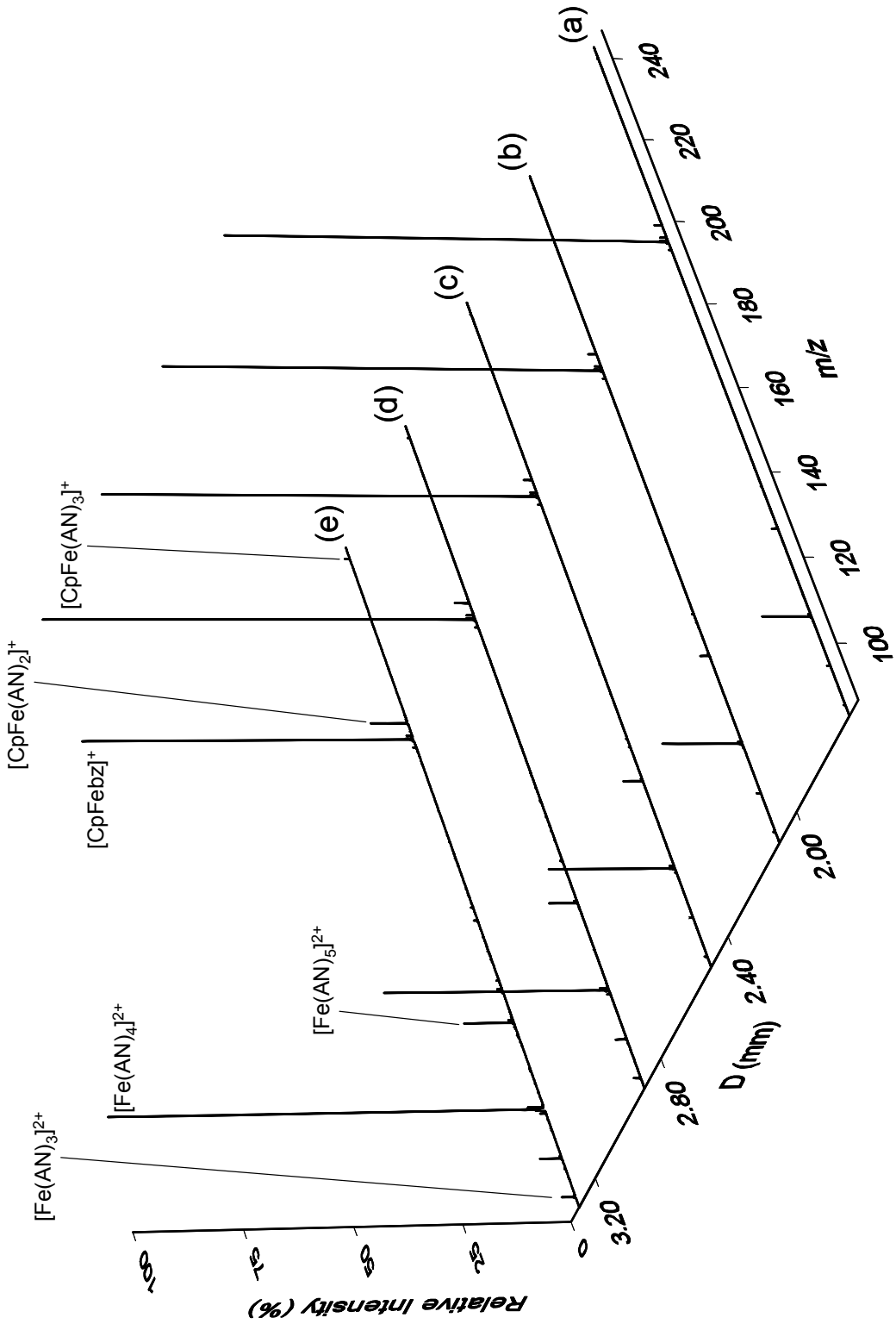
(a)
(b)
(c)
(d)
(e)
[Fe(AN)3]2+
[Fe(AN)4]2+
[Fe(AN)5]2+
[CpFebz]+
[CpFe(AN)2]+
[CpFe(AN)3]+
Relative Intensity (%)
0
20
40
60
80
100
3.20
2.80
2.40
2.00
D (mm)
100
120
140
160
180
200
220
240
m/z

Figure 11

ESI-TOF mass spectrum of products from the photolysis of 200 μM [CpFebz]PF_6 in acetonitrile with 8 mM cyclohexene oxide (CHO). The spectrum was acquired at a flow rate of 40 μL/h and D = 3.0 mm. Inset: the blow-up of the X^+ at m/z = 140.1 Da.

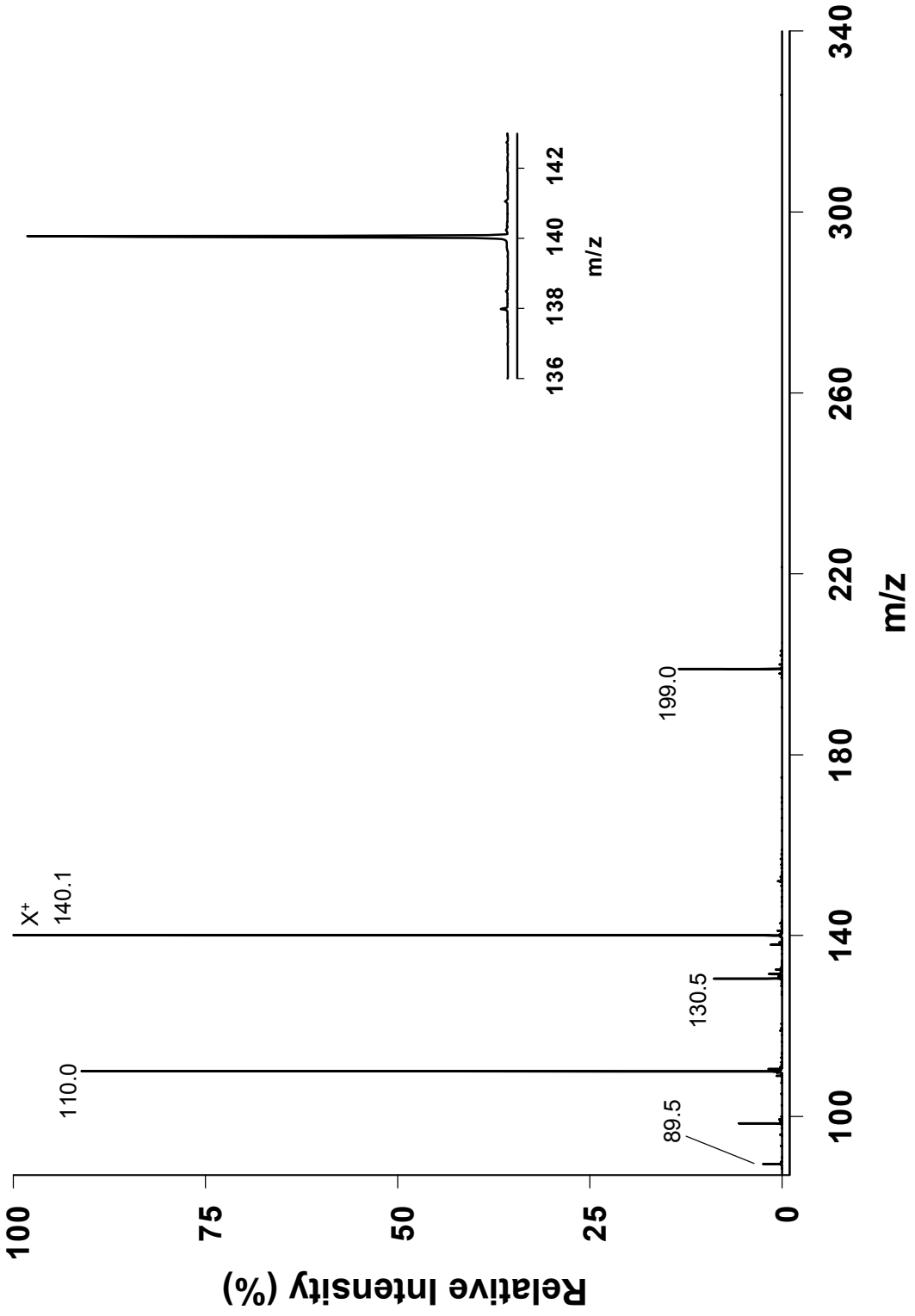
Relative Intensity (%)
100
75
50
25
0
100
140
180
220
260
300
340
m/z
X+
140.1
110.0
89.5
130.5
199.0
136
138
140
142
m/z

the monocation feature, and the peak at m/z = 138.1 Da seems to suggest the presence of iron in the species at first glance. A closer look enables the recognition of a tiny but distinguishable peak at m/z = 138.6 Da, suggesting that the peak at 138.1 arises from the monoisotopic species of a dication. Further study was focused on observing the behavior of X^+ or other potential initiating centers in a reaction system with higher monomer concentration. When 50 mM of CHO was added into an acetonitrile solution of 40μM $[CpFebz]^+$, new species at m/z = 238.2 Da showed up in the product spectrum (Figure 12a). External calibration with tetraethylammonium hexafluorophosphate (m/z = 130.1596 Da for $[N(Et)_4]^+$) and tetrabutylammonium hexafluorophosphate (m/z = 242.2848 Da for $[N(Bu)_4]^+$) assigns 140.11 Da and 238.17 Da to X^+ and the new species, respectively, with a measurement precision of ± 0.03 Da based on their spectral resolution levels. The mass difference of the two is 98.07 Da while the theoretical monoisotopic mass of CHO is 98.0732. The match on the mass difference is supportive of forming an $[X\text{-}CHO]^+$ species with m/z = 238.2 Da at higher CHO concentration. Further increasing the CHO concentration to 400 mM allows the detection of $[X(CHO)]^+$ in significant intensity in the mass spectrum of products, as well as the appearance of the species with probably the second CHO attachment in a mass/charge ratio of 336.2 for $[X(CHO)_2]^+$ (see Figure 12b). The high concentration of CHO and high ratio of CHO to photoinitiator, here 10,000 to 1 in the case of Figure 12b, promoted more involvement of CHO molecules in the reaction in the acetonitrile medium, but signals from iron-containing species including ferricenium at m/z = 186.0 showed relative minor intensities. Increasing

Figure 12

ESI-TOF mass spectra of products from the photolysis of 40 μM [CpFebz]PF_6 in acetonitrile with (a) 50 mM CHO and (b) 400 mM CHO. Inset in (a): the blow-up of the species at m/z = 238.2 Da.

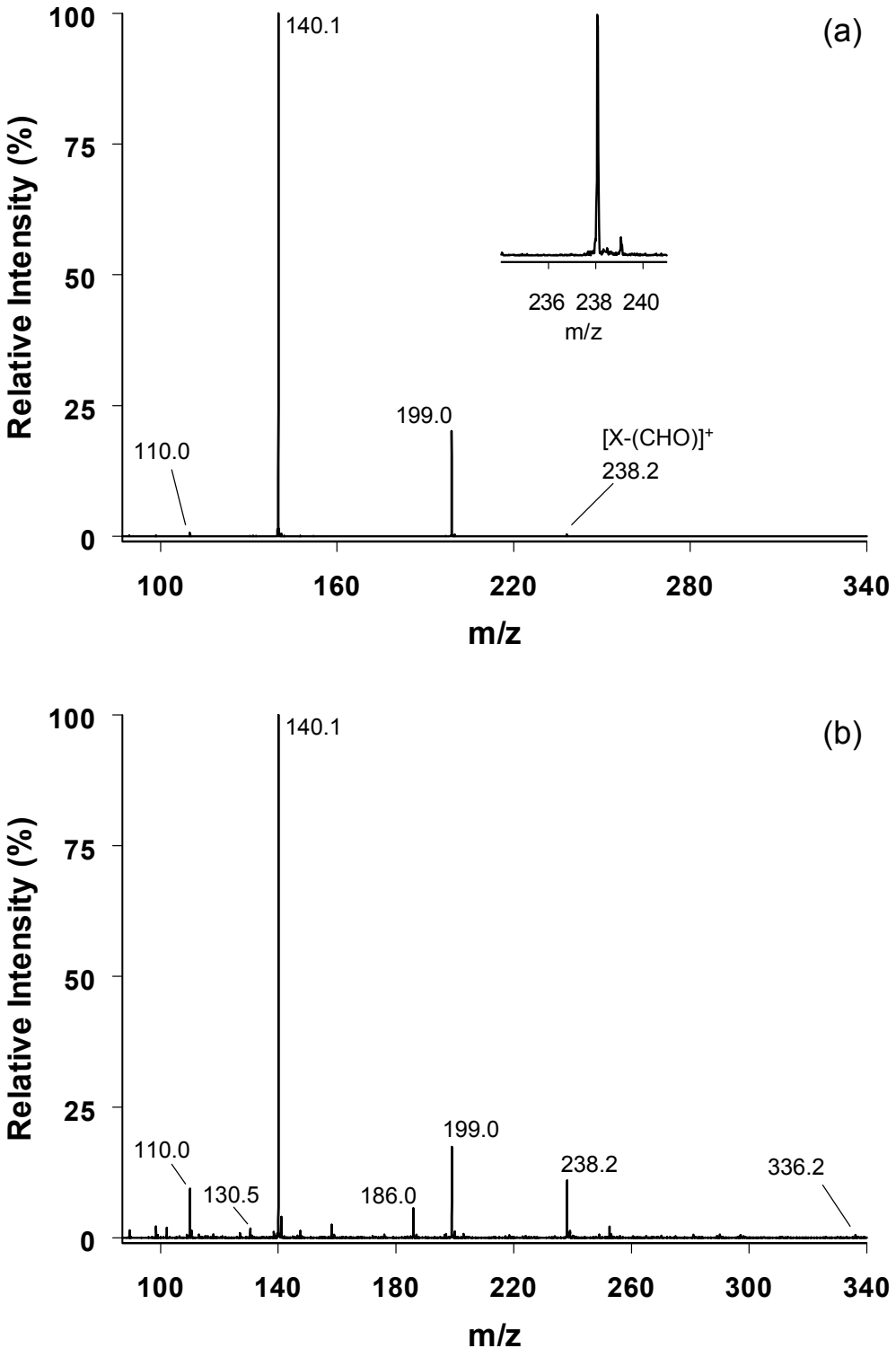
(a)
Relative Intensity (%)
100
75
50
25
0
140.1
199.0
110.0
[X-(CHO)]+
238.2
236 238 240
m/z
100
160
220
280
340
m/z
(b)
Relative Intensity (%)
100
75
50
25
0
140.1
110.0
130.5
186.0
199.0
238.2
336.2
100
140
180
220
260
300
340
m/z

the initiator concentration tenfold up to 400 μM, while maintaining the CHO concentration at 400 mM, provided more information on the chemistry as shown in Figure 13. Firstly, the intensities of $[Fe(AN)_m]^{2+}$ series were enhanced. Secondly, the $[X(CHO)_2]^+$ could be confirmed by its outstanding peak (m/z = 336.2 Da) with a mass difference of 98.07 Da from that of $[X(CHO)]^+$ owing to one more CHO attachment. Lastly, iron(II) complex ions containing CHO ligand in addition to solvent molecules were detected as $[Fe(AN)_2(CHO)]^{2+}$, $[Fe(AN)_3(CHO)]^{2+}$, and $[Fe(AN)_4(CHO)]^{2+}$.

3.4 Photoinitiated polymerization study in 1,2-dichloroethane

Irradiating $[CpFebz]PF_6$ and CHO in the poorly-coordinating solvent, 1,2-dichloroethane (DCE), yielded a rich array of photoproducts. The electronic spectrum of $[CpFebz]PF_6$ in DCE, shown in Figure 14, revealed two bands in the visible region at 455 nm and 384 nm with extinction coefficients of 73 ($M^{-1}cm^{-1}$) and 62 ($M^{-1}cm^{-1}$), respectively. The very similar features shown by the photoinitiator in DCE and acetonitrile (Figure 6) suggest that the same excited state is populated in both solvents upon irradiation at 488 nm. The photoexcitation of a solution of 32 μM $[CpFebz]PF_6$ with 40 mM CHO in freshly and rigorously dried DCE yielded the X-CHO series, as seen in acetonitrile solutions, but with up to three CHO attached to the X^+ (Figure 15). Also in the spectrum are two new species at mass/charge ratios of 282.1 and 331.2 Da with relatively low intensities. They can be assigned tentatively as $[Fe(H_2O)(CHO)_5]^{2+}$ and $[Fe(H_2O)(CHO)_6]^{2+}$ based on their charge status and masses but need to be

Figure 13

ESI-TOF mass spectrum of products from the photolysis of 400 μM $[CpFebz]PF_6$ in acetonitrile with 400 mM CHO at a flow rate of 10 μL/h and D = 2 mm. Insets I, II, and II are the blow-ups for $[Fe(AN)_3(CHO)]^{2+}$, $[Fe(AN)_4(CHO)]^{2+}$, and $[X(CHO)_2]^{+}$, respectively.

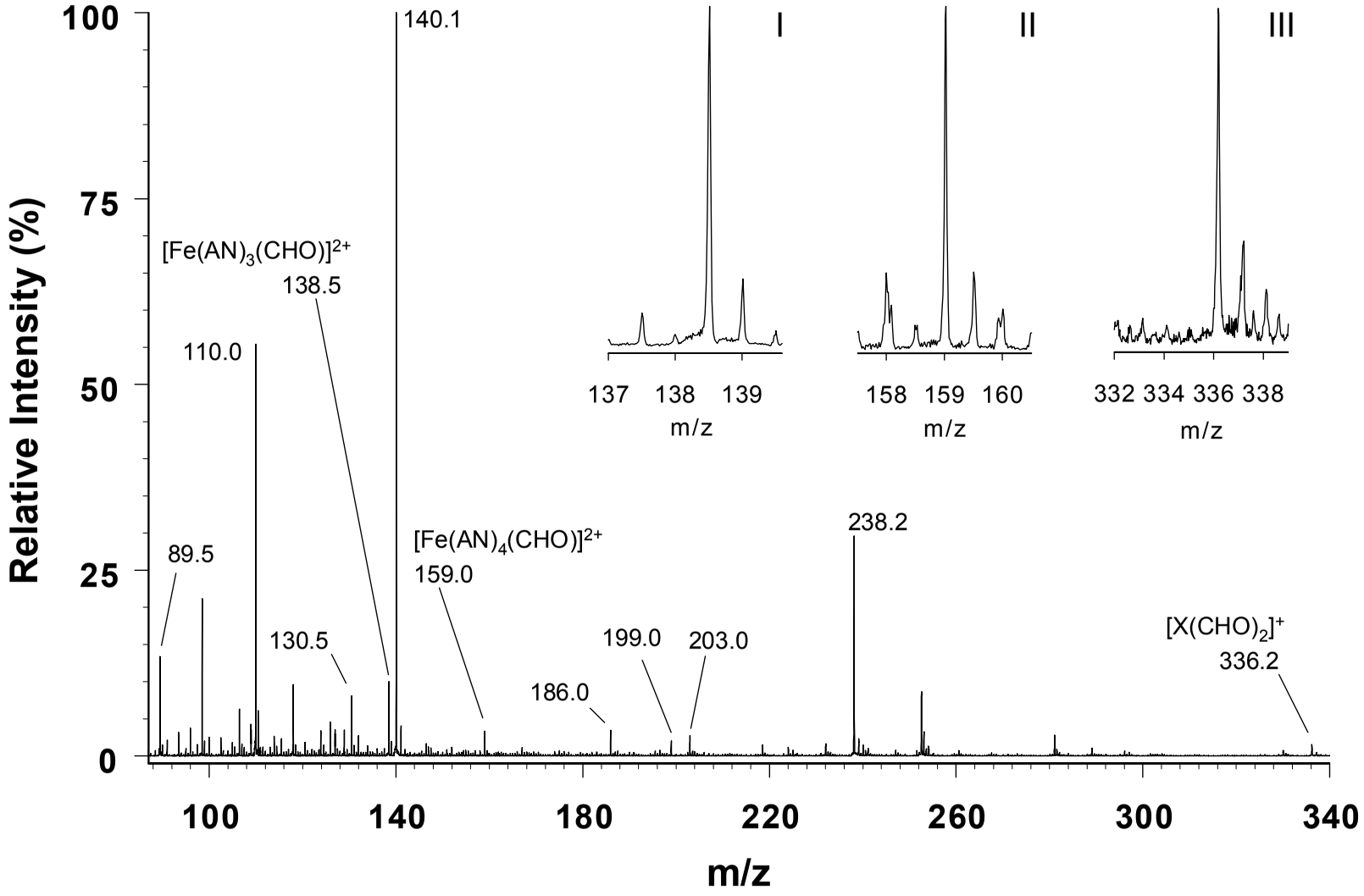
Relative Intensity (%)
100
75
50
25
0
100
140
180
220
260
300
340
m/z
140.1
[Fe(AN)3(CHO)]2+
138.5
110.0
89.5
130.5
[Fe(AN)4(CHO)]2+
159.0
186.0
199.0
203.0
238.2
[X(CHO)2]+
336.2
I
II
III
137 138 139
m/z
158 159 160
m/z
332 334 336 338
m/z

Figure 14

Room temperature electronic absorption spectrum of [CpFebz]PF_6 in 1,2-dichloroethane.

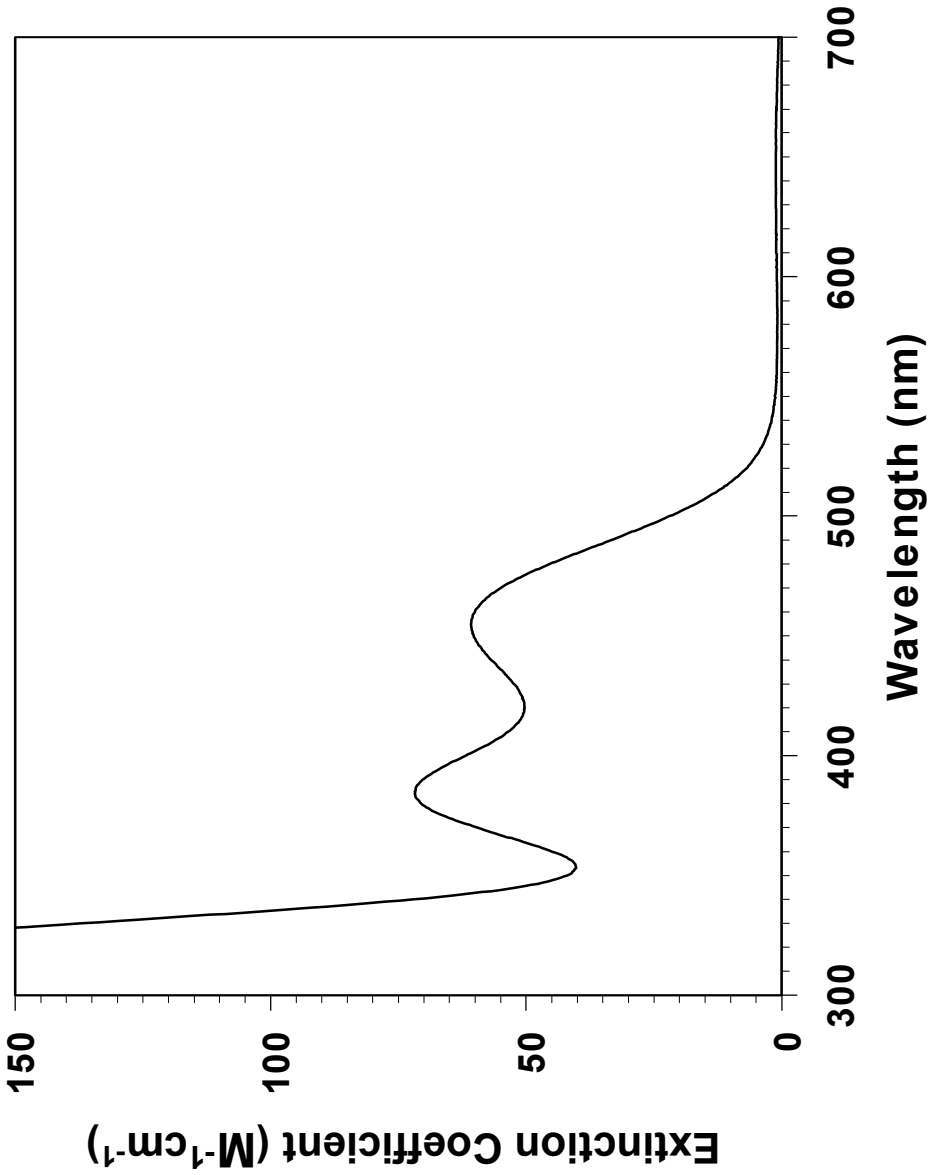
Extinction Coefficient (M-1cm-1)
150
100
50
0
300
400
500
600
700
Wavelength (nm)

Figure 15

ESI-TOF mass spectrum of photolysis products from a 32 μM $[CpFebz]PF_6$ solution with 40 mM CHO in 1,2-dichloroethane. The spectrum was acquired at a sampling flow rate of 20 μL/h when irradiated at 488 nm with D = 10.4 mm. Insets I through IV are enlarged peaks for $[X(CHO)]^+$, $[X(CHO)_2]^+$, $[X(CHO)_3]^+$, and $[Fe(H_2O)(CHO)_6]^{2+}$ with identical magnification.

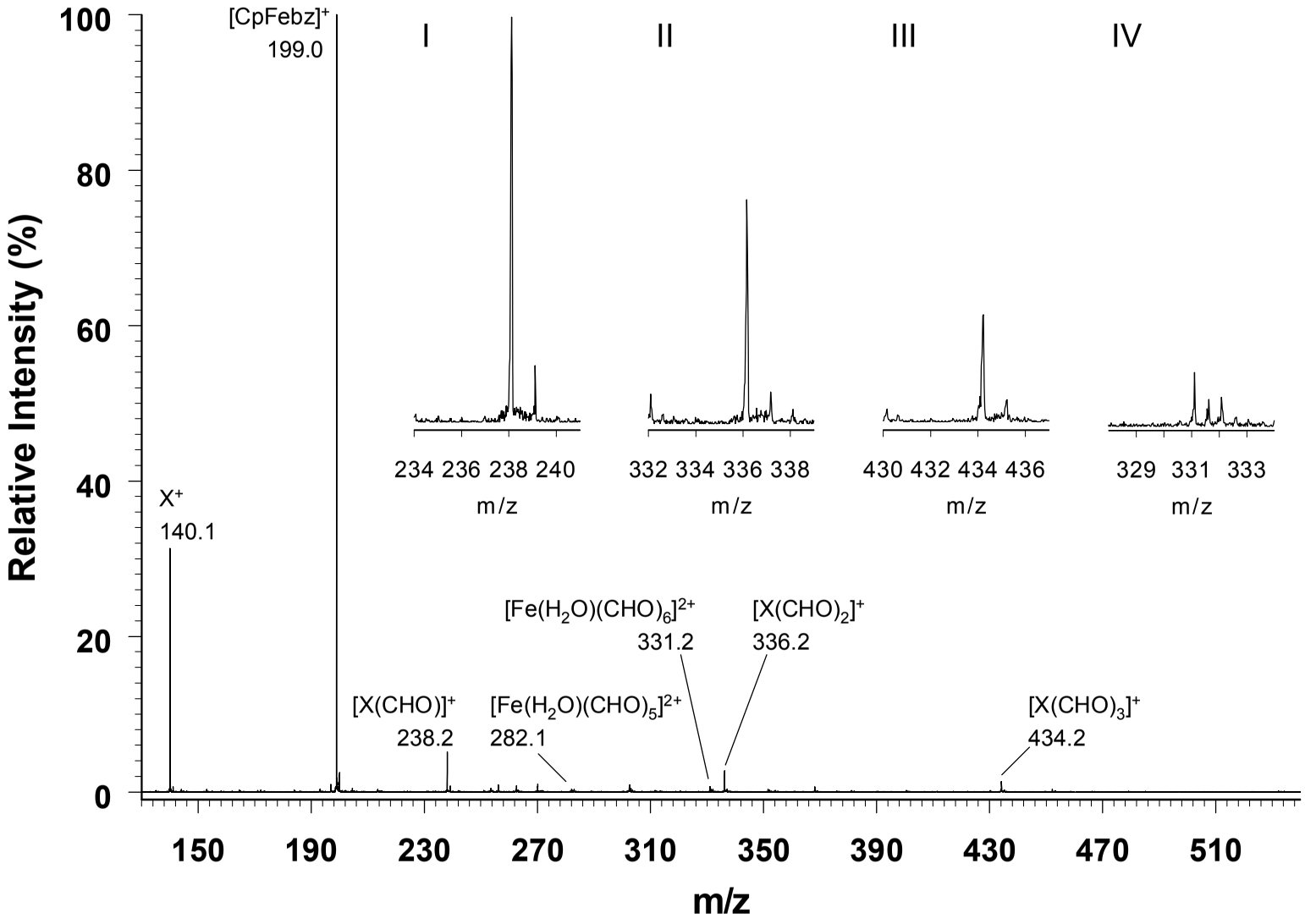
100
80
60
40
20
0
Relative Intensity (%)
[CpFebz]+
199.0
X+
140.1
[X(CHO)]+
238.2
[Fe(H2O)(CHO)5]2+
282.1
[Fe(H2O)(CHO)6]2+
331.2
[X(CHO)2]+
336.2
[X(CHO)3]+
434.2
150
190
230
270
310
350
390
430
470
510
m/z
I
II
III
IV
234 236 238 240
m/z
332 334 336 338
m/z
430 432 434 436
m/z
329 331 333
m/z

further confirmed. When the DCE solvent was not highly anhydrous, for instance stored in a flask for a few days, a mixture of two major product series was detected (see Figure 16). In addition to the $[X(CHO)_q]^+$ (q = 1 - 3) series, the iron-containing species with a general formula $[Fe(H_2O)(CHO)_m]^{2+}$ (m = 4 - 15) appeared as the major photoproducts. In remarkable contrast to the $[Fe(AN)_{2-4}(CHO)]^{2+}$ series detected in acetonitrile at high concentrations of [CpFebz]PF_6 (400 μM) and CHO (400 mM) in the experiment shown in Figure 13, the modest concentration of both photoinitiator (40 μM) and monomer (40 mM) in the DCE solvent yielded products with not only more than one CHO molecule associated with the metal, but also with the total number of attached potential ligands far beyond six and in a consecutive manner. Photolysis in DCE also results in up to four CHO molecules bond to X^+, in contrast to the single CHO bond to X^+ in an acetonitrile solution with the same levels of initiator and monomer concentrations, as illustrated in Figure 12a. Minor series in the spectrum are identified as $[Fe(CHO)_{5-8}]^{2+}$, $[Fe(H_2O)_2(CHO)_{3-6}]^{2+}$, and $[(H_3O)(CHO)_{2-5}]^+$. The first two along with the major series of $[Fe(H_2O)(CHO)_{4-15}]^{2+}$ products reflect the competition for binding sites on the Fe(II) center between CHO and the trace amount of water. The H_3O^+-containing series suggest the possibility of proton initiation with $[CpFe(\eta^6\text{-arene})]^+$ type photoinitiators that had been ruled out in literature.[27] Interestingly, the ferricenium ion, presumably from the oxidation of the ferrocene formed from the thermal decomposition of half-sandwich species (see Scheme 4), yielded a more prominent peak in the spectrum.

Figure 16

ESI-TOF mass spectrum of photolysis products from a 40 μM [CpFebz]PF_6 and 40 mM CHO solution in slightly moist 1,2-dichloroethane. The spectrum was acquired at a sampling flow rate of 20 μL/h when irradiated at 488 nm with D = 6 mm.

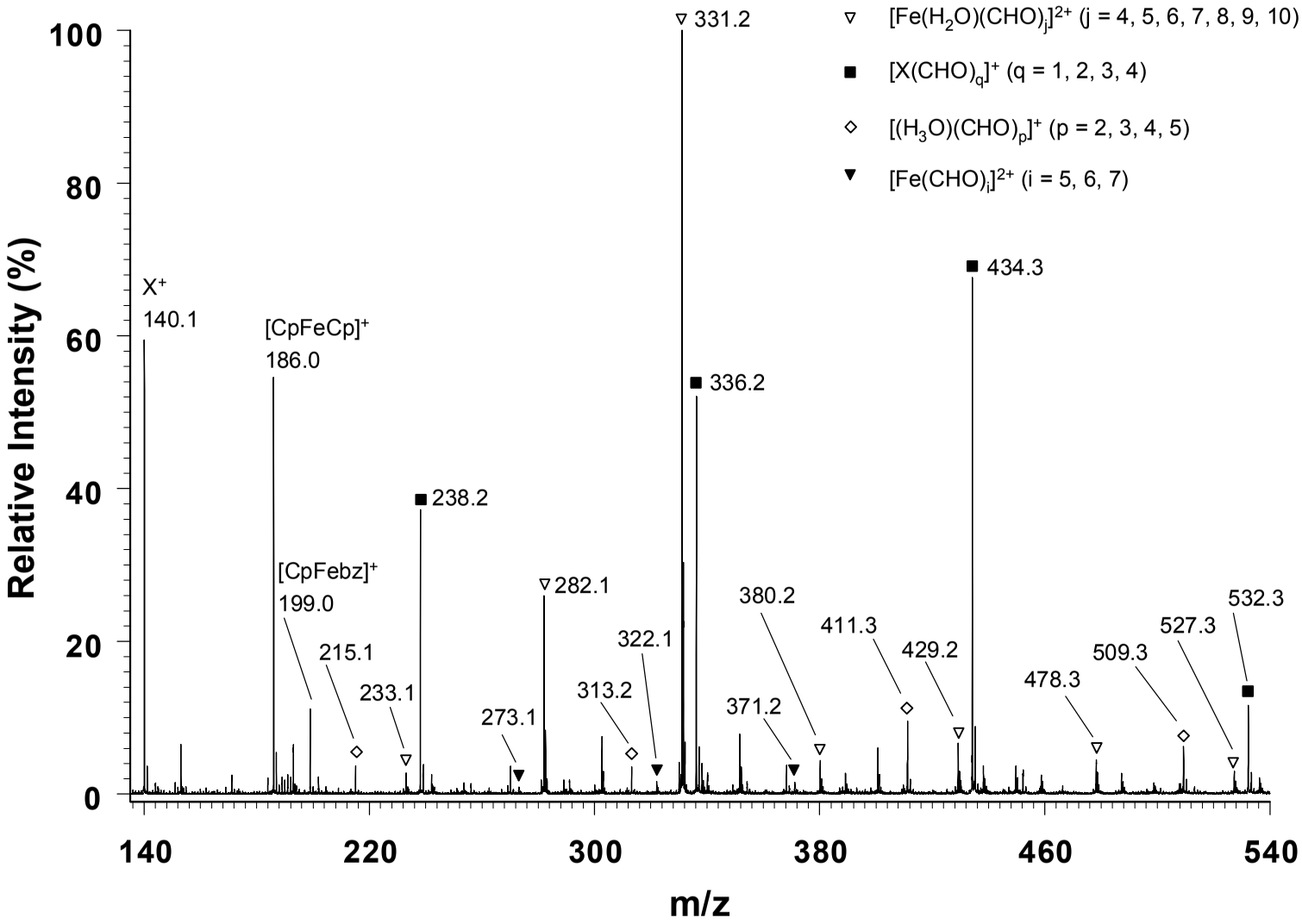
Relative Intensity (%)
m/z
100
80
60
40
20
0
140
220
300
380
460
540
X+
140.1
[CpFeCp]+
186.0
[CpFebz]+
199.0
215.1
233.1
238.2
273.1
282.1
313.2
322.1
331.2
336.2
371.2
380.2
411.3
429.2
434.3
478.3
509.3
527.3
532.3
[Fe(H2O)(CHO)j]2+ (j = 4, 5, 6, 7, 8, 9, 10)
[X(CHO)q]+ (q = 1, 2, 3, 4)
[(H3O)(CHO)p]+ (p = 2, 3, 4, 5)
[Fe(CHO)i]2+ (i = 5, 6, 7)

These results suggest that several products result from the photolysis of mixed sandwich iron(II) complexes in solution. The product ratio is sensitive to the trace amount of water that either exists in the DCE solvent or is introduced to the rigorously dried solvent during sample preparation. Figure 17 demonstrates the effects of trace moisture on the types of epoxide oligomers when the 40 μM $[CpFebz]^+$ and 40 mM CHO solution in rigorously dried DCE solvent was prepared in a glove bag instead of using the glove box as usual. Compared with that in Figure 15, species of the type $[Fe(H_2O)(CHO)_{4\text{-}15}]^{2+}$ are now the dominant products. In addition, peaks corresponding to $[X(CHO)_{1\text{-}2}]^+$ diminish in relative intensity and X^+ at m/z = 140.1 disappears completely. Interestingly, the relative abundance of ferricenium, m/z = 186.0, appears to correlate with the water content of the solvent. That is, more of this oxidized iron species is generated as the solvent becomes wetter.

3.5 Investigation of intermediates in the photoinitiated polymerization reaction

On-line irradiation of $[CpFebz]^+$ in DCE containing CHO at a thermal reaction time scale of 5 ms revealed the predominance of the half-sandwich series of the form $[CpFe(H_2O)(CHO)_{0\text{-}4}]^+$ as shown in Figure 18. Accompanying these new species were $[Fe(H_2O)(CHO)_{4\text{-}10}]^{2+}$ and $[X(CHO)_{0\text{-}4}]^+$ series that were the prevalent ones when the thermal reaction times were greater than 170 ms (see Figure 16 and 17). Presented in the same mass spectrum are the distinguishable, though minor in terms of relative intensities, $[CpFe(CHO)_m]^+$,

Figure 17

ESI-TOF mass spectrum of photolysis products from a DCE solution containing 40 μM [CpFebz]PF_6 and 40 mM CHO. Sample preparation was performed in a glove box with rigorously dried DCE and the spectrum was acquired at a sampling flow rate of 20 μL/h when irradiated at 488 nm with D = 8 mm.

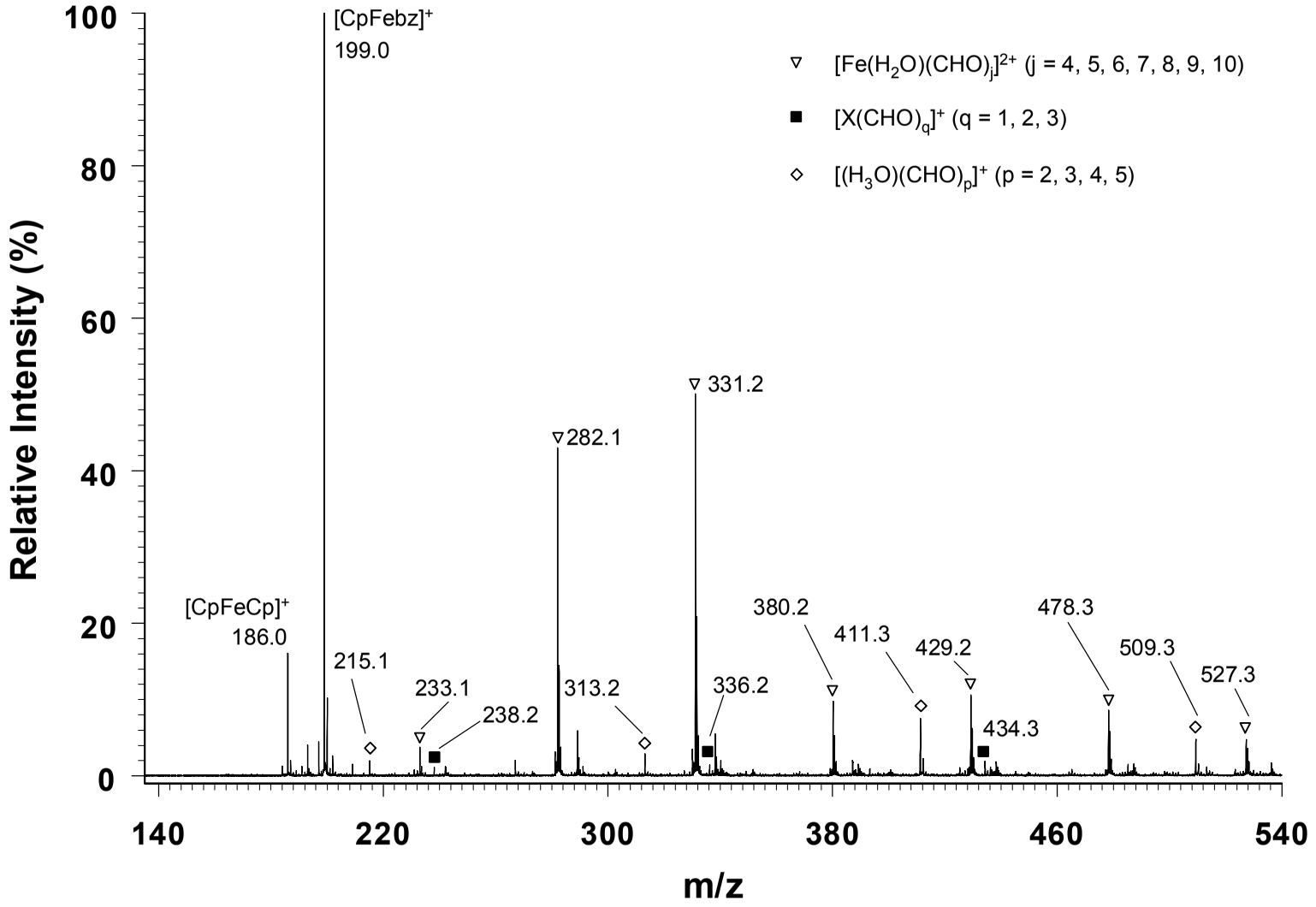
100
80
60
40
20
0
Relative Intensity (%)
140
220
300
380
460
540
m/z
[CpFebz]+
199.0
[CpFeCp]+
186.0
215.1
233.1
238.2
282.1
313.2
331.2
336.2
380.2
411.3
429.2
434.3
478.3
509.3
527.3
▽ [Fe(H2O)(CHO)j]2+ (j = 4, 5, 6, 7, 8, 9, 10)
■ [X(CHO)q]+ (q = 1, 2, 3)
◇ [(H3O)(CHO)p]+ (p = 2, 3, 4, 5)

Figure 18

ESI-TOF mass spectrum of photolysis products from a DCE solution containing 100 μM [CpFebz]PF_6 and 40 mM CHO at a thermal reaction time of 5 ms in the tip. The spectrum was acquired at a sampling flow rate of 60 μL/h when irradiated at 488 nm with D = 0.55 mm.

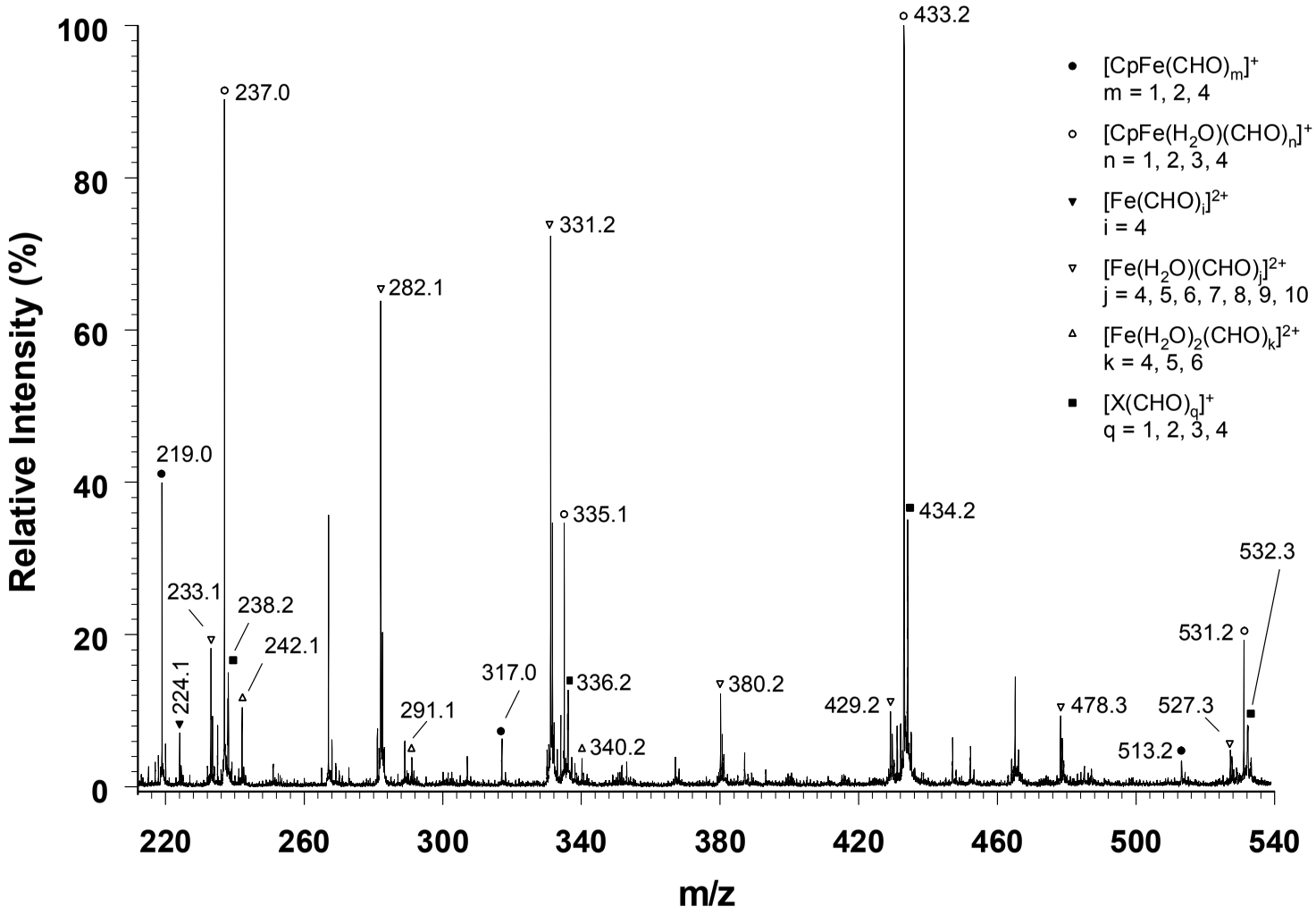
Relative Intensity (%)
100
80
60
40
20
0
220
260
300
340
380
420
460
500
540
m/z
433.2
237.0
331.2
282.1
219.0
335.1
434.2
532.3
233.1
238.2
242.1
531.2
224.1
317.0
336.2
380.2
291.1
429.2
478.3
527.3
340.2
513.2
[CpFe(CHO)m]+
m = 1, 2, 4
[CpFe(H2O)(CHO)n]+
n = 1, 2, 3, 4
[Fe(CHO)i]2+
i = 4
[Fe(H2O)(CHO)j]2+
j = 4, 5, 6, 7, 8, 9, 10
[Fe(H2O)2(CHO)k]2+
k = 4, 5, 6
[X(CHO)q]+
q = 1, 2, 3, 4

$[Fe(CHO)_4]^{2+}$, and $[Fe(H_2O)_2(CHO)_k]^{2+}$ species. The low signal intensity of the non-water product families, $[CpFe(CHO)_m]^+$ and $[Fe(CHO)_4]^{2+}$, suggested the stabilizing role of water towards the formation of half-sandwich and the fully ring-deligated Fe(II) complexes, though species with more than one water molecule, like $[Fe(H_2O)_2(CHO)_{4-6}]^{2+}$, are not favored.

In order to verify the intermediate characteristics of the half-sandwich species, the dependence of their intensity on the thermal reaction times after irradiation was investigated. Figure 19 specifically compares the relative intensities of $[CpFe(H_2O)]^+$ and its two neighboring products, $[Fe(H_2O)(CHO)_2]^{2+}$ and $[X]^+$ as the value of D is changed. The species presented in this figure are the representative half-sandwich and fully ring-deligated Fe(II) complex ions and the iron-free species $[X]^+$. As the D value, i.e., thermal reaction time for intermediate, increases, the disappearance of the parent species $[CpFe(H_2O)]^+$ and the growth of offspring series $[Fe(H_2O)(CHO)_2]^{2+}$ and $[X]^+$ can be visualized. The same trends can be seen from Figure 20 and Figure 21 when more CHO molecules are introduced. In Figure 22, the consecutive addition of CHO molecules has not stopped, while the disappearance of the half-sandwich series still accompanies the growth of the $[Fe(H_2O)(CHO)_j]^{2+}$ and $[X(CHO)_q]^+$ in each of the comparison groups.

3.6 Identity study of species X^+

The identity of the photogenerated species X^+, a monocation with a mass to charge ratio of 140.11±0.03 Da, was studied by using the photoinitiators that

Figure 19

Comparison of relative peak intensities in the mass spectra of $[CpFe(H_2O)]^+$, $[Fe(H_2O)(CHO)_2)]^{2+}$, and X^+ at varied D values. The spectra were acquired with an irradiated DCE solution containing 100 μM $[CpFebz]PF_6$ and 40 mM CHO at a sampling flow rate of 60 μL/h and D = 0.55, 0.88, 1.21, 1.54, 1.87 mm. Laser wavelength was 488nm.


■ X+
[CpFe(H2O)]+
[Fe(H2O)(CHO)2]2+
Relative Intensity (%)
0
25
50
75
100
D (mm)
0.66
0.99
1.32
1.65
m/z
133
134
135
136
137
138
139
140
141
142

Figure 20

Comparison of relative peak intensities in the mass spectra of $[CpFe(H_2O)(CHO)]^+$, $[Fe(H_2O)(CHO)_4)]^{2+}$, and $[X(CHO)]^+$ at varied D values. The spectra were acquired with an irradiated DCE solution containing 100 μM $[CpFebz]PF_6$ and 40 mM CHO at a sampling flow rate of 60 μL/h and D = 0.55, 0.88, 1.21, 1.54, 1.87 mm. Laser wavelength was 488nm.

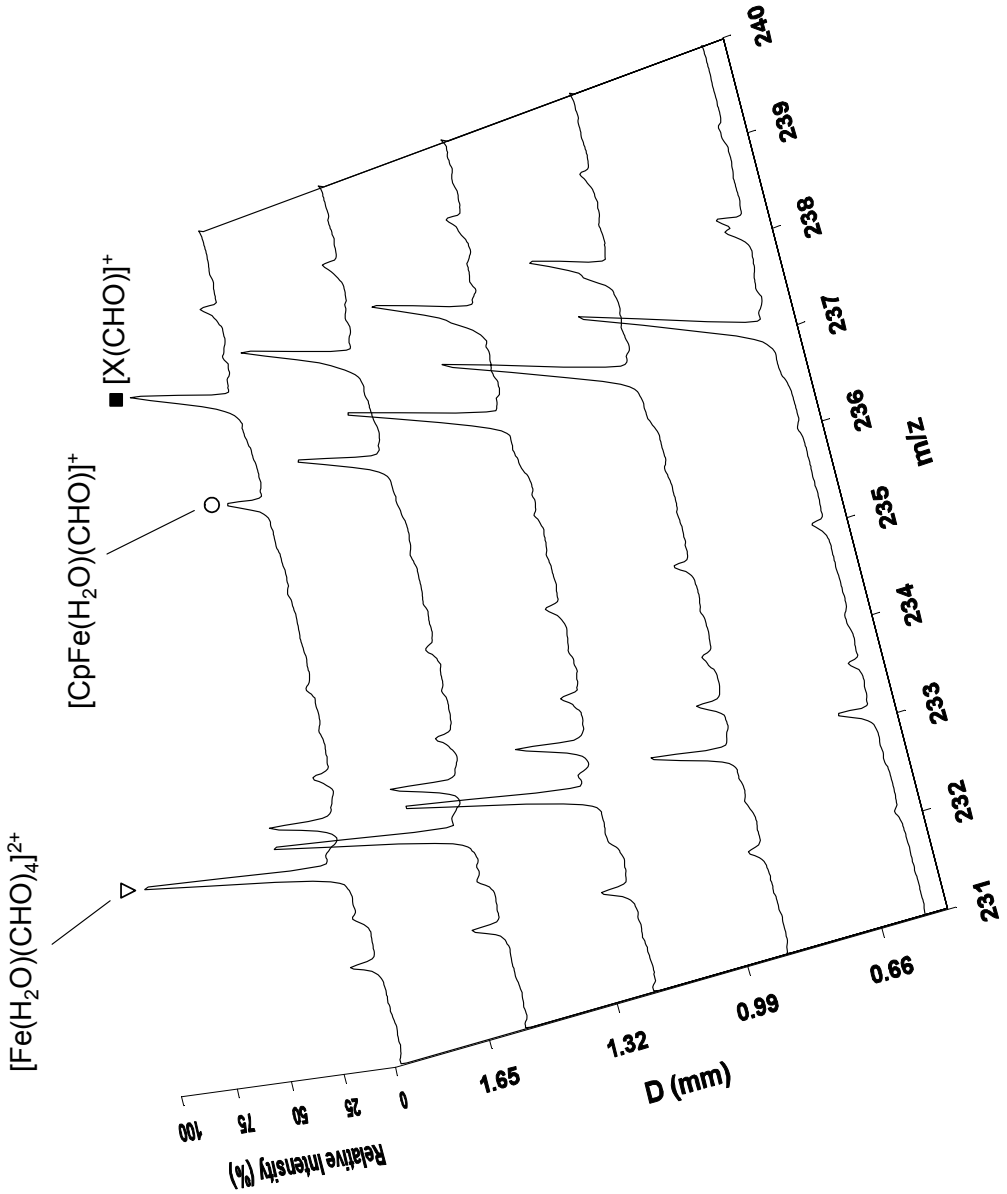
[Fe(H2O)(CHO)4]2+
[CpFe(H2O)(CHO)]+
[X(CHO)]+
Relative Intensity (%)
0
25
50
75
100
D (mm)
1.65
1.32
0.99
0.66
m/z
231
232
233
234
235
236
237
238
239
240

Figure 21

Comparison of relative peak intensities in the mass spectra of $[CpFe(H_2O)(CHO)_2]^+$, $[Fe(H_2O)(CHO)_6)]^{2+}$, and $[X(CHO)_2]^+$ at varied D values. The spectra were acquired with an irradiated DCE solution containing 100 μM $[CpFebz]PF_6$ and 40 mM CHO at a sampling flow rate of 60 μL/h and D = 0.55, 0.88, 1.21, 1.54, 1.87 mm. Laser wavelength was 488nm.

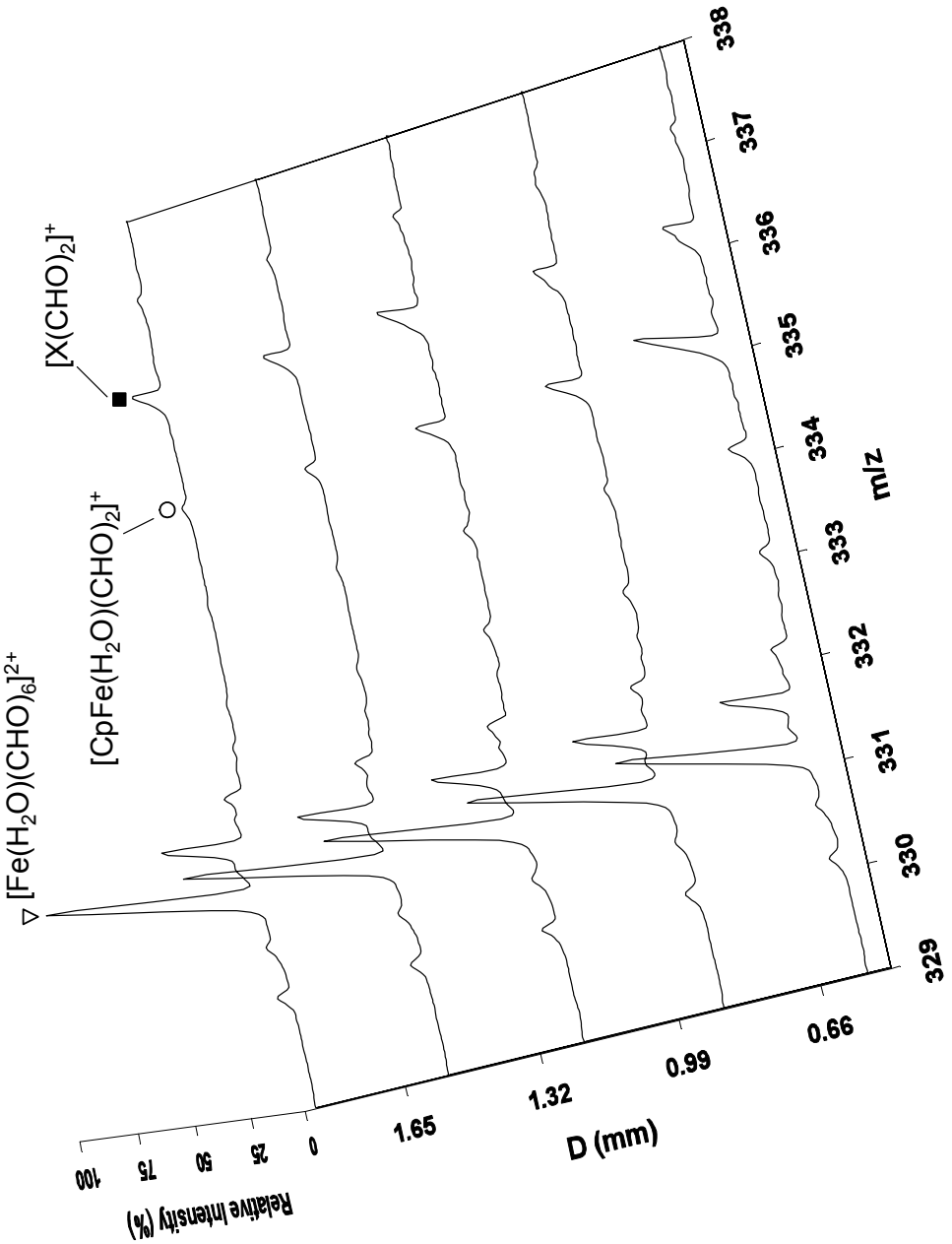
[Fe(H2O)(CHO)6]2+
[CpFe(H2O)(CHO)2]+
[X(CHO)2]+
Relative Intensity (%)
100
75
50
25
0
D (mm)
1.65
1.32
0.99
0.66
m/z
329
330
331
332
333
334
335
336
337
338

Figure 22

Comparison of relative peak intensities in the mass spectra of $[CpFe(H_2O)(CHO)_3]^+$, $[Fe(H_2O)(CHO)_8)]^{2+}$, and $[X(CHO)_4]^+$ at varied D values. The spectra were acquired with an irradiated DCE solution containing 100 μM $[CpFebz]PF_6$ and 40 mM CHO at a sampling flow rate of 60 μL/h and D = 0.55, 0.88, 1.21, 1.54, 1.87 mm. Laser wavelength was 488nm.

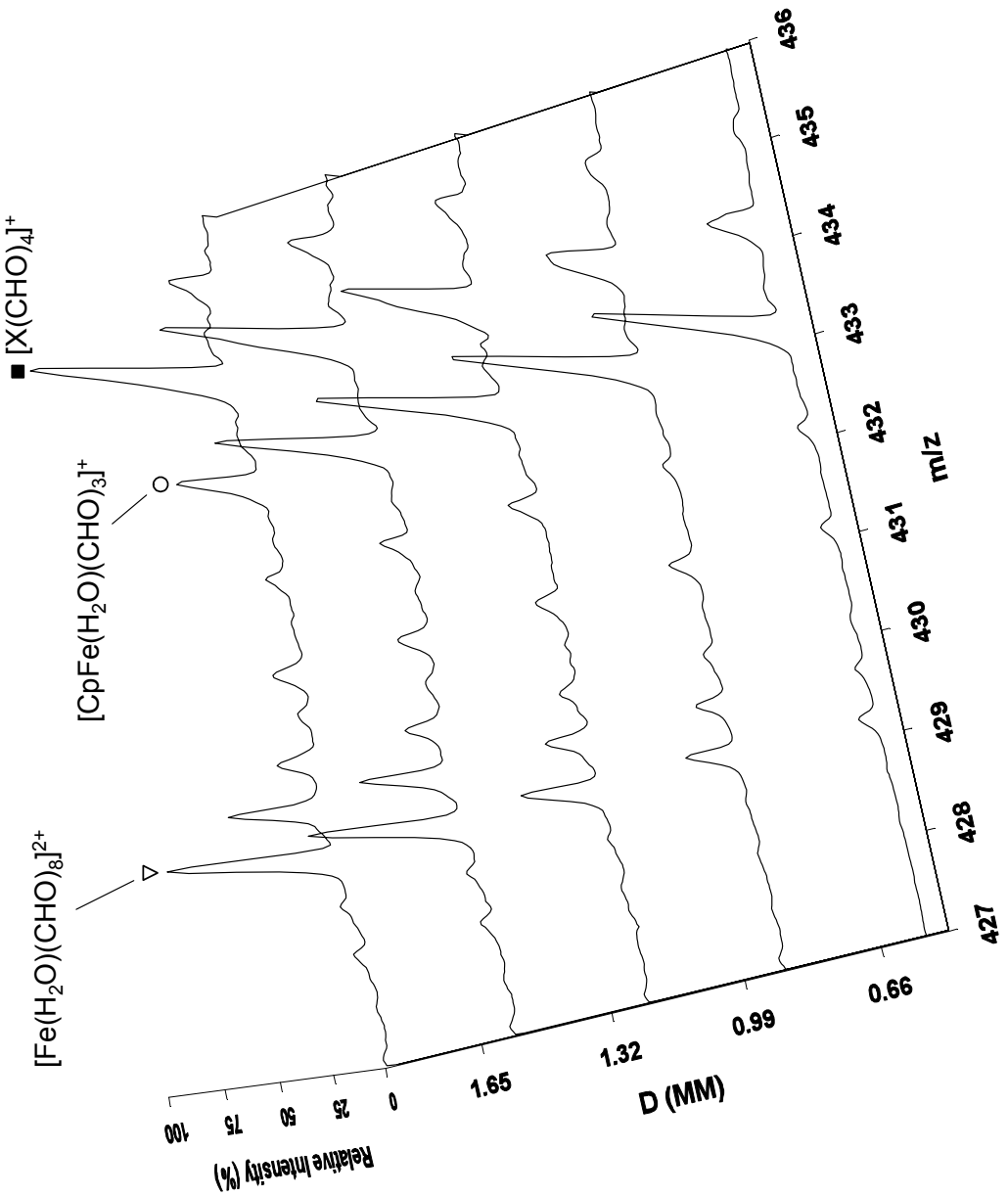
■ [X(CHO)4]+
○ [CpFe(H2O)(CHO)3]+
▽ [Fe(H2O)(CHO)8]2+
Relative Intensity (%)
100
75
50
25
0
D (MM)
1.65
1.32
0.99
0.66
m/z
427
428
429
430
431
432
433
434
435
436

were deuterium-labeled on the Cp and benzene rings and by employing varied counterions. When irradiated at 488 nm, a solution containing 40 μM deuterated initiator, $[CpFe(\eta^6\text{-}C_6D_6)]PF_6$, and 40 mM CHO in DCE yielded the identical $[X(CHO)_{0\text{-}3}]^+$ product series in addition to the deuterium labeled precursor with m/z at 205.1 for $[CpFe(\eta^6\text{-}C_6D_6)]^+$ (Figure 23), which ruled out the involvement of benzene in the formation of X^+.

The $[(\eta^5\text{-}C_5D_5)Febz]PF_6$ complex with 86% incorporation of deuterium on the Cp ring then was tested. Irradiating a solution containing 120 μM initiator and 40 mM CHO in DCE generated the major series of $[X(CHO)_{0\text{-}4}]^+$ and a minor series of $[Fe(H_2O)(CHO)_{5\text{-}8}]^{2+}$ as well as the $[(H_3O)(CHO)_{2\text{-}5}]^+$ series (see Figure 24). No deuterium incorporation can be identified from the characteristic isotopic patterns of the three product series, especially those from $[X(CHO)_{0\text{-}4}]^+$. These results suggest that X^+ from the photolysis of $[(\eta^5\text{-}C_5D_5)Febz]PF_6$ did not originate from the Cp ring in the initiator molecule.

Further studies on the identity of X^+ involve the use of initiators with the same $[CpFebz]^+$ cation but different types of anions. These studies were based on a hypothesis that the anion may be involved in some fashion with the formation of X^+. One initiator tested is $[CpFebz]SbF_6$, which gives the highest speed for epoxy polymerization using photoinitiators of the type $[CpFebz]^+Z^-$, where Z is SbF_6^-, AsF_6^-, PF_6^-, or BF_4^-. Greater polymerization speed correlates with a decrease in the nucleophilicity of the anion.[27] The 100 μM $[CpFebz]SbF_6$ and 90 mM CHO solution in DCE gave a clean mass spectral background with $[CpFebz]^+$ as the only detected species when the laser was off. However,

Figure 23

ESI-TOF mass spectrum of photolysis products from a DCE solution containing 40 μM [CpFe(η^6-C_6D_6)]PF_6 and 40 mM CHO. The spectrum was acquired at a sampling flow rate of 20 μL/h when irradiated at 488 nm with D = 2 mm.

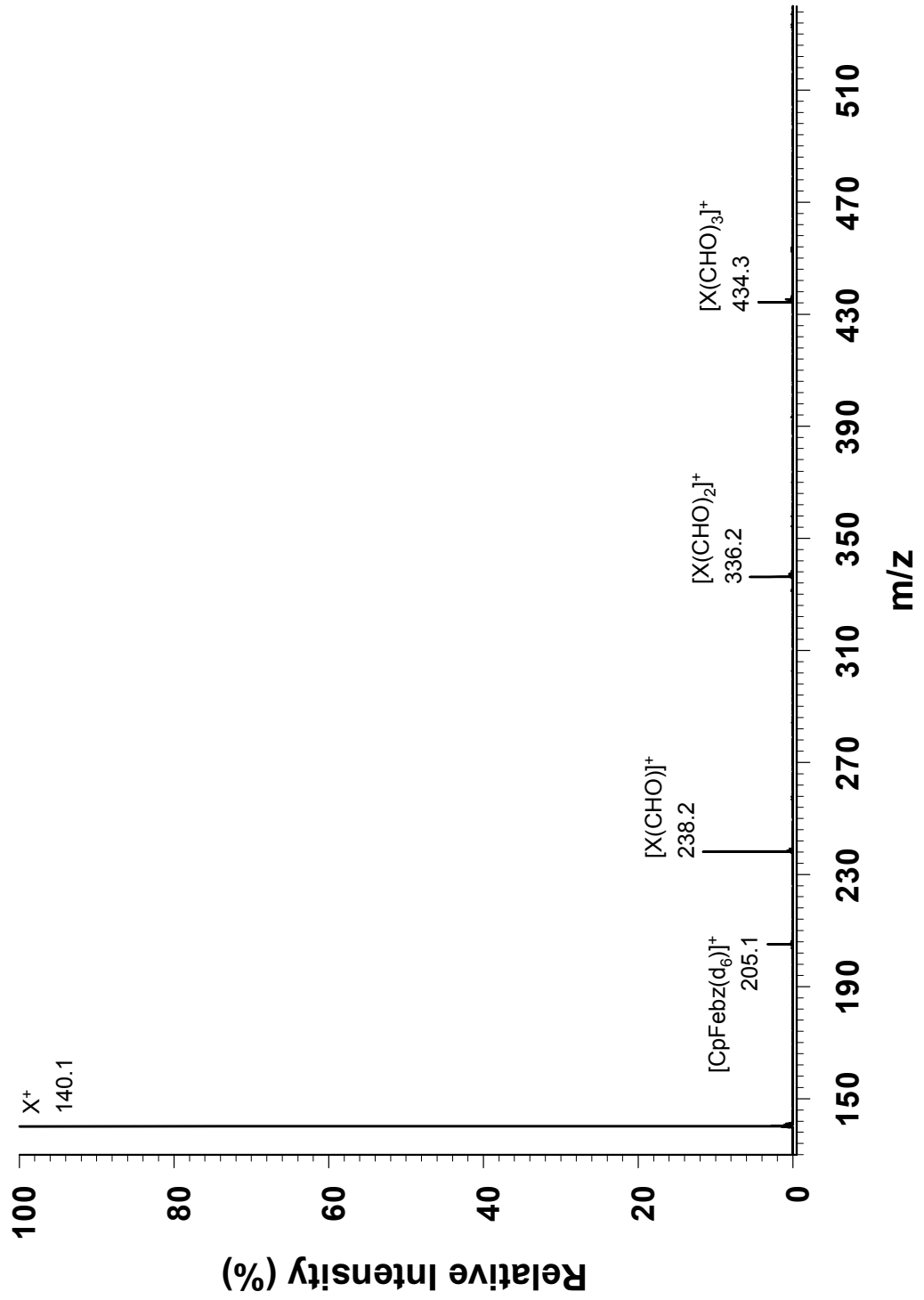
Relative Intensity (%)
100
80
60
40
20
0
150
190
230
270
310
350
390
430
470
510
m/z
X+
140.1
[CpFebz(d6)]+
205.1
[X(CHO)]+
238.2
[X(CHO)2]+
336.2
[X(CHO)3]+
434.3

Figure 24

ESI-TOF mass spectrum of photolysis products from a DCE solution containing 120 μM photoinitiator with 86% deuterated cyclopentadienyl, $[Cp(d_5)Febz]PF_6$, and 40 mM CHO. The spectrum was acquired at a sampling flow rate of 20 μL/h when irradiated at 488 nm with D = 6.7 mm.

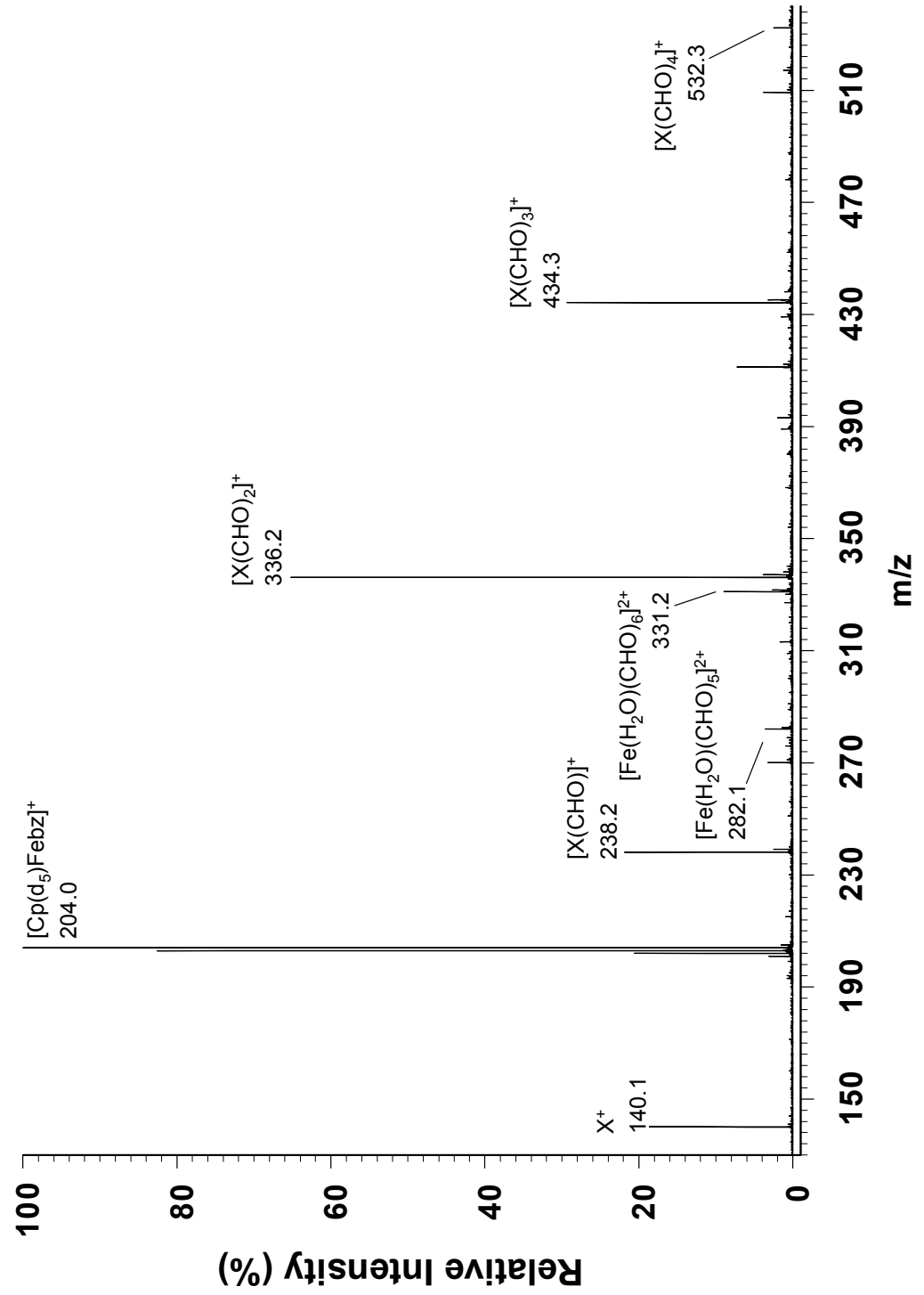
Relative Intensity (%)
100
80
60
40
20
0
150
190
230
270
310
350
390
430
470
510
m/z
[Cp(d5)Febz]+
204.0
X+
140.1
[X(CHO)]+
238.2
[Fe(H2O)(CHO)6]2+
331.2
[Fe(H2O)(CHO)5]2+
282.1
[X(CHO)2]+
336.2
[X(CHO)3]+
434.3
[X(CHO)4]+
532.3

irradiation at 488 nm brought about a richer mass spectrum with the familiar photolysis product $[CpFeCp]^+$ at m/z of 186.0, $[X(CHO)_q]^+$ (q = 0 – 3) species, $[Fe(H_2O)_i(CHO)_q]^{2+}$ with one through three water molecules in the coordination sphere, as well as a more complicated family of dipositive ions containing CHO (Figure 25). From the latter family, four series with a consecutive molecular mass difference of one water molecule were located; the identity of this family will be discussed later. The hexafluoroantimonate anion experiment did not solve the mystery of X^+ but at least partially explained the accelerating effect of the anion, i.e., it helped generate more initiating species compared to those found in hexafluorophosphate anion system. The presence of antimony in the photoproducts seems unlikely, because the characteristic isotope pattern originating from $_{51}Sb^{121}$ and $_{51}Sb^{123}$ with natural abundance of 57.25% and 42.75%, respectively, was not found from the mass spectrum.

The study next turned to a more nucleophilic anion with different chemical structure from the aforementioned family. Trifluoromethanesulfonate (Tf^-) was chosen based on the consideration that it has been compared along with other anions in terms of counterion effect on the photolysis of $[CpFe(\eta^6\text{-arene})]^+$. Figure 26 displays the mass spectrum of identified products generated from the on-line photolysis of a 60 μM [CpFebz]Tf and 40 mM CHO solution in DCE. The photochemistry for the mixed-sandwich cation is the same as that observed from previous systems, as evidenced by the detection of ferricenium (m/z = 186.0) that is formed in the thermal decomposition of the half-sandwich intermediate following the photorelease of benzene. The inset of Figure 26 reveals several

Figure 25

ESI-TOF mass spectrum of photolysis products from a DCE solution containing 100 μM [CpFebz]SbF_6 and 90 mM CHO. The spectrum was acquired at a sampling flow rate of 20 μL/h when irradiated at 488 nm with D = 2 mm.

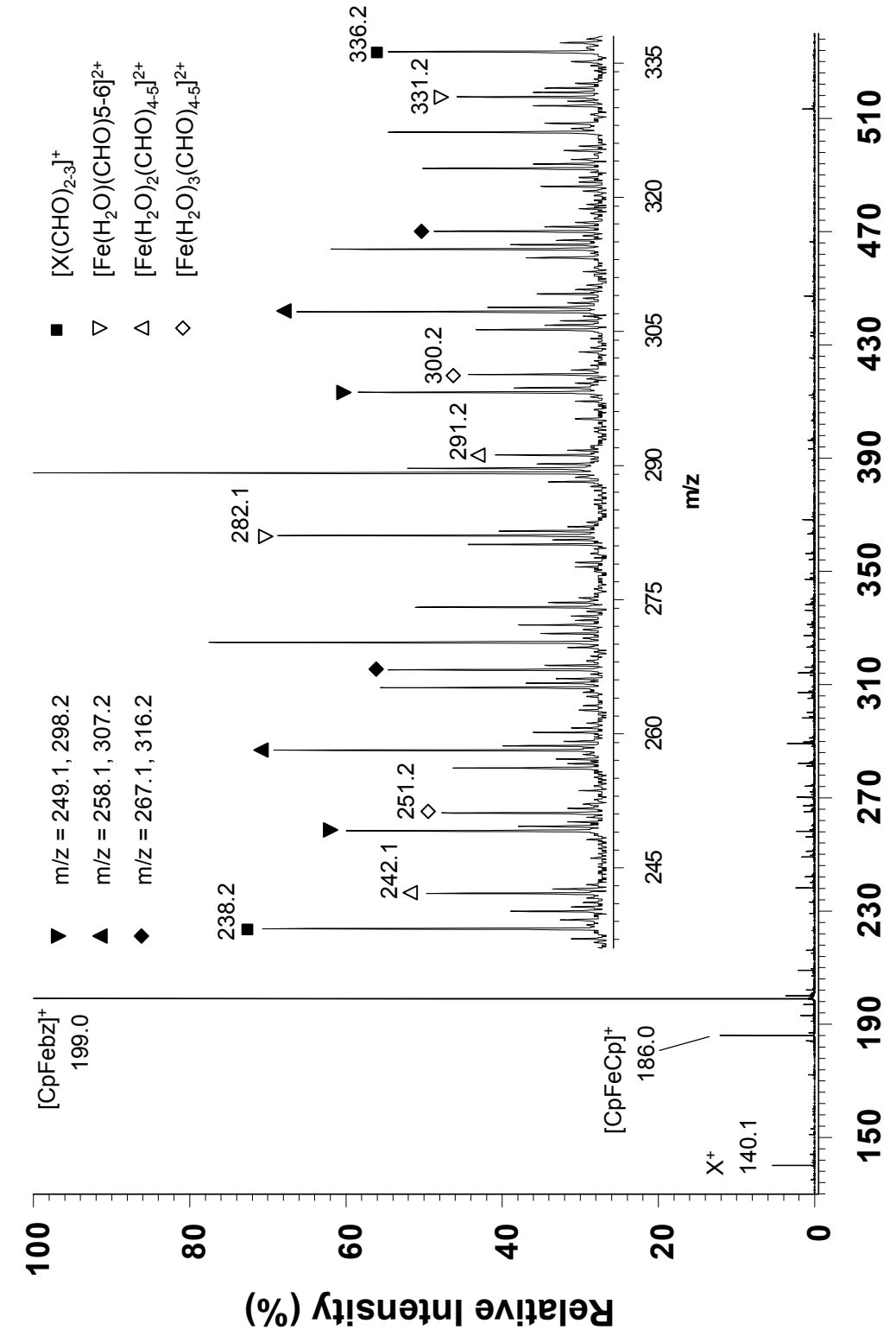
Relative Intensity (%)
m/z
[CpFebz]+
199.0
[CpFeCp]+
186.0
X+
140.1
m/z = 249.1, 298.2
m/z = 258.1, 307.2
m/z = 267.1, 316.2
[X(CHO)2-3]+
[Fe(H2O)(CHO)5-6]2+
[Fe(H2O)2(CHO)4-5]2+
[Fe(H2O)3(CHO)4-5]2+
238.2
242.1
251.2
282.1
291.2
300.2
331.2
336.2

Figure 26

ESI-TOF mass spectrum of photolysis products from a DCE solution containing 60 μM [CpFebz]Tf and 40 mM CHO. The spectrum was acquired at a sampling flow rate of 20 μL/h when irradiated at 488 nm with D = 8 mm. Tf is trifluoromethanesulfonate. Inset: the enlarged region of mass/charge ratio from 230 to 450.

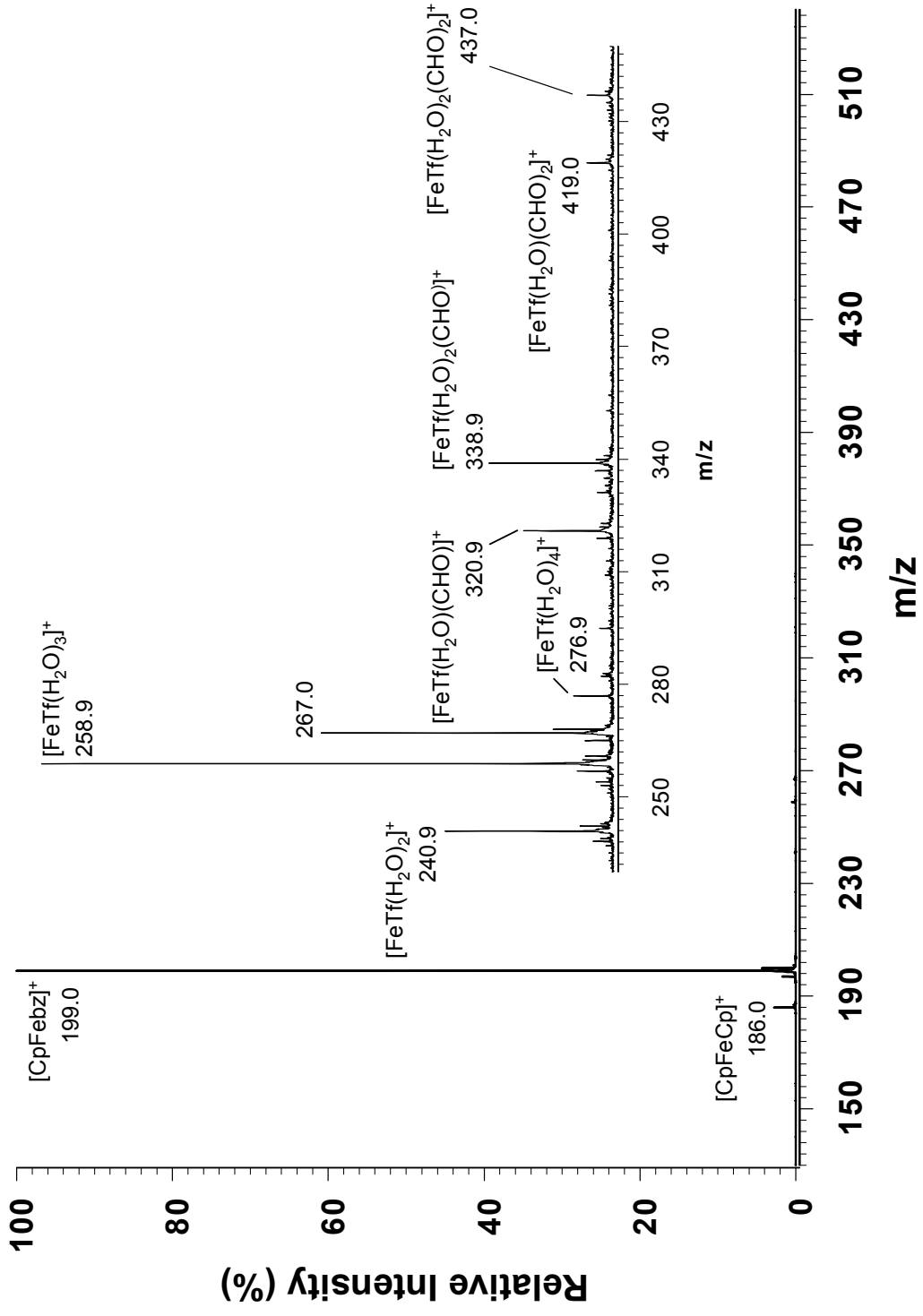
Relative Intensity (%)
100
80
60
40
20
0
150
190
230
270
310
350
390
430
470
510
m/z
[CpFebz]+
199.0
[CpFeCp]+
186.0
[FeTf(H2O)2]+
240.9
[FeTf(H2O)3]+
258.9
267.0
[FeTf(H2O)4]+
276.9
[FeTf(H2O)(CHO)]+
320.9
[FeTf(H2O)2(CHO)]+
338.9
[FeTf(H2O)(CHO)2]+
419.0
[FeTf(H2O)2(CHO)2]+
437.0
250
280
310
340
370
400
430
m/z

fully ring-deligated Fe(II) complex series involving the coordination of water and CHO molecules to the iron(II) center. It is worth noting that all of the species contain a Tf^- ion that helps stabilize the complex ions in the weak nucleophilic medium, DCE. For each of the identified species, there are no more than six ligands within the coordination sphere of iron; meanwhile, complex ions with more than three water ligands cannot accommodate the coordination of a CHO molecule. These species are identified from the match of their isotope patterns with those from theoretical calculation (see Figure 27) in addition to the accurate mass measurements as listed in Table 5. Other than the fully ring-deligated Fe(II) complexes, only a tiny peak at m/z = 140.1 was found in the spectrum, implying that the formation of X^+ from previously studied initiators is related to the anion of fluorine-containing types.

3.7 Continuous photolysis study of 1,1'-dibenzoylferrocene

The room temperature electronic spectrum of 1,1'-dibenzoylferrocene (DBF) along with its parent complex, ferrocene, is shown in Figure 28, reflecting the effects of the substituent on the Cp ring on spectral properties. The absorption bands at 326 nm and 442 nm that arise from the weak ligand field transitions in ferrocene are replaced by the high intensity bands that have red-shifted to 354 nm and 486 nm in DBF. These profound spectral changes have been attributed to the metal-to-ligand charge transfer character of the transitions in the benzoyl-substituted complex.[119] In addition to spectral differences, the two compounds exhibit very different photochemical behaviors. Ferrocene is inert

Figure 27

Comparison on isotopic patterns in mass spectra of photolysis products from a DCE solution containing 60 μM [CpFebz]Tf and 40 mM CHO. (a) $[FeTf(H_2O)_3]^+$; (b) $[FeTf(H_2O)_2(CHO)]^+$. Tf is trifluoromethanesulfonate.

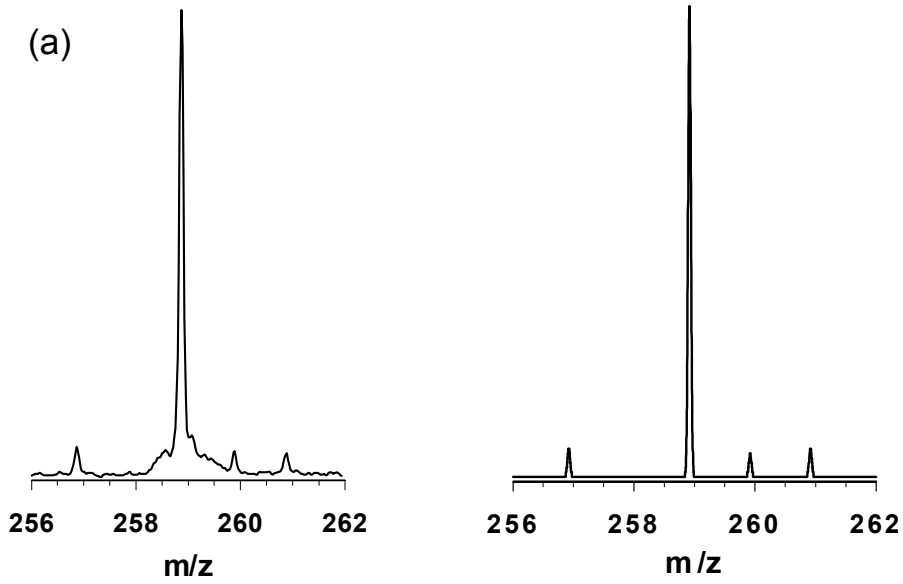
(a)
256
258
260
262
m/z
Measured
256
258
260
262
m/z
Calculated

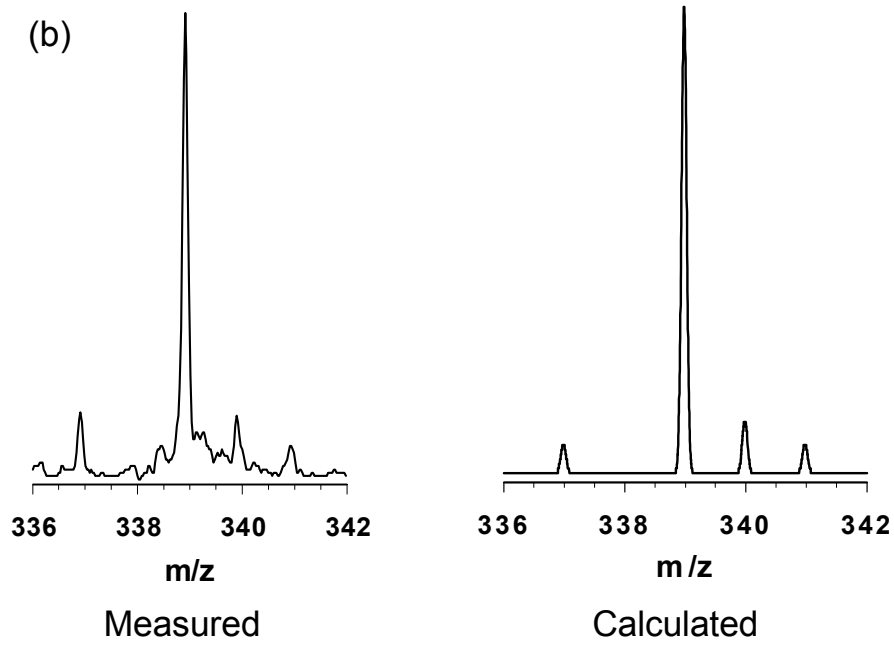
(b)
336
338
340
342
m/z
Measured
336
338
340
342
m/z
Calculated

Table 5 List of observed and expected mass/charge ratios of the products from the photolysis of [CpFebz]Tf in DCE solution containing CHO

Formula	Measured m/z	Resolution Power	Calculated m/z	Error (Da)	Δm of the attached CHO*	Error in Δm (Da)
$[FeTf(H_2O)_2]^+$	240.901	3142	240.9081	-0.007	98.075	0.002
$[FeTf(H_2O)_2(CHO)]^+$	338.976	3248	338.9812	-0.005	98.078	0.005
$[FeTf(H_2O)_2(CHO)_2]^+$	437.054	2964	437.0544	0.000		
$[FeTf(H_2O)(CHO)]^+$	320.955	3032	320.9706	-0.016	98.091	0.018
$[FeTf(H_2O)(CHO)_2]^+$	419.046	7873	419.0438	0.002		
$[FeTf(H_2O)_3]^+$	258.913	4583	258.9186	-0.006		
$[FeTf(H_2O)_4]^+$	276.930	3027	276.9292	0.001		
$[FeTf(H_2O)_5]^+$	294.920	3027	249.9398	-0.007		

* The theoretical monoisotopic m/z for CHO is 98.0732 Da.

Figure 28

Room temperature electronic absorption spectra of ferrocene and 1,1'-dibenzoylferrocene in methanol. I, ferrocene; II, 1,1'dibenzoylferrocene.

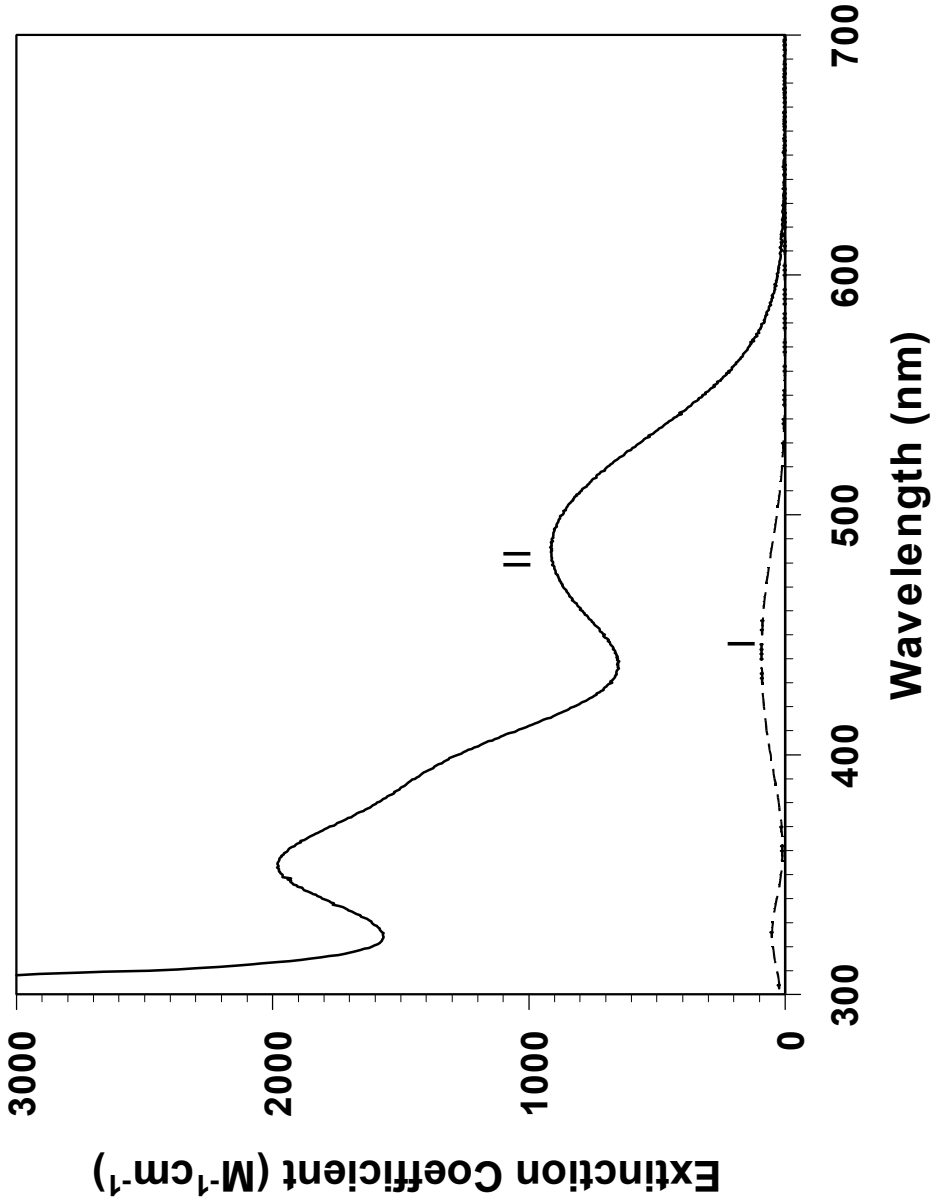
Extinction Coefficient (M-1cm-1)
3000
2000
1000
0
300
400
500
600
700
Wavelength (nm)
I
II

towards photolysis in non-halogenated solvents. In contrast, DBF undergoes photoreaction readily in methanol solution when irradiated with 546 nm light. Figure 29 displays representative spectral changes during photolysis. Along the time course of continuous irradiation at 546 nm, a steady bleaching of the long-wavelength band (λ_{max} = 486 nm) of DBF is accompanied by the sharp increase of absorbance in the ultraviolet region. Shown in the figure is an isosbestic point at 372 nm, indicating that secondary photolysis is negligible. A similar experiment was performed with a higher concentration of DBF in methanol for the purpose of estimating the quantum yield. The extent of photoreaction was calculated spectrometrically by measuring the decrease in absorbance intensity of the long-wavelength band in the UV-Vis spectrum of a 2.38 mM DBF solution (Figure 30). Equation 23 is applied for determining the percent of DBF reacted, where A_0 is the absorbance at the band maximum with zero time of irradiation, A_t represents the absorbance with time t irradiation, and A_f is the absorbance when no further bleaching of the band can be observed with extended time of irradiation. The limiting quantum yield for the initial complex solution with zero percent of reaction was obtained by linearly extrapolating the plot of quantum yield vs the extent of reaction to zero irradiation time. A quantum yield of 0.36 was determined for the 2.38 mM argon-saturated DBF solution in methanol.

$$\% \text{ reaction} = \frac{A_0 - A_t}{A_0 - A_f} \times 100 \qquad (23)$$

Figure 29

UV-Vis spectral changes resulting from the 546 nm photolysis of 1,1'-dibenzoylferrocene (0.476 mM) in argon-saturated methanol. Spectra were acquired in a 1 cm pathlength cell after 0, 36, 60, 108, 156, 252 seconds of irradiation with a source of light intensity at 1.24×10^{-7} einsteins/sec; arrows indicate the direction of spectral changes as photolysis proceeds.

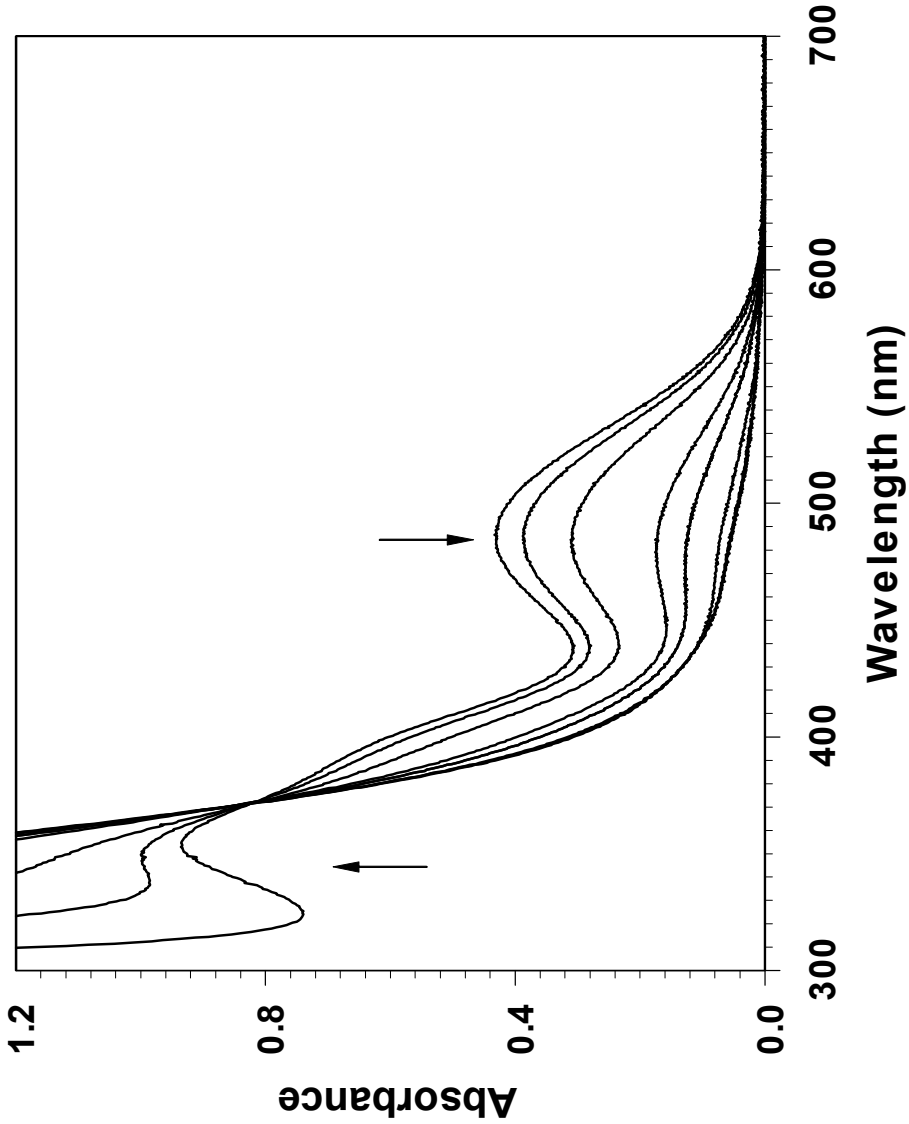
Absorbance
1.2
0.8
0.4
0.0
300
400
500
600
700
Wavelength (nm)

Figure 30

UV-Vis spectral changes arising from the 546 nm photolysis of 1,1'-dibenzoylferrocene (2.38 mM) in argon-saturated methanol. Spectra were acquired in a 1 cm pathlength cell after 0, 30, 60, 120, 180, 480, and 720 seconds of irradiation with a source of light intensity at 1.24×10^{-7} einsteins/sec; arrow indicates the direction of spectral changes as photolysis proceeds.

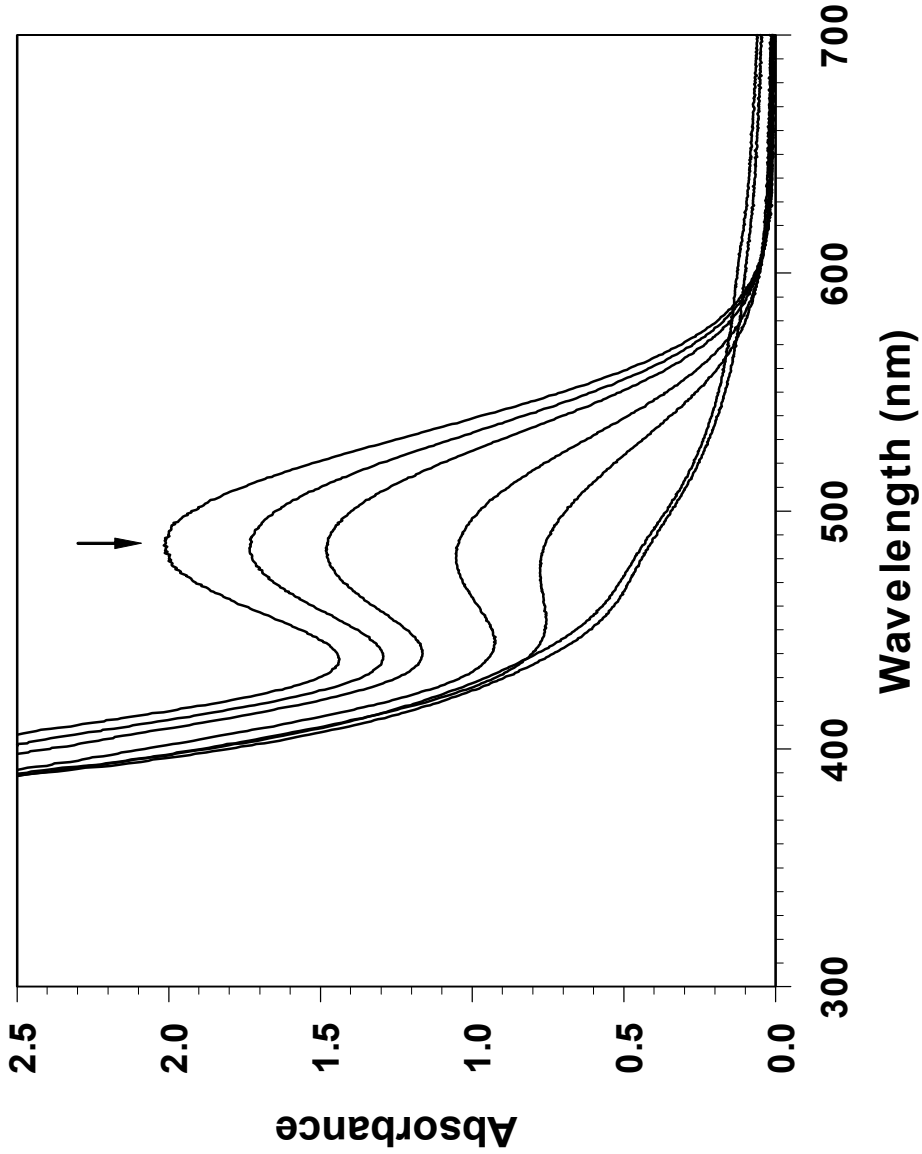
Absorbance
2.5
2.0
1.5
1.0
0.5
0.0
300
400
500
600
700
Wavelength (nm)

The high photochemical reactivity greatly facilitates the mechanistic study of the reaction of DBF, while the bleaching feature can be used to monitor the extent of reaction in the following mechanistic experiments.

3.8 Photolysis mechanism study of 1,1'-dibenzoylferrocene

^{1}H NMR spectroscopy was employed to identify the products formed upon photolysis of 1,1'-dibenzoylferrocene (DBF) at 546 nm. A major photoproduct previously identified by GC-MS[62] and X-ray crystallography[61] is the benzoyl-cyclopentadienide anion. The NMR spectrum of this anion, in the form of its sodium salt, was used as a standard for comparison to the spectra of the photoproducts from DBF. ^{1}H and ^{13}C NMR data collected in this study along with those from other research groups are summarized in Table 6 and Table 7, respectively. As seen from the tables, most of the band assignments found in this study are consistent with the data reported in the literature, though minor discrepancy exists. Proton NMR spectra of 24 mM DBF in CD_3OD at 0, 200, and 400 seconds of irradiation are shown in Figure 31, and the corresponding electronic absorption measurements are displayed in Figure 32, indicating a decomposition of approximately 30% to 40 % of the initial DBF after 400 seconds of irradiation. A pair of new peaks at 6.71 and 6.92 ppm is indicative of photoproducts and the shoulder (3.38 ppm) on the low field side of the band at 3.35 ppm looks like an overlap of a reaction product with a broadened solvent peak at 3.31 ppm (see Figure 31b, c). However, formation of precipitate[62] resulted in band broadening in each signal peak, including the solvent peaks at

Table 6 Chemical shifts (ppm) in ^{1}H NMR spectra of sodium benzoylcyclopentadienide[a]

In CD_3CN (Na^+ Salt)[b]	In DMSO-d_6 (Na^+ Salt)[b]	In THF-d_8 (Na^+ Salt)[c]	In DMSO-d_6 (Tl^+ Salt)[d]	Band Assignment
7.66-7.69	7.55-7.58	7.272-7.76	7.64	Ortho- in Ph
7.36-7.37	7.30-7.32	7.27-7.28	7.36	Para- and meta- in Ph
6.42	6.17	6.38	6.28	$H_{2,5}$ in Cp
5.91	5.70	5.98	5.81	$H_{3,4}$ in Cp
3.66	3.60	3.55-3.60		$H_{2,5}$ in THF
1.81	1.76	1.68-1.75		$H_{3,4}$ in THF

a. Contains one molecule of THF.

b. This study.

c. From Burger, P.; Brintzinger, H. H. *J. Organomet. Chem.* **1991**, *407*, 207-213.

d. From Jones S. S.; Rausch, M.D.; Bitterwolf, T. E. *J. Organomet. Chem.* **1993**, *450*, 27-31.

Table 7 Chemical shifts (ppm) in ^{13}C NMR spectra of sodium benzoylcyclopentadienide[a]

In DMSO-d_6 (Na^+ Salt)[b]	In DMSO-d_6 (Na^+ Salt)[c]	In DMSO-d_6 (Tl^+ Salt)[c]	In DMSO-d_6 (Tl^+ Salt)[d]	Band Assignment
183.65	185.85	189.17	187.34	Carbonyl C
122.11	123.77	124.65	122.93	C_1 in Cp
	116.28	116.03	114.22	$C_{2,5}$ in Cp
112.24	114.27	114.13	112.22	$C_{3,4}$ in Cp
145.33			142.93	C_1 in Ph
128.36			128.74	$C_{2,6}$ in Ph
127.68			128.00	C_4 in Ph
126.93			127.09	$C_{3,5}$ in Ph

a. Contains one molecule of THF.

b. This study.

c. From Arthurs, M.; Bickerton, J. C.; Hogarth, G.; Morton-Blake, D. A.; Kubal, G.; Truter, M. R. *J. Organomet. Chem.* **1998**, *571*, 43-53.

d. From Jones S. S.; Rausch, M.D.; Bitterwolf, T. E. *J. Organomet. Chem.* **1993**, *450*, 27-31.

Figure 31

Proton NMR spectral changes resulting from the 546 nm photolysis of 23.7 mM DBF in CD_3OD after irradiation for (a) 0 s; (b) 200 s; and (c) 400 s.

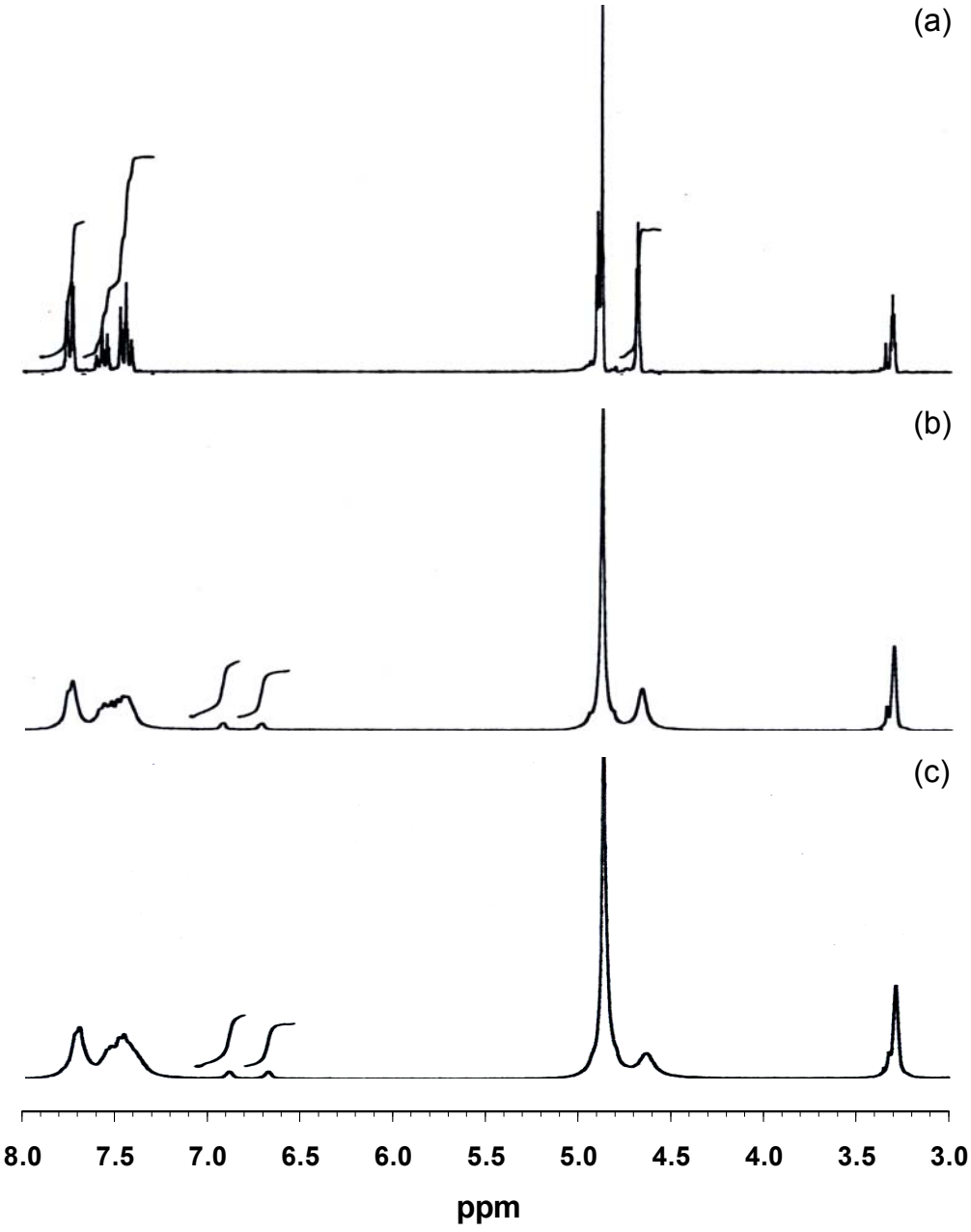
(a)
(b)
(c)
8.0
7.5
7.0
6.5
6.0
5.5
5.0
4.5
4.0
3.5
3.0
ppm

Figure 32

UV-Vis spectral changes resulting from the 546 nm photolysis of 23.7 mM DBF in CD_3OD after irradiation for (I) 0 s; (II) 200 s; and (III) 400 s.

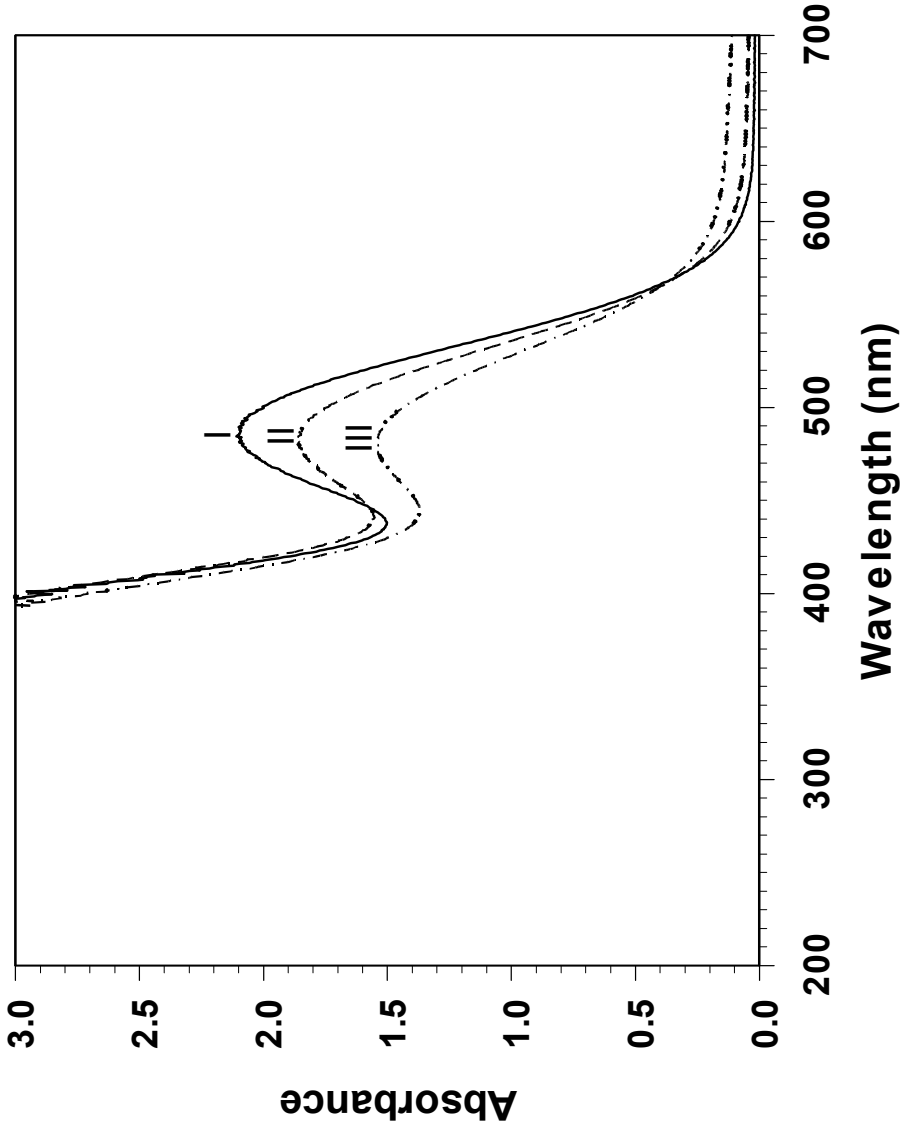
Absorbance
3.0
2.5
2.0
1.5
1.0
0.5
0.0
200
300
400
500
600
700
Wavelength (nm)
I
II
III

3.31 and 4.88 ppm, thereby making it difficult to identify the product solely based on the spectrum.

Switching the solvent to deuterated acetonitrile lessened this problem. Figure 33b shows the spectrum of an 18 mM DBF solution that was exposed to a 546 nm light source for 586 seconds. In addition to the three new bands at 7.2, 6.8, and 6.6 ppm with equivalent signal areas in the spectrum of the irradiated sample, a signal with twice the area of each of the three peaks is observed at 3.46 ppm. The phenyl ring in the product seems intact in the photoprocess as evident from its multiple peaks at 7.77, 7.58, and 7.48 ppm attributable to ortho-, para-, and meta-protons, respectively (refer to data in Table 6 for sodium benzoylcyclopentadienide in CD_3CN). However, the cyclopentadienide anion is unlikely in this case, since the number of protons and their distribution according to the peak integration for the new species in the spectrum suggest that there are five protons, instead of four protons for the cyclopentadienide, on the Cp ring. Moreover, the two protons at 3.46 ppm are in a very similar shielding environment. We may tentatively assign the product as 1-benzoyl-1,3-cyclopentadiene that resulted from protonation of the benzoylcyclopentadienide anion generated from the primary photoreaction.

The photoreaction in deuterated dimethyl sulfoxide (DMSO) with 23 mM of DBF displays the same band broadening as seen in the CD_3OD experiment and peaks from DBF remain even after 40 minutes of irradiation (see Figure 34). An unresolved cluster of product bands in the region of 7.2 – 7.4 ppm appears upon irradiation for 200 seconds (Figure 34b), accompanied by a broad band at 3.42

Figure 33

Proton NMR spectral changes resulting from the 546 nm photolysis of 18 mM DBF in CD_3CN after irradiation for (a) 0 s; and (b) 586 s.

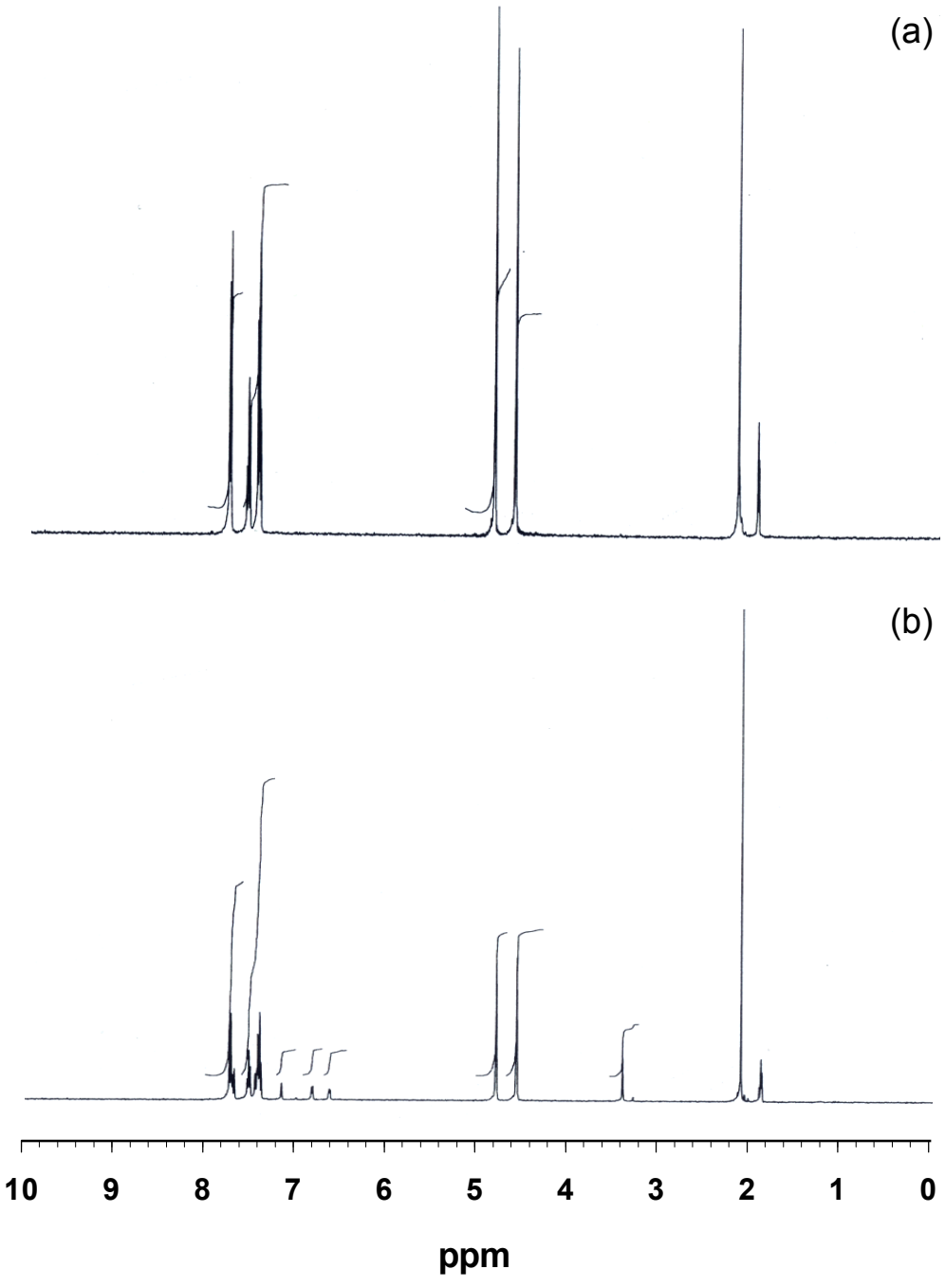
(a)
(b)
10
9
8
7
6
5
4
3
2
1
0
ppm

Figure 34

Proton NMR spectral changes resulting from the 546 nm photolysis of 23 mM DBF in deuterated dimethyl sulfoxide after irradiation for (a) 0 s; (b) 200 s; (c) 800 s; and (d) 2400 s.

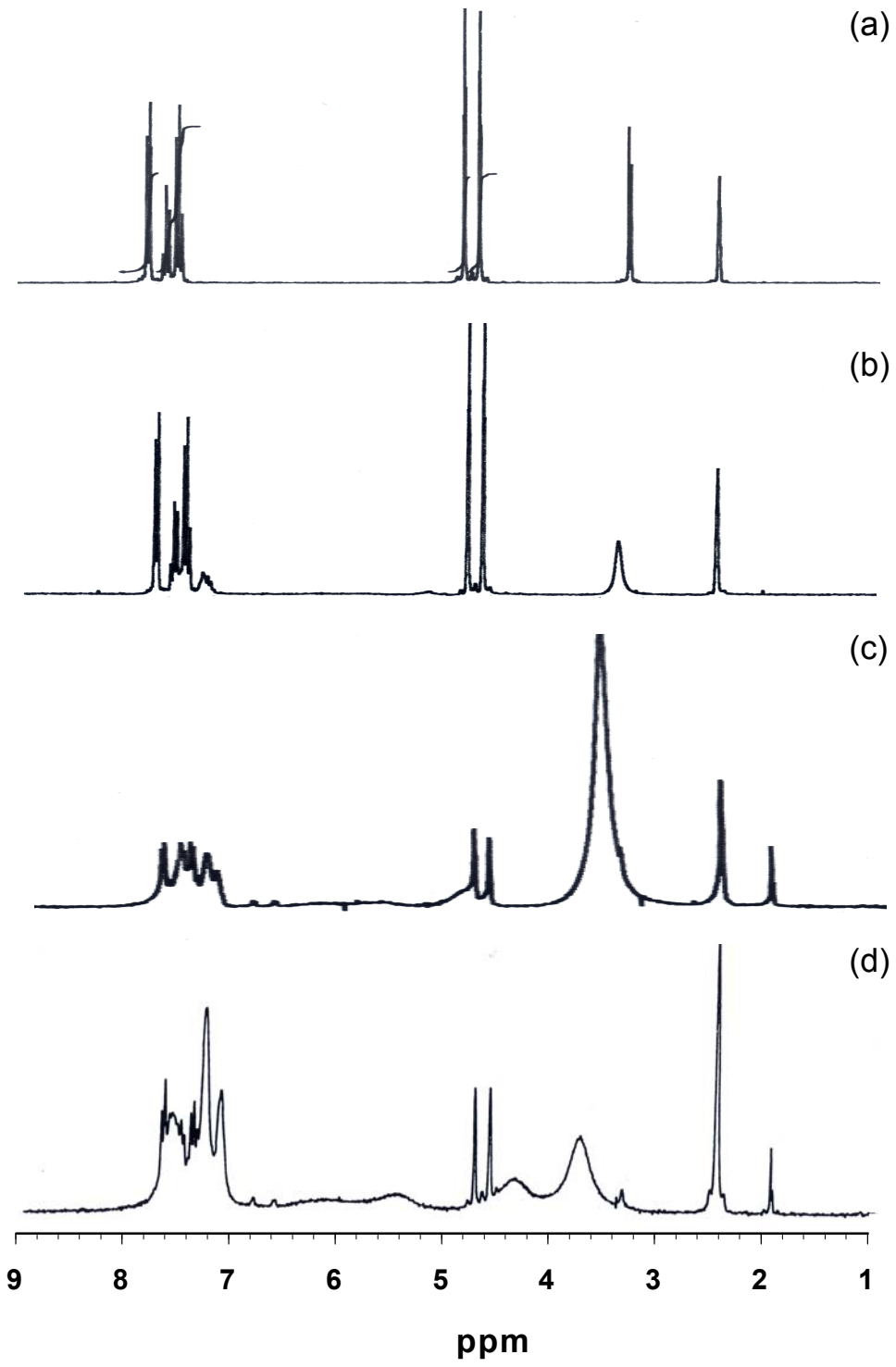
(a)
(b)
(c)
(d)
9
8
7
6
5
4
3
2
1
ppm

ppm which may overlap with the 3.3 ppm band of HDO in the solvent. As the irradiation proceeds, the band at 3.42 ppm shifts to low field and at the same time two bands, also broadened, at 5.4 and 4.3 ppm, develop in the spectrum. Once the irradiation time reaches 40 minutes, two tiny, but distinguishable, bands at 6.8 and 6.6 ppm can been seen in the spectrum, while the band at 7.2 ppm found in the CD_3CN experiment may be buried in the growing cluster at 7.2 - 7.4 ppm which may be attributed to the photoproduct. At this point no conclusive characterization can be made for the product(s), but the anion of benzoylcyclopentadienide seems difficult to identify from NMR spectra without the assistance of some other techniques.

Further studies on the mechanism of the photoinduced deligation from DBF were conducted by using the established on-line ESI-MS technique. In the positive ion mode, sodium or potassium iodide was added into the DBF solution in acetonitrile (AN) to create sodium or potassium adducts for electrospray ionization. As seen from Figure 35, at relatively low concentrations of NaI, two species in the forms of one and two DBF molecules associated with one sodium showed up as the only peaks in the mass spectrum with a clean background (Figure 35a), while more NaI in the sample solution changed the intensity ratio of the two in addition to bringing in some impurities (Figure 35b). The identities of the DBF adduct species from the mass spectra were confirmed by changing the carrier ion from Na^+ to K^+ with KI instead of NaI in the solution. Referring to the spectrum in Figure 35b, the identical peak distribution and isotopic patterns, and accurate mass differences from the carrier change in Figure 35c are all

Figure 35

ESI-TOF mass spectra of 1,1'-dibenzoylferrocene (DBF) in acetonitrile with sodium iodide or potassium iodide as ion carrier. (a) A sample of 100 μM DBF and 160 μM NaI; (b) a sample of 70 μM DBF and 1.4 mM NaI; and (c) a sample of 90 μM DBF and 1.2 mM KI.

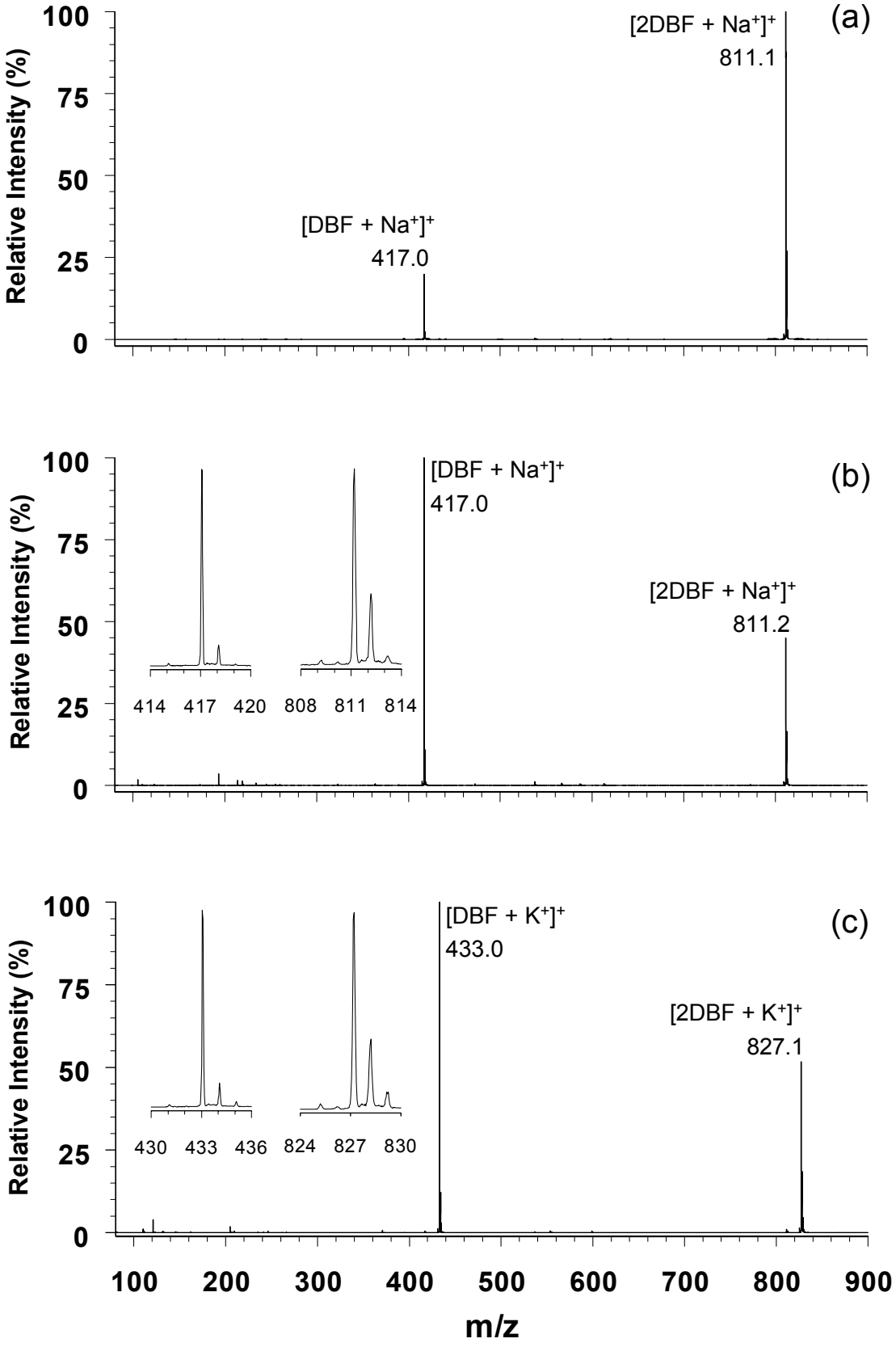
(a)
[2DBF + Na+]+
811.1
[DBF + Na+]+
417.0
Relative Intensity (%)
100
75
50
25
0
(b)
[DBF + Na+]+
417.0
[2DBF + Na+]+
811.2
414 417 420 808 811 814
(c)
[DBF + K+]+
433.0
[2DBF + K+]+
827.1
430 433 436 824 827 830
100 200 300 400 500 600 700 800 900
m/z

supportive of the proposed identities of the DBF-containing ions in the system with NaI. The laser irradiation at 488 nm, followed by a controlled thermal reaction of 12 milliseconds, enabled the identification of an assortment of products from an acetonitrile solution containing 130 μM DBF and 120 μM NaI. Shown in Figure 36 is the parent ion, $[DBF + Na^+]^+$, along with three groups of products: (i) half-sandwich complex intermediates with one added proton; (ii) the benzoylcyclopentadienide anion with one added proton and a carrier ion of either proton or sodium; (iii) fully ring-deligated Fe(II) complex ions as products from the thermal decomposition of the half-sandwich intermediate. The nucleophilic nature of the benzoylcyclopentadienyl moiety is demonstrated by the first two product groups, especially by the anion-related species. The half-sandwich complex ions coordinated with two and three solvent molecules accept a proton to form dipositive ions with mass/charge ratio of 154.0 and 174.5, respectively, while the anion formed from the deligation of DBF in the photoreaction gains a proton from the environment to form the neutral 1-benzoyl-1,3-cyclopentadiene that is then cationized by the carrier ion. Analogous to its $[2DBF + Na^+]^+$ parent, two 1-benzoyl-1,3-cyclopentadiene molecules can also share a sodium carrier, which gives the major anion-related peak in the spectrum at m/z = 363.1. The measured mass/charge values of the DBF parent and its three groups of products generated from photoreaction and identified by the on-line ESI-MS, and the mass measurement errors for each of them are summarized in Table 8.

Figure 36

ESI-TOF mass spectrum of photolysis products from an AN solution containing 130 μM DBF and 120 μM NaI. The spectrum was acquired at a sampling flow rate of 40 μL/h when irradiated at 488 nm with D = 0.84 mm.

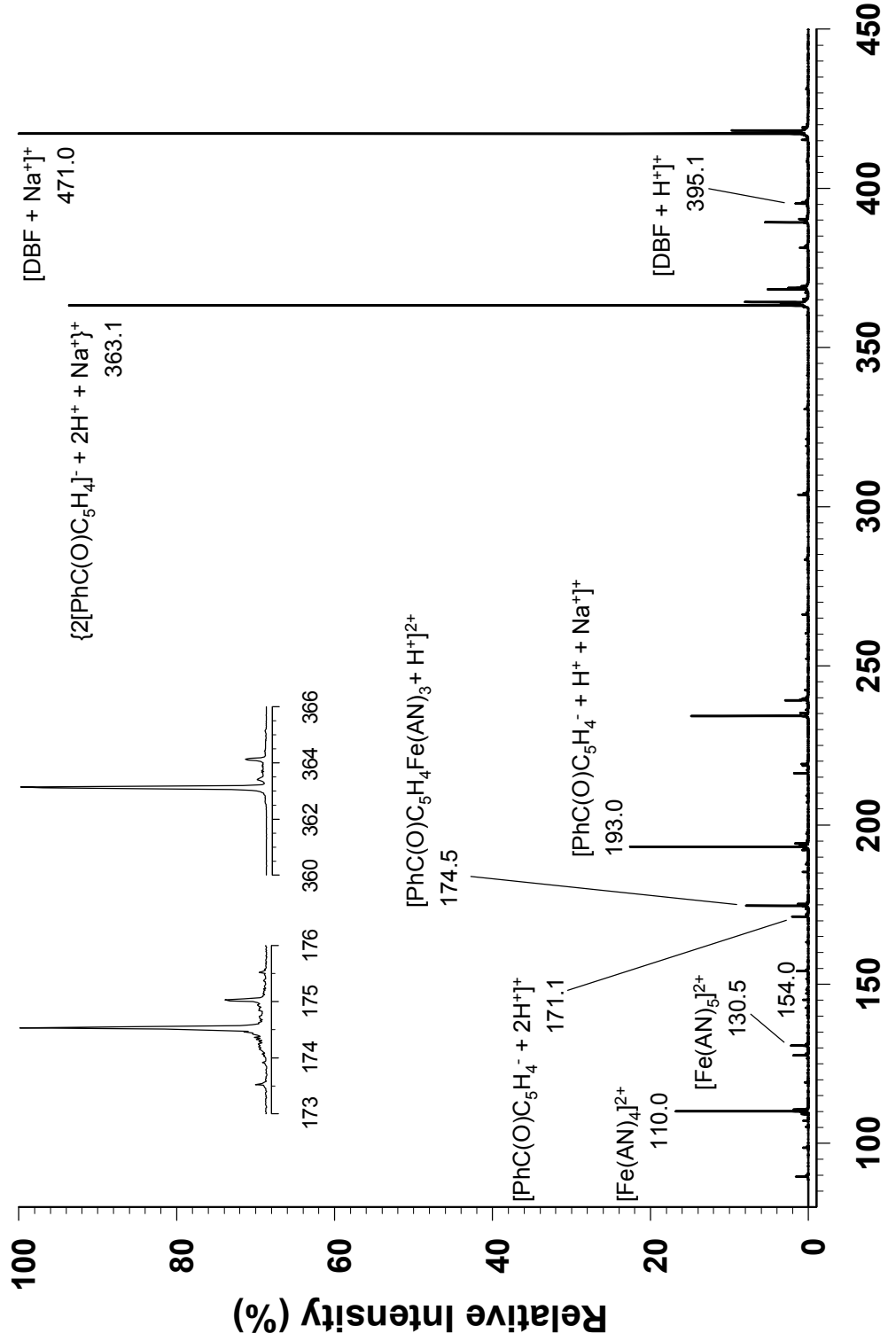
Relative Intensity (%)
m/z
100
80
60
40
20
0
100
150
200
250
300
350
400
450
[DBF + Na+]+
471.0
{2[PhC(O)C5H4]- + 2H+ + Na+}+
363.1
[DBF + H+]+
395.1
[PhC(O)C5H4Fe(AN)3 + H+]2+
174.5
[PhC(O)C5H4- + H+ + Na+]+
193.0
[PhC(O)C5H4- + 2H+]+
171.1
[Fe(AN)4]2+
110.0
[Fe(AN)5]2+
130.5
154.0
173
174
175
176
360
362
364
366

Table 8 List of observed mass/charge ratios for DBF and its photolysis products

Formula	Measured m/z	Resolution Power	Calculated m/z	Error (Da)
$[DBF + Na^+]^+$	417.048	5137	417.0554	-0.007
$\{[PhC(O)C_5H_4Fe(AN)_2]^+\} + H^+]^{2+}$	154.020	5455	154.0306	-0.011
$\{[PhC(O)C_5H_4Fe(AN)_3]^+ + H^+\}^{2+}$	174.535	4650	174.5439	-0.009
$\{[PhC(O)C_5H_4]^- + 2H^+\}^+$	171.065	4440	171.0810	-0.016
$\{[PhC(O)C_5H_4]^- + H^+ + Na^+\}^+$	193.047	3395	193.0630	-0.016
$\{2[PhC(O)C_5H_4]^- + Na^+\}^+$	363.127	5031	363.1361	-0.009
$[Fe(AN)_3]^{2+}$	89.491	2577	89.5073	-0.016
$[Fe(AN)_4]^{2+}$	110.011	3197	110.0206	-0.010
$[Fe(AN)_5]^{2+}$	130.527	3341	130.5338	-0.007

3.9 On-line photolysis of $[Fe(\eta^6\text{-mes})_2](PF_6)_2$

In acetonitrile (AN) medium, $[Fe(\eta^6\text{-mes})_2]^{2+}$ exhibits three low-intensity bands at 515, 432, and 334 nm in its electronic spectrum attributable to spin-allowed ligand field transitions.[57] Photoexcitation at wavelengths corresponding to these bands results in the labilization of the metal-ligand bond, and therefore facilitates the substitution of arene by solvent molecules. On-line irradiation at 488 nm with the laser light source yielded the family of $[Fe(AN)_{3\text{-}5}]^{2+}$ ions at thermal reaction times longer than 20 ms as the only products. Half-sandwich species of the type $[Fe(mes)(AN)_{2\text{-}3}]^{2+}$ were not found in the spectrum with a thermal reaction time as small as 10 ms (see Figure 37). The peak at m/z = 128.979 in the figure is very weak and the recognition of its isotopic pattern is not feasible. Its mass/charge ratio is 0.062 Da off the calculated theoretical value (129.0409) for $[Fe(mes)(AN)_2]^{2+}$, an unlikely error for the mass measurement by the TOF spectrometer. Owing to technical difficulties, this experiment was conducted only once. Further work will be undertaken to search for the short-lived half-sandwich intermediates in photolyzed solutions.

Figure 37

ESI-TOF mass spectrum of the products from the photolysis of an 80 μM $[Fe(mes)_2](PF_6)_2$ solution in acetonitrile (AN). The spectrum was acquired with a flow rate of 40 μL/h and at D = 0.7 mm, corresponding to a thermal reaction time of 10 ms.

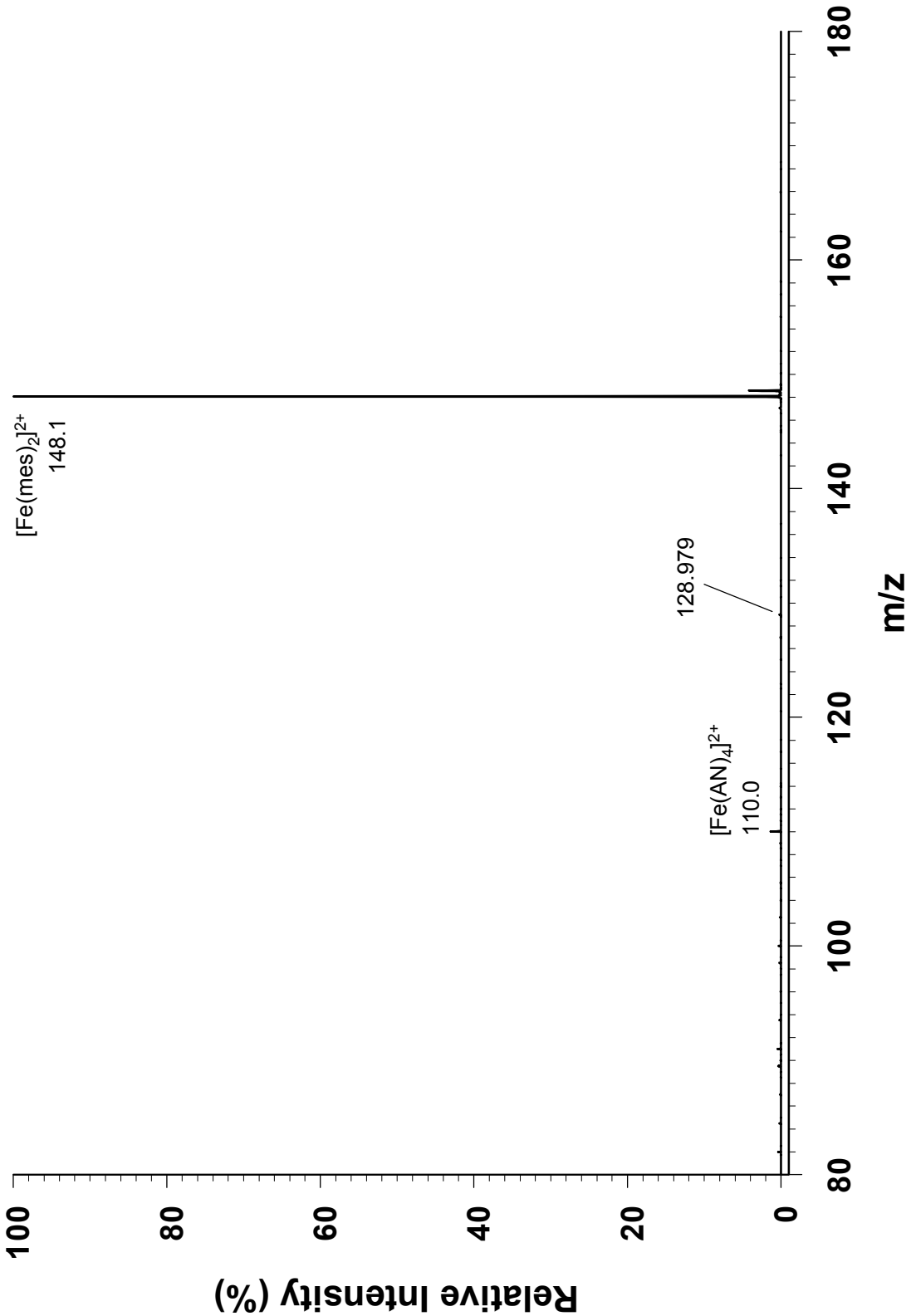
Relative Intensity (%)
100
80
60
40
20
0
80
100
120
140
160
180
m/z
[Fe(mes)2]2+
148.1
128.979
[Fe(AN)4]2+
110.0

CHAPTER 4

DISCUSSION

4.1 Photochemistry in the ESI nanospray tip

The irradiated section of the silica nanospray tip for ESI in this study functions as a micro flow cell. The cell can be approximated as a cylinder with inner diameter of 14 μm, as measured from a working tip in Figure 8, and a length of ca. 0.6 mm, resulting from the light beam emerging from an optical fiber (core o.d. 0.3 mm) that is positioned close to the tip and lying at an angle of 30 degrees relative to the tip. With a flowing sample solution at a concentration level of micromoles per liter of the photosensitive substance, the effect of light intensity and sample flow rate on the nature of the photoprocess was investigated. As shown in Figure 38, at a constant flow rate and D value, laser power at the irradiation zone was varied from 112 mW to 280 mW for the 40 μM acetonitrile solution of $[CpFebz]PF_6$. Although the absolute counts of product ions increased with the corresponding increase of laser power, no new products besides the $[CpFe(AN)_{2\text{-}3}]^+$ and $[Fe(AN)_{3\text{-}6}]^{2+}$ series were found and the photoproduct patterns in terms of relative intensities were basically identical. The ratio of products to the precursor $[CpFebz]^+$, as measured by peak intensities, changed dramatically, however, which gave evidence of the increasing importance of a primary photo-deligation of the precursor. On the other hand, the time that a given volume of sample solution is exposed to the light beam is determined by the solution flow rate through the cylindrical cell. More photons are absorbed by a sample passing through the irradiation zone as the flow rate decreases at a fixed intensity of laser irradiation. The product distribution in the photolysis of a 70 μM $[CpFebz]PF_6$ solution in acetonitrile with constant light intensity and D value but varied flow

Figure 38

Products from the photolysis of a 40 μM [CpFebz]PF_6 solution in acetonitrile (AN) at varied irradiation intensities. Mass spectra were acquired at a flow rate of 160 μL/h with laser power output at the optical fiber of (a) 112 mW, (b) 145 mW, (c) 190 mW, (d) 235 mW, and (e) 280 mW.

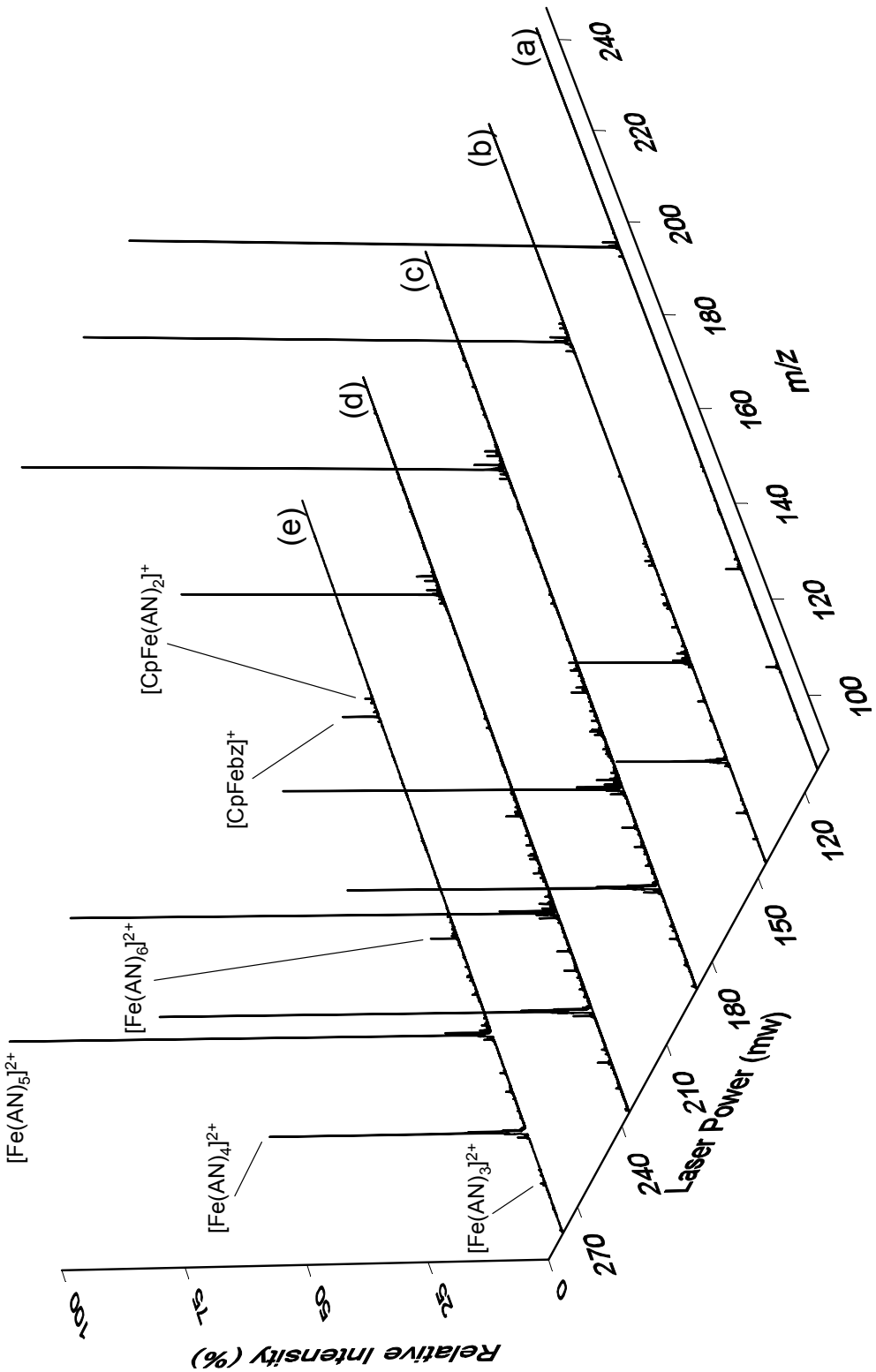
Relative Intensity (%)
0
25
50
75
100
m/z
100
120
140
160
180
200
220
240
Laser Power (mW)
120
150
180
210
240
270
(a)
(b)
(c)
(d)
(e)
[Fe(AN)3]2+
[Fe(AN)4]2+
[Fe(AN)5]2+
[Fe(AN)6]2+
[CpFebz]+
[CpFe(AN)2]+

rate is shown in Figure 39. The finding that no new products appear as flow rate changes indicates that secondary photoprocesses are not important with the flow cell and the light source used in this study.

4.2 Photolysis mechanism of [CpFebz]PF_6 at room temperature

The photolysis of [CpFe(η^6-arene)]PF_6 in acetonitrile at -40^{o}C releases the arene and forms the half-sandwich complex, $[CpFe(AN)_3]^+$, a purple intermediate stable for several hours at that temperature. This intermediate was characterized at low temperature by ^{1}H NMR, electronic spectroscopy, and cyclic voltammetry with a rotating photoelectrode.[32]. Warming the irradiated solution from -40^{o}C to 20^{o}C made the purple color disappear from the system and yielded ferrocene and fully solvated Fe(II) species. The $[CpFe(AN)_3]^+$ species was assigned as an intermediate generated from the photoreaction, and the ferrocene and $[Fe(AN)_6]^{2+}$, as shown in Scheme 4, were believed to be the products from a subsequent thermal reaction in which the intermediate lost the Cp ring.

The successful identification of $[CpFe(AN)_{2\text{-}3}]^+$ at room temperature by the on-line ESI-MS technique in this study establishes the existence of the half-sandwich intermediate. Moreover, the dramatic change in relative abundance as the residence time of this species in the nanospray tip is changed from 17 ms (Figure 9a) to 50 ms (Figure 9b) illustrates that it possesses a short lifetime in solution at room temperature. Deciphering the overall relationship of the two types of species, $[CpFe(AN)_{2\text{-}3}]^+$ and $[Fe(AN)_{3\text{-}6}]^{2+}$, generated from the photoreaction becomes the key in elucidating the mechanism. A quantitative

Figure 39

Product distribution from the photolysis of a 70 μM [CpFebz]PF_6 solution in acetonitrile (AN) at varied flow rates. Mass spectra were acquired with constant laser intensity, D = 1.25 mm, and at a flow rate of (a) 20 μL/h, (b) 40 μL/h, (c) 60 μL/h.

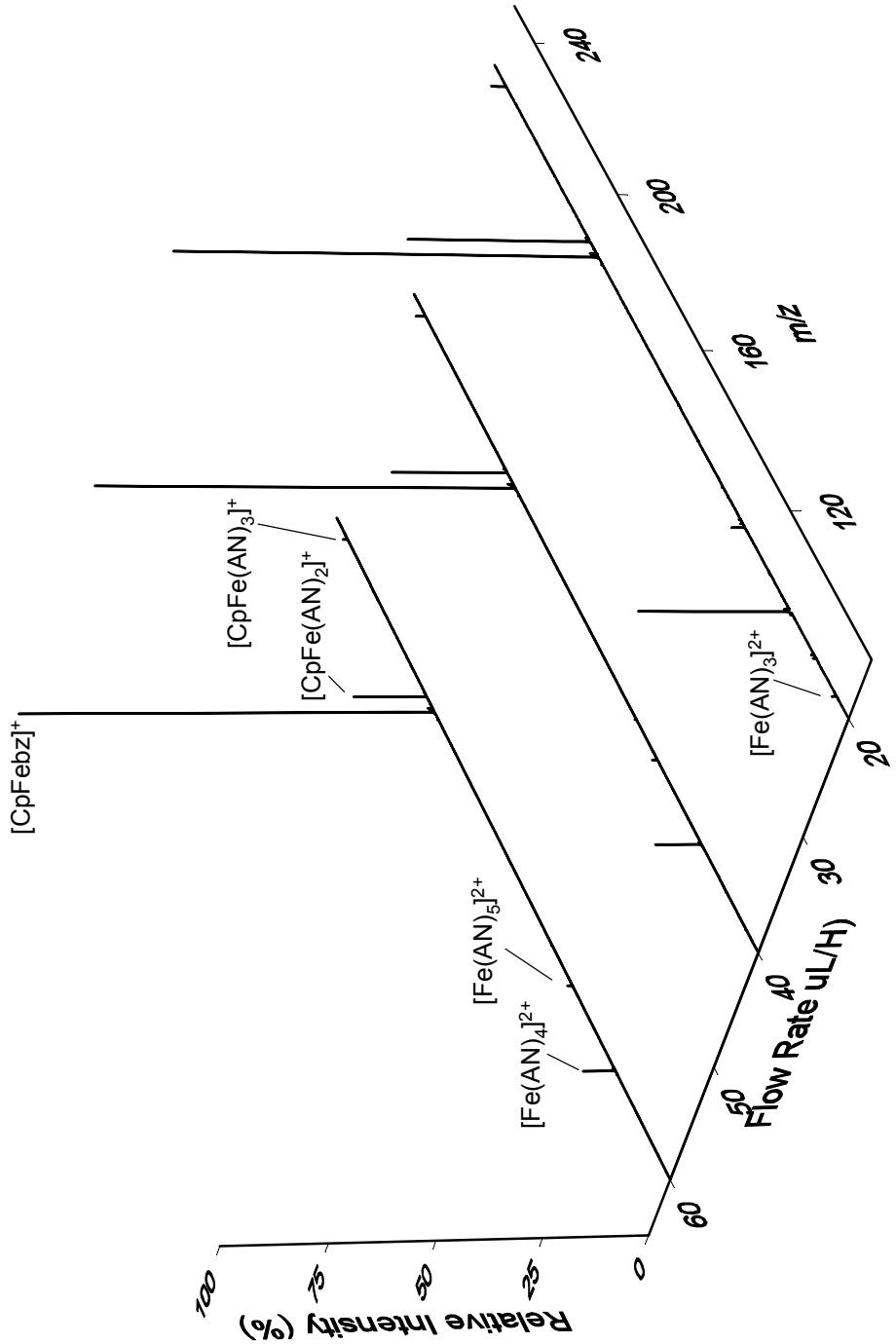
[CpFebz]+
[CpFe(AN)2]+
[CpFe(AN)3]+
[Fe(AN)4]2+
[Fe(AN)5]2+
[Fe(AN)3]2+
Relative Intensity (%)
m/z
Flow Rate uL/H)

measurement of the distribution pattern was obtained by calculating the intensity (I) ratio, R, of the signals arising from members of the two families, $\Sigma I_{\{[Fe(AN)_m]^{2+}\}}/\Sigma I_{\{[CpFe(AN)_n]^{+}\}}$. Presented in Figure 40 is the plot of R against D, corresponding to the thermal reaction time for the intermediate at a constant flow rate. It reveals the simultaneous disappearance of the half-sandwich intermediate and the growth of the $[Fe(AN)_m]^{2+}$ family as the thermal reaction time increases. A parent-offspring relationship between $[CpFe(AN)_n]^{+}$ and $[Fe(AN)_m]^{2+}$ is thus recognized as well as the time frame of milliseconds for the short-lived intermediate. The lifetime of $[CpFe(AN)_3]^{+}$ at room temperature can be estimated as ca. 50 ms based on the data obtained in this study. The room temperature photochemistry of $[CpFebz]^{+}$ is explicitly depicted in Scheme 6.

Scheme 6

$$2[CpFe(\eta^6\text{-benzene})]^{+} \xrightarrow[CH_3CN]{h\nu,\ 20^oC} 2[CpFe(CH_3CN)_3]^{+} + 2\text{benzene}$$

$$2[CpFe(CH_3CN)_3]^{+} \xrightarrow[\text{fast}\ \ 20^oC]{} FeCp_2 + [Fe(CH_3CN)_6]^{2+}$$

The coordinatively-unsaturated species observed in the mass spectrum of a photolyzed solution of $[CpFebz]^{+}$ in acetonitrile, e.g., five-coordinated $[CpFe(AN)_2]^{+}$ and four-coordinated $[Fe(AN)_4]^{2+}$, most likely resulted from collisionally-induced dissociation (CID) of AN from $[CpFe(AN)_3]^{+}$ and $[Fe(AN)_6]^{2+}$, respectively, in the region following the first skimmer. Similar dissociation of AN

Figure 40

Product distribution represented by ratio, R of $[Fe(AN)_m]^{2+}$ to $[CpFe(AN)_n]^+$ series generated from the photolysis of a 40 μM $[CpFebz]PF_6$ solution in acetonitrile, as a function of distance D from the laser beam to the nanospray tip end. Corresponding thermal reaction time T is also shown. $R = \Sigma I_{\{[Fe(AN)_m]^{2+}\}} / \Sigma I_{\{[CpFe(AN)_n]^+\}}$; m = 3 - 5; n = 1 - 3.

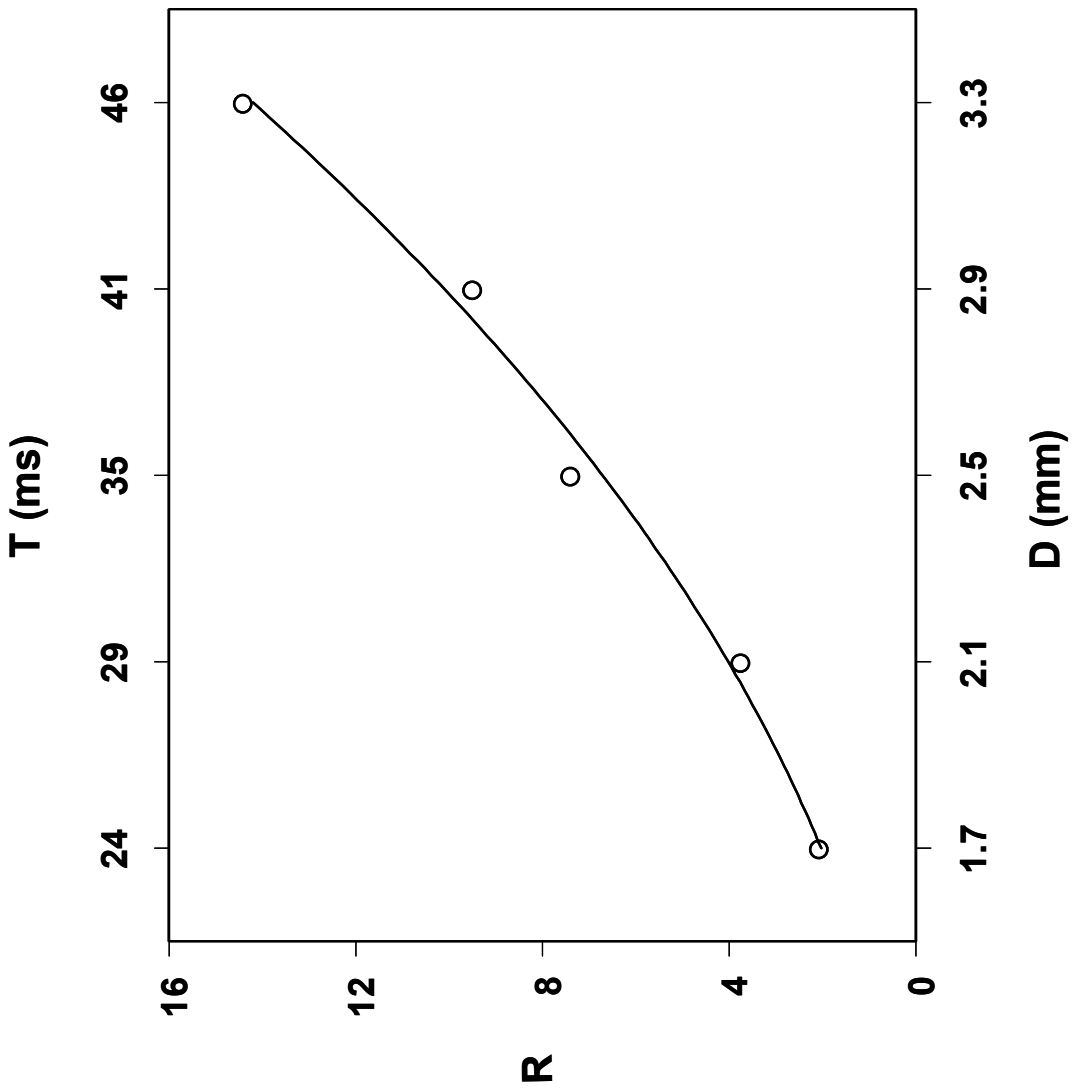
T (ms)
24
29
35
41
46
R
16
12
8
4
0
D (mm)
1.7
2.1
2.5
2.9
3.3

from a dipositive transition metal ion was also observed[104] in the ESI-MS study of the photoproducts from $[Ru(bpy)_2(dmbpy)](ClO_4)_2$ in AN solution (bpy is 2,2'-bipyridine; dmbpy is 3,3'-dimethyl-2,2'-bipyridine). Consistent with this explanation, we observed (Table 9) that increasing the kinetic energy of the electrosprayed ions by raising the skimmer 1 voltage favored the production of species with fewer coordinated AN molecules and decreased the abundance of ions with more coordinated AN molecules in the mass spectra.

It has also been noted that with rigorously dried solvent, no ferricenium (m/z = 186.0), resulting from the oxidation of ferrocene during the ESI process, was observed. In contrast, the oxidation of ferrocene in the ESI process with samples prepared with either HPLC-grade acetonitrile[101] or 50% aqueous acetonitrile[120] was reported and predicted in the computational simulation of a ferrocene sample in CH_3CN/H_2O (90/10 v/v).[121] To investigate this discrepancy, ferrocene samples in DCE solvents with and without drying/distilling treatment were run under the same ESI-MS conditions. In Figure 41a, the mass spectrum of 200 μM Cp_2Fe with 20 μM tetrabutylammonium (TBA) showed no signal from ferricenium. However, once the solution was prepared with non-treated DCE, a peak with about 20% relative intensity at m/z = 186.0 as that of TBA was readily recorded (Figure 41b), even though the ferrocene concentration was scaled down to 20 μM with the same concentration of TBA. Samples from the photolysis study of $[CpFebz]PF_6$ prepared with two types of DCE solvents exhibit an impressive effect of trace amounts of water on the capacity to detect by ESI-MS the ferrocene that is formed from the reaction in Scheme 6. As shown in Figure 42,

Table 9 Observed relative intensity* (RI) of $[Fe(AN)_{3\text{-}5}]^{2+}$ as a function of the skimmer 1 potential

Skimmer 1 Potential (V)	$RI_{[Fe(AN)_3]^{2+}}$ (%)	$RI_{[Fe(AN)_4]^{2+}}$ (%)	$RI_{[Fe(AN)_5]^{2+}}$ (%)
11	0.029	28.30	3.57
16	0.036	20.10	2.87
20	0.073	17.80	2.19

* Setting the intensity of $[CpFebz]^+$ equal to 100%.

Figure 41

ESI-TOF mass spectra of solutions of ferrocene and tetrabutylammonium (TBA) hexafluorophosphate prepared with dried and non-dried 1,2-dichloroethane (DCE) solvents. (a) 200 μM Cp_2Fe and 20 μM TBA in dried DCE; (b) 20 μM Cp_2Fe and 20 μM TBA in non-dried DCE.

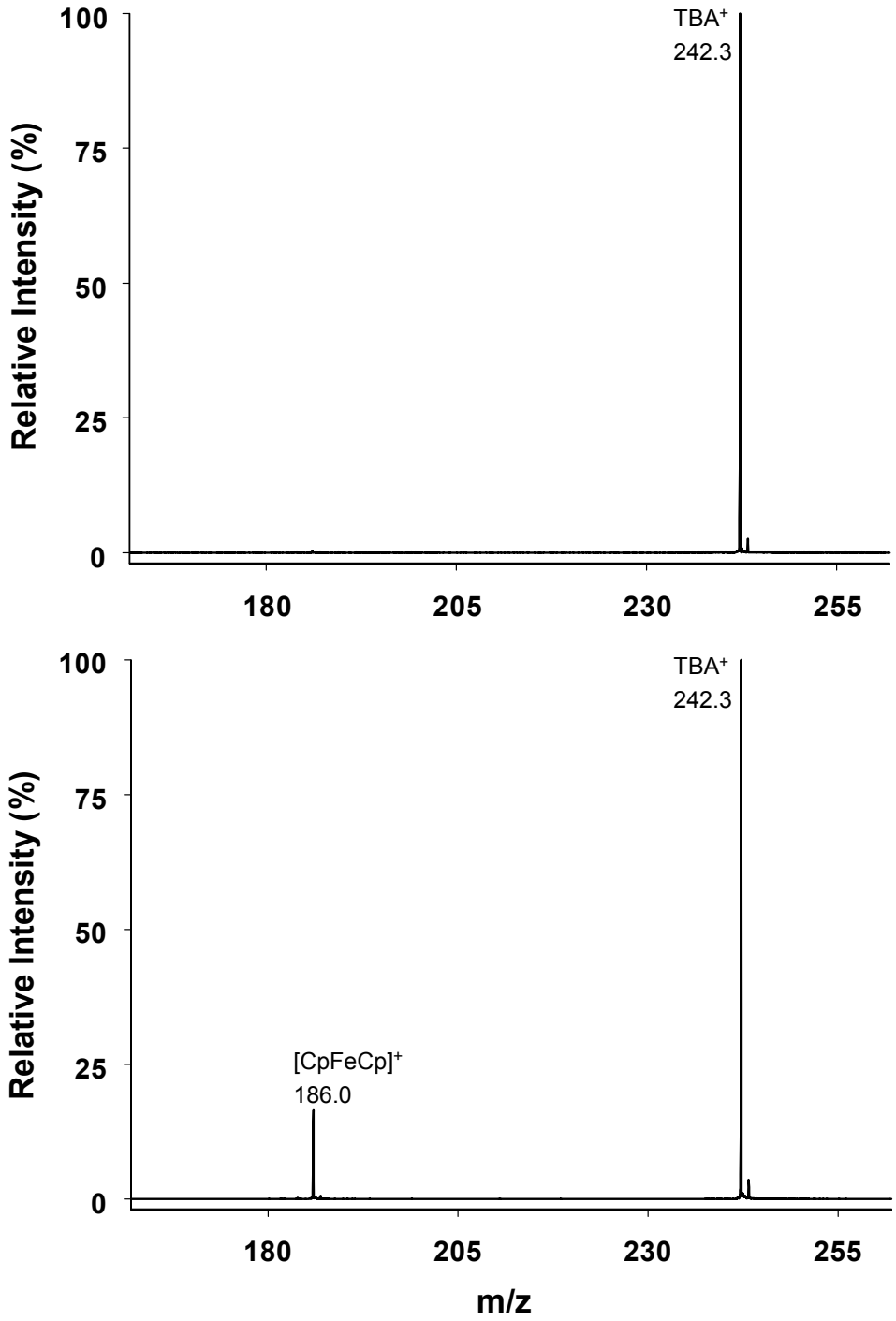
100
75
50
25
0
Relative Intensity (%)
TBA+
242.3
180
205
230
255
100
75
50
25
0
Relative Intensity (%)
TBA+
242.3
[CpFeCp]+
186.0
180
205
230
255
m/z

irradiation of a 40 μM [CpFebz]PF_6 solution prepared with freshly dried DCE gave a tiny ferricenium signal with a relative intensity of less than 0.2% of the precursor's base peak (Figure 42a and inset I), while no signal for the ferricenium was found in the spectrum with the same sample when the laser was off (inset II of Figure 42a). The ferricenium ion, as demonstrated in Figure 42b, with significant intensity and the unambiguous isotopic patterns was identified from the on-line 488 nm irradiation of a 20 μM [CpFebz]PF_6 solution prepared with the DCE that was pre-dried but stored for 46 days prior to use. In both cases, no ferricenium was detected from the non-irradiated samples. These results confirm that the oxidation of ferrocene occurs in the ESI process when the sample solution contains at least a trace amount of water, and more importantly, provides evidence of the detection of the ferrocene generated from the reaction outlined in Scheme 6. Here we have a similar situation to that reported by Berkel and Zhou[122] in their study on the extent of oxidation of nickel (II) octaethylporphyrin in the ESI process as a function of solution conductivity.

4.3 Mechanism of photoinitiated polymerization of CHO

Photolysis of [CpFebz]PF_6 in AN solution containing 0.8 - 400 mM of cyclohexene oxide (CHO) yielded the same products as those observed in pure AN, as well as a few new species. At the highest CHO concentration (400 mM), the fully ring-deligated Fe(II) complexes associated with CHO were identified as $[Fe(AN)_2(CHO)]^{2+}$, $[Fe(AN)_3(CHO)]^{2+}$, and $[Fe(AN)_4(CHO)]^{2+}$, along with $[Fe(AN)_{3\text{-}5}]^{2+}$. The latter also were observed both in lower CHO concentration

Figure 42

ESI-TOF mass spectra of photolyzed samples containing [CpFebz]PF_6 prepared with freshly dried and stored DCE solvents. (a) 40 μM [CpFebz]PF_6 in freshly dried DCE. Insets: I, no-light blank; II, peak at m/z = 186.0 magnified 546 times. (b) 20 μM [CpFebz]PF_6 in DCE stored for 46 days. Insets: I, no-light blank; II, peak at m/z = 186.0 magnified 3.3 times.

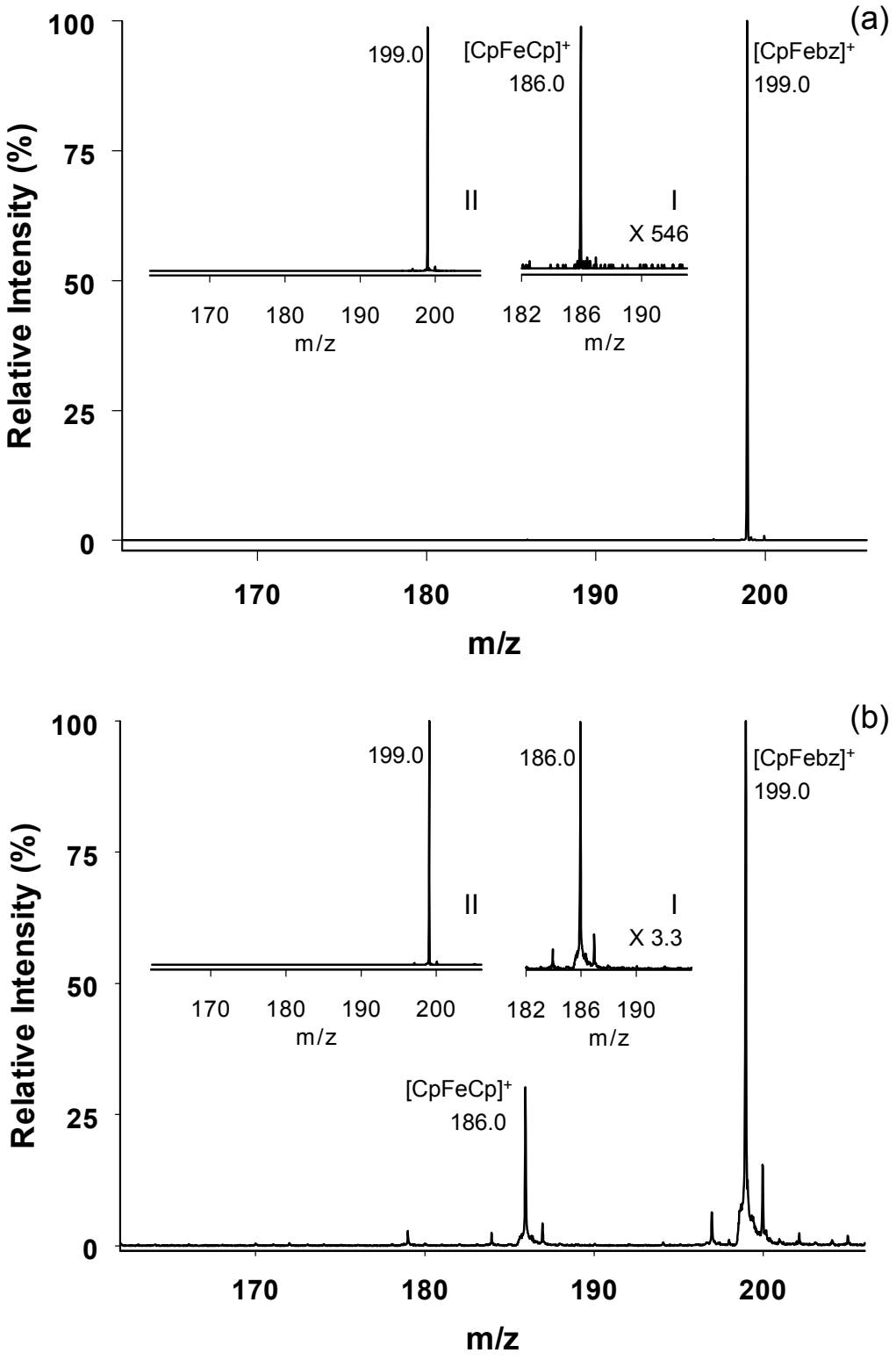
(a)
100
75
50
25
0
Relative Intensity (%)
199.0
[CpFeCp]+
186.0
[CpFebz]+
199.0
II
I
X 546
170 180 190 200
m/z
182 186 190
m/z
170
180
190
200
m/z
(b)
100
75
50
25
0
Relative Intensity (%)
199.0
186.0
[CpFebz]+
199.0
II
I
X 3.3
170 180 190 200
m/z
182 186 190
m/z
[CpFeCp]+
186.0
170
180
190
200
m/z

(≤ 40mM) and in pure AN solution. An identical parent-offspring relationship between $[CpFe(AN)_n]^+$ and $[Fe(AN)_m]^{2+}$ series is maintained with the CHO concentrations employed. In other words, the participation of CHO in the photoreaction of $[CpFebz]PF_6$ basically does not alter the photolysis mechanism. However, noticeable features are present in the new products as one looks at their formula. No AN in the coordination shell of $[CpFe(AN)_n]^+$ is substituted by CHO, though the substitution for $[Fe(AN)_m]^{2+}$ happens when CHO is as high as 400 mM. However, none of the substituted species involves more than one epoxide molecule in the iron complex ions in acetonitrile medium, and the total number of ligands, as already noted in the case of $[Fe(AN)_m]^{2+}$, is less than six. These results indicate that the poorly coordinating CHO does not compete effectively with AN for binding sites about the Fe(II) center in an AN environment, and the access of uncoordinated CHO to the CHO already bound to the iron(II) center is blocked in the AN medium.

When CHO was present in an AN solution of $[CpFebz]PF_6$, another product, X^+ (m/z = 140.1) was observed. This product has not yet been identified, but an analysis of its isotope pattern has established that it does not contain iron. X^+ was observed as long as CHO was present in the irradiated solutions. At high CHO concentrations (≥ 50 mM), a species corresponding to $[X(CHO)]^+$ was detected.

As a moderately polar solvent, acetonitrile accommodates the solvation of ions in its environment. The strong solvation effect inhibits other species like CHO from coordinating to the iron metal center, and to further start initiation and

propagation processes. Thus, it is not surprising to see no oligomers associated with iron species here. A similar reasoning, explaining only one CHO attachment at such high CHO concentrations, can be made for X^+. Accordingly, it was worthwhile to switch to a solvent that is less polar than AN for the CHO polymerization study, though we have kept it in mind that the polarity of the target solvent has to be high enough to maintain the ESI ionization process. That led us to 1,2-dichloroethane (DCE). It happened to be the same solvent used for the system of $[CpFe(\eta^6\text{-arene})]^+$ and CHO in the mechanistic study of photochemical arene release[38] and in the kinetic investigation of CHO polymerization caused by active species that had not been characterized.[44]

Irradiating the $[CpFebz]PF_6$ and CHO solutions in DCE yielded a rich vein of new products. Unlike those obtained from the AN solutions that show no ions with CHO molecule attachment outside the first coordination sphere of the metal, two major series of products from the DCE system were obtained as $[X(CHO)_q]^+$ (q = 1 – 4) and $[Fe(H_2O)(CHO)_j]^{2+}$ (j = 4 – 10), in addition to the two minor series, $[Fe(CHO)_i]^{2+}$ (i = 5 – 7) and $[(H_3O)(CHO)_p]^+$ (p = 2 – 5), in the photolysis followed by a 170 ms thermal reaction in the ESI tip (see Figure 16). The number of CHO units attached to the Fe-containing species is now far beyond that necessary for a coordinatively saturated Fe(II) complex.

The photolysis mechanism of $[CpFebz]PF_6$ in DCE with 400-fold molar excess of CHO was investigated in a much shorter post-irradiation thermal reaction time that ranged from 5 ms to 20 ms. In addition to product families of $[X(CHO)_q]^+$ and $[Fe(H_2O)(CHO)_j]^{2+}$ that were observed in the experiments with a

longer thermal reaction time, a new major product family with general formula $[CpFe(H_2O)(CHO)_n]^{2+}$ (n = 1 - 4) was detected. Notice the chemically analogous structural character of the new species to those probed in acetonitrile solution in the absence of CHO. The intermediate nature of this half-sandwich product series can be recognized, at least qualitatively, by comparing the changes of its peak intensities in the mass spectra relative to the peak intensities of two neighboring species, $[X(CHO)_q]^+$ and $[Fe(H_2O)(CHO)_j]^{2+}$, as a function of thermal reaction time. Figure 19 – 22 reveal that species containing one Cp ring diminish in abundance, with concomitant increases in the abundances of members of the other families, as the thermal reaction time increases. The overall trend of product distribution for all members of the three families is shown in Figure 43, in which the R, defined as the ratio of $\Sigma I_{\{[Fe(H_2O)(CHO)_{2-11}]^{2+}\}}$ to $\Sigma I_{\{[CpFe(H_2O)(CHO)_{0-4}]^+\}}$ and the ratio of $\Sigma I_{\{[X(CHO)_{0-4}]^+\}}$ to $\Sigma\{I_{\{[CpFe(H_2O)(CHO)_{0-4}]+\}}$ with symbol ∇ and ■, respectively, are plotted against the variation of D. As D changed from 0.55 mm to 2.22 mm, corresponding to a thermal reaction time from 5 ms to 20 ms, more of the $[Fe(H_2O)(CHO)_j]^{2+}$ and $[X(CHO)_q]^+$ family members replace those from the $[CpFe(H_2O)(CHO)_n]^+$ family. Reflected in the curves is the intermediate character of $[CpFe(H_2O)(CHO)_n]^+$ in the photochemical reaction. It dominates in the mass spectrum at short reaction time, since most of its members survive the transit to the spray end without decomposition, but diminishes as the time exceeds 20 ms. Based on its dependence on the thermal reaction time, the lifetimes of the half-sandwich intermediates at room temperature can be estimated at ca. 20 ms, much shorter than similar intermediates belonging to the $[CpFe(AN)_{2-3}]^+$ family

Figure 43

Product distribution, represented by ratio R, among $[CpFe(H_2O)(CHO)_n]^+$, $[Fe(H_2O)(CHO)_j]^{2+}$, and $[X(CHO)_q]^+$ series generated from the photolysis of a 1,2-dichloroethane solution containing 100 μM $CpFebzPF_6$ and 40 mM cyclohexene oxide (CHO) as a function of distance D from the laser beam to the nanospray tip end. Corresponding thermal reaction time T is also shown. R is the ratio of $\Sigma I_{\{[Fe(H_2O)(CHO)_j]^{2+}\}}/\Sigma I_{\{[CpFe(H_2O)(CHO)_n]^+\}}$ (symbolized by ∇); or $\Sigma I_{\{[X(CHO)_q]^+\}}/\Sigma I_{\{[CpFe(H_2O)(CHO)_i]^+\}}$ (symbolized by ■); n = 0 - 4; j = 2 - 11; q = 0 - 4.

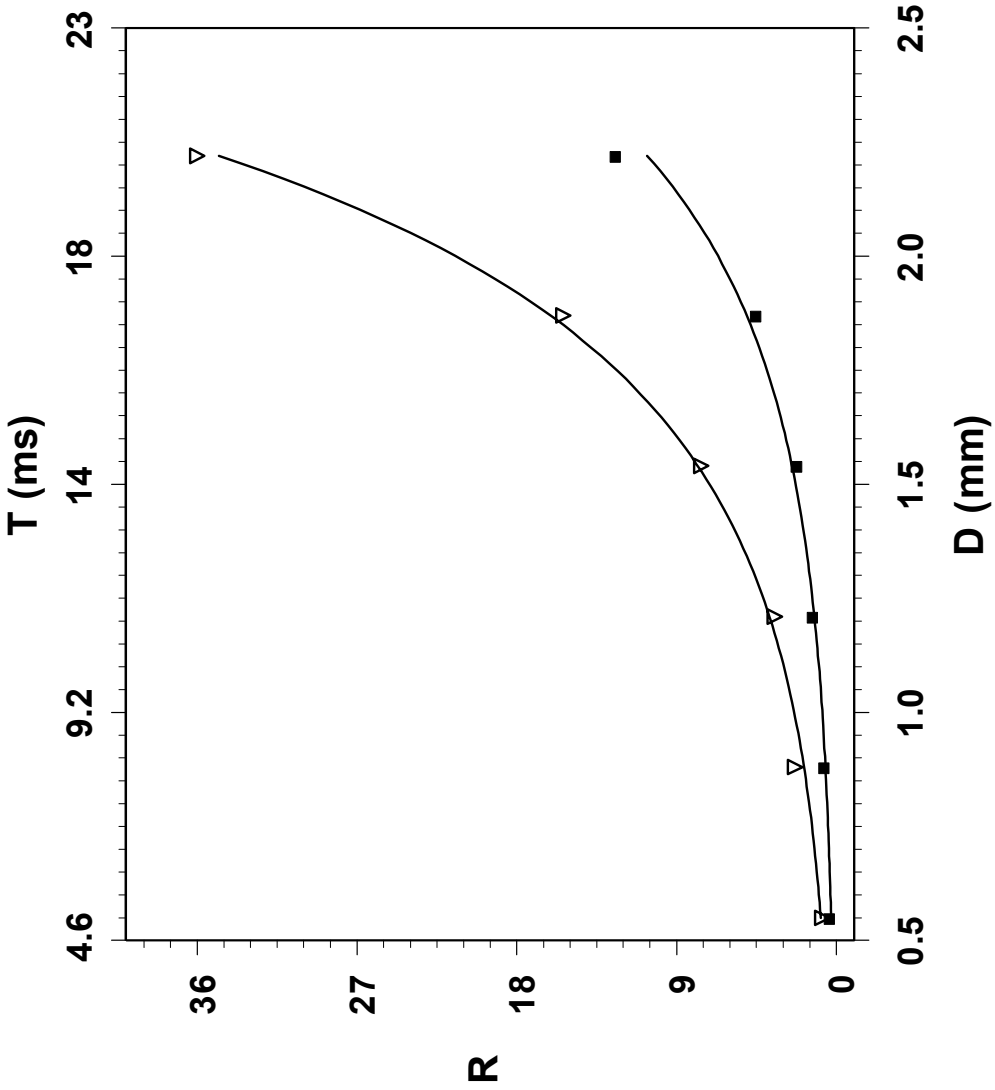
T (ms)
23
18
14
9.2
4.6
D (mm)
2.5
2.0
1.5
1.0
0.5
R
36
27
18
9
0

that are stabilized by acetonitrile ligands. This is consistent with the previous conclusion that CHO is a weaker ligand than acetonitrile and is less able to form a stable half-sandwich complex ion with $[CpFe]^+$. The curves in Figure 43 also support the parent-offspring relationship in general for the families of $[Fe(H_2O)(CHO)_j]^{2+}$ and $[X(CHO)_q]^+$ that are generated from the intermediate family, $[CpFe(H_2O)(CHO)_n]^+$, in a thermal reaction following the photolysis of $[CpFebz]PF_6$. It should be noted from the development of the two offspring families that the iron-containing series grows faster than the $[X(CHO)_q]^+$ series.

To confirm the identities of the Fe(II) products for the purpose of elucidating the initiation/polymerization mechanism, the observed mass information for the four Fe(II) species, specifically comprising five through eight CHO molecules in the family $[Fe(H_2O)(CHO)_m]^{2+}$ (m = 5, 6, 7, 8), were scrutinized by comparing the calibrated mass/charge ratios and isotopic patterns with those from theoretical prediction. Summarized in Table 10 are comparisons of mass/charge ratios for monoisotopic peaks of $[Fe(H_2O)(CHO)_m]^{2+}$ and the mass differences among them for each added CHO molecule with respect to the corresponding theoretical monoisotopic mass of CHO. The mass/charge measurement errors for both the species themselves and the mass difference due to the consecutive addition of CHO molecules are less than 0.01 Da. The accuracy of these measurements is sufficient for identifying the products, given the resolution power of about 4000 for the mass/charge analysis by the TOF spectrometer.

Table 10 List of observed and expected mass/charge ratios, the measurement errors for $[Fe(H_2O)(CHO)_{5\text{-}8}]^{2+}$, and the mass of attached CHO molecules

Formula	Measured m/z	Resolution Power	Calculated m/z	Error (Da)	∆m of the Attached CHO*	Error in ∆m (Da)
$[Fe(H_2O)(CHO)_5]^{2+}$	282.155	3675	282.1557	-0.001		
					49.033	-0.004
$[Fe(H_2O)(CHO)_6]^{2+}$	331.188	3909	331.1923	-0.004		
					49.034	-0.003
$[Fe(H_2O)(CHO)_7]^{2+}$	380.222	4125	380.2289	-0.007		
					49.036	-0.001
$[Fe(H_2O)(CHO)_8]^{2+}$	429.258	4217	429.2654	-0.007		

* The monoisotopic m/z values for CHO are 98.0732 and 49.0366 for z = 1 and z = 2, respectively.

The identities of the Fe-containing species can be further confirmed by the consistency of their measured isotopic patterns with those by theoretical calculation, as demonstrated in Figure 44. For the $[Fe(H_2O)(CHO)_m]^{2+}$ species, their isotopic features in terms of the peak positions and relative intensities for the isotopic peaks of the mass spectra are mainly determined by the contribution from non-monoisotopes of $_{26}Fe^{54}$, $_{26}Fe^{57}$, and $_{6}C^{13}$ with natural abundances of 5.83%, 2.19%, and 1.11%, respectively. Monoisotopic peaks of these species stem from the corresponding monoisotopes of $_{26}Fe^{56}$ and $_{6}C^{12}$, while the two peaks at mass/charge ratio less than the monoisotopic one by 1 Da and 0.5 Da with appropriate intensity ratio confirm the existence of iron in these species due to the contribution of $_{26}Fe^{54}$. The three peaks at mass/charge ratio larger by 0.5, 1, 1.5 Da than the monoisotopic one reflect the combined contribution of $_{6}C^{13}$ and $_{26}Fe^{57}$. Identical abundance distributions among the isotopic peaks for the observed $[Fe(H_2O)(CHO)_{5-6}]^{2+}$ species with high intensity in the mass spectra can be seen with respect to the calculated peak distributions. When the signal intensity becomes weaker as in the cases of the $[Fe(H_2O)(CHO)_{7-8}]^{2+}$ species upon addition of CHO monomers, the intensities at mass/charge ratios of 379.7 and 428.7 for $\{[Fe(H_2O)(CHO)_7]^{2+} - 0.5\}$ and $\{[Fe(H_2O)(CHO)_7]^{2+} - 0.5\}$, respectively, are relatively higher than those from theoretical prediction, probably due to the contribution of peaks from other minor species at these m/z positions. However, the same general isotopic patterns compared to the calculated ones establish the identities of these iron-containing species.

Figure 44

Comparison of isotopic patterns for $[Fe(H_2O)(CHO)_m]^{2+}$ (m = 5, 6, 7, 8) observed in the spectrum of Figure 17 with those from theoretical calculation. (a) $[Fe(H_2O)(CHO)_5]^{2+}$; (b) $[Fe(H_2O)(CHO)_6]^{2+}$; (c) $[Fe(H_2O)(CHO)_7]^{2+}$; and (d) $[Fe(H_2O)(CHO)_8]^{2+}$.

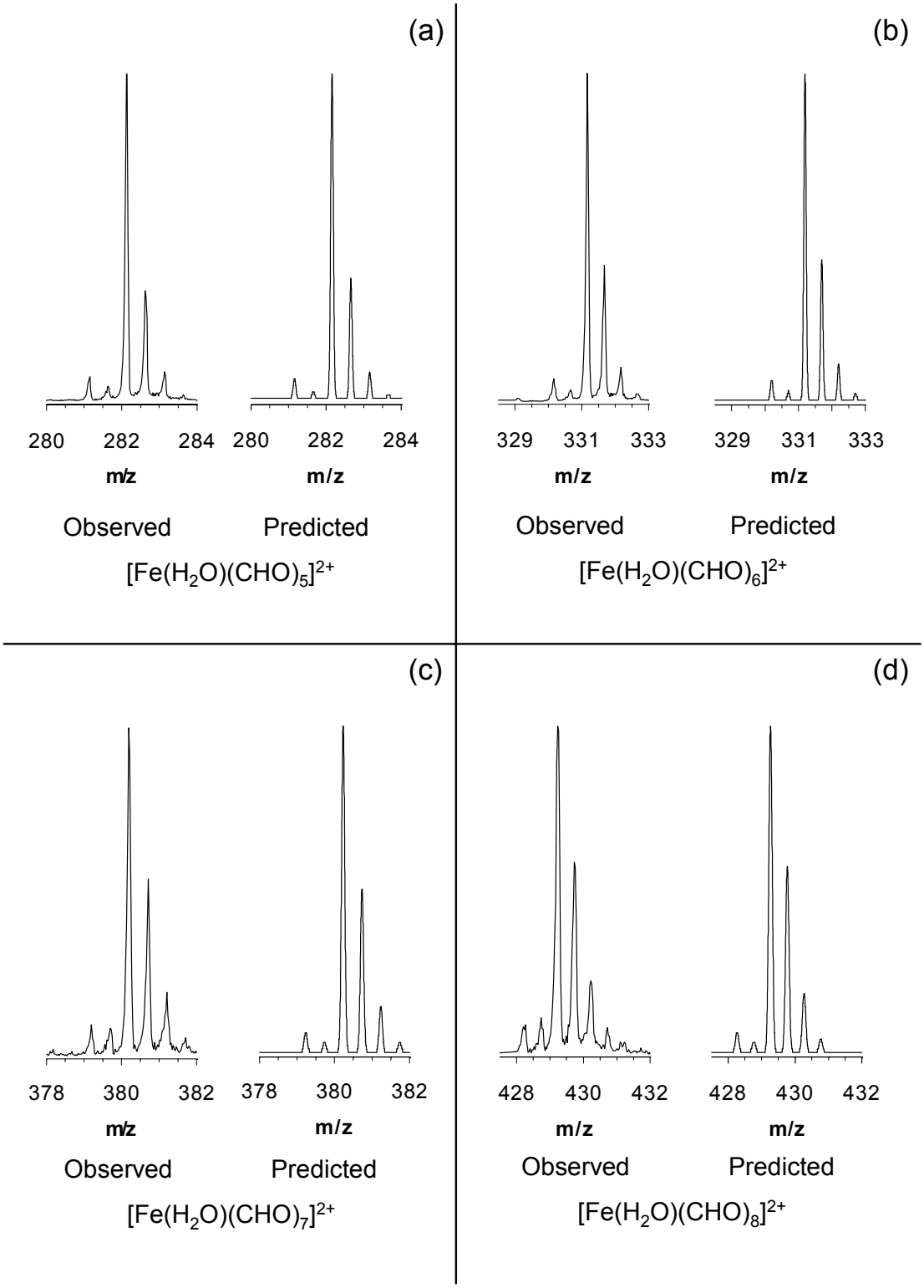
(a)
280 282 284
m/z
Observed
280 282 284
m/z
Predicted
$[Fe(H_2O)(CHO)_5]^{2+}$
(b)
329 331 333
m/z
Observed
329 331 333
m/z
Predicted
$[Fe(H_2O)(CHO)_6]^{2+}$
(c)
378 380 382
m/z
Observed
378 380 382
m/z
Predicted
$[Fe(H_2O)(CHO)_7]^{2+}$
(d)
428 430 432
m/z
Observed
428 430 432
m/z
Predicted
$[Fe(H_2O)(CHO)_8]^{2+}$

Similarly, the addition of up to four CHO molecules onto X^+ can be verified from the mass difference of the series formed by consecutive addition of CHO, at a mass error of less than 0.01 Da (see Table 11). The measured mass for each added CHO unit is in agreement with the predicted value to an accuracy of better than 100 ppm.

The identities of $[CpFe(H_2O)(CHO)_{0-4}]^+$ are confirmed in the same way by comparing the masses of their monoisotopic peaks with the theoretical values and the mass difference among them for each added CHO molecule with the calculated CHO monoisotope mass, as summarized in Table 12. The errors for the mass measurements of the intermediate type ions are within 110 ppm of the calculated values and the mass measurement accuracy for each added CHO is at the same level of agreement as for the other two product families.

The water present in the Fe-containing products most likely originated from moisture introduced to the rigorously dried solvent during sample preparation. The stabilization function of the water ligand toward both the half-sandwich intermediates and the fully ring-deligated Fe(II) complexes in the poorly coordinating medium DCE is essential to keep these active species living long enough to add CHO molecules in the reaction system. Signals corresponding to the water-free products, $[CpFe(CHO)_{1-5}]^+$ and $[Fe(CHO)_{5-8}]^{2+}$, as well as the products with more than one water, namely, $[Fe(H_2O)_2(CHO)_{3-11}]^{2+}$ and $[Fe(H_2O)_3(CHO)_{2-4}]^{2+}$, also appeared in the mass spectra, but with diminished intensities. No Fe-containing species with more than three water molecules was observed.

Table 11 List of observed mass/charge ratios for $[X(CHO)_{0-4}]^+$ and the measurement errors for the mass of attached CHO molecules

Formula	Measured m/z	Resolution Power	Δm of the Attached CHO*	Error in Δm (Da)
$[X]^+$	140.112	3121		
			98.081	0.008
$[X(CHO)]^+$	238.193	3406		
			98.082	0.009
$[X(CHO)_2]^+$	336.275	4294		
			98.079	0.006
$[X(CHO)_3]^+$	434.354	4382		
			98.078	0.005
$[X(CHO)_4]^+$	532.453	4111		

* The theoretical monoisotopic m/z for CHO is 98.0732 Da.

Table 12 List of observed and expected mass/charge ratios, the measurement errors for $[CpFe(H_2O)(CHO)_{0\text{-}4}]^+$, and the mass of attached CHO molecules

Formula	Measured m/z	Resolution Power	Calculated m/z	Error (Da)	Δm of the Attached CHO *	Error in Δm (Da)
$[CpFe(H_2O)]^+$	138.970	3509	138.9846	-0.015		
					98.073	0.000
$[CpFe(H_2O)(CHO)]^+$	237.043	3735	237.0578	-0.015		
					98.071	-0.002
$[CpFe(H_2O)(CHO)_2]^+$	335.114	4060	335.1310	-0.017		
					98.068	-0.005
$[CpFe(H_2O)(CHO)_3]^+$	433.182	3848	433.2041	-0.022		
					98.067	-0.006
$[CpFe(H_2O)(CHO)_4]^+$	531.249	4282	531.2773	-0.028		

* The monoisotopic m/z values of CHO are 98.0732 and 49.0366 for z = 1 and z = 2, respectively.

It is unlikely that all of the molecules present in the heavier members of the $[Fe(H_2O)(CHO)_j]^{2+}$ and $[CpFe(H_2O)(CHO)_n]^+$ series are bound directly to the metal, since Fe(II) rarely exhibits coordination numbers above six.[123] Recall the difficulty of CHO in competing with AN for the coordination sites on Fe(II) and the fact that no more than six acetonitrile molecules as ligands of Fe(II) are observed from the photolysis of $[CpFebz]PF_6$ in acetonitrile. Consequently, other chemical structures for the identified $[Fe(H_2O)(CHO)_j]^{2+}$ and $[CpFe(H_2O)(CHO)_n]^+$ product series have to be deduced. We have considered two alternative models to describe the structures of these species resulting from ion-molecule association in the condensed phase. A similar analysis was reported for the cationic oligomerization of CHO with perfluorinated compounds in the gas phase.[82] Common to each model is the assumption that the metal forms up to six strong coordinate-covalent bonds to ligands in its first coordination sphere. In the cluster model (Equation 24), the remaining molecules reside on the periphery as a kind of loose “solvation shell” held by weaker ion-dipole forces. Many examples of such van der Waals clusters of solvent molecules surrounding a cationic core have been reported.[124] Nonetheless, we discount this model in our system on grounds that similar clusters are absent in samples electrosprayed from AN (see Figure 7), a solvent possessing a larger dipole moment than that of CHO (3.92 vs. 2.08 Debye[125,126]). In the polymer model (Equation 25), a coordinated CHO monomer undergoes nucleophilic attack by the oxygen atom of an uncoordinated monomer unit.[127] The ensuing C-O bond formation opens the strained three-membered ring and creates another cationic site for continued chain growth.

According to this model, which accommodates all of our experimental observations, products such as $[(H_2O)Fe(CHO)_{15}]^{2+}$, $[Fe(CHO)_8]^{2+}$, and $[CpFe(H_2O)(CHO)_5]^{2+}$ contain a growing polymer chain bound directly to the metal center. The observation that X^+ forms products containing up to five CHO units also is consistent with the polymer model, and we tentatively propose that this non-iron species is an active initiator for epoxide polymerization.

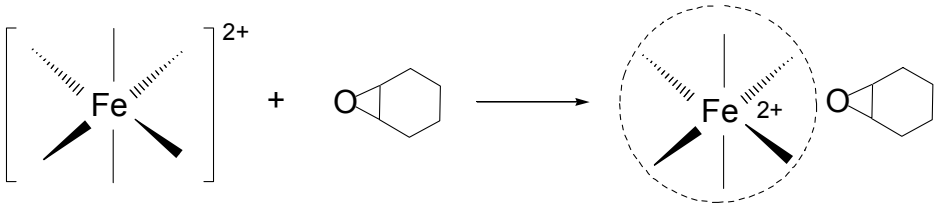

(24)

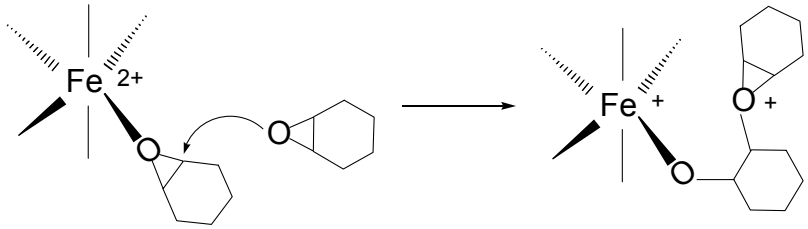

(25)

The chain growth nature of the $[X(CHO)_q]^+$ series was examined in a CID experiment by changing the effective potential felt by the electrosprayed ions to study their behavior in gas phase. Figure 45a displays the relative intensity of $[X(CHO)_{1\text{-}4}]^+$ species relative to that of initiating species, X^+, as a function of skimmer 1 potential in the range of 11.5 V to 50 V, the maximum set for the instrument. When the skimmer 1 was increased from 11.5 V to 23 V, the intensities of the species formed in the propagation step, i.e., $[X(CHO)_{2\text{-}4}]^+$,

Figure 45

Intensity distribution of initiating species and oligomers from $[X(CHO)_q]^+$ series in CID experiments. The sample contained 75 μM $[CpFebz]PF_6$ and 40 mM CHO in DCE and was pumped at 20 μL/h to the ESI while irradiated at 488 nm with D = 8.7 mm. (a) R represents the intensity ratios of $[X(CHO)_{1-4}]^+$ to $[X]^+$; (b) R' is the intensity ratio of $[X]^+$ to $[CpFebz]^+$.

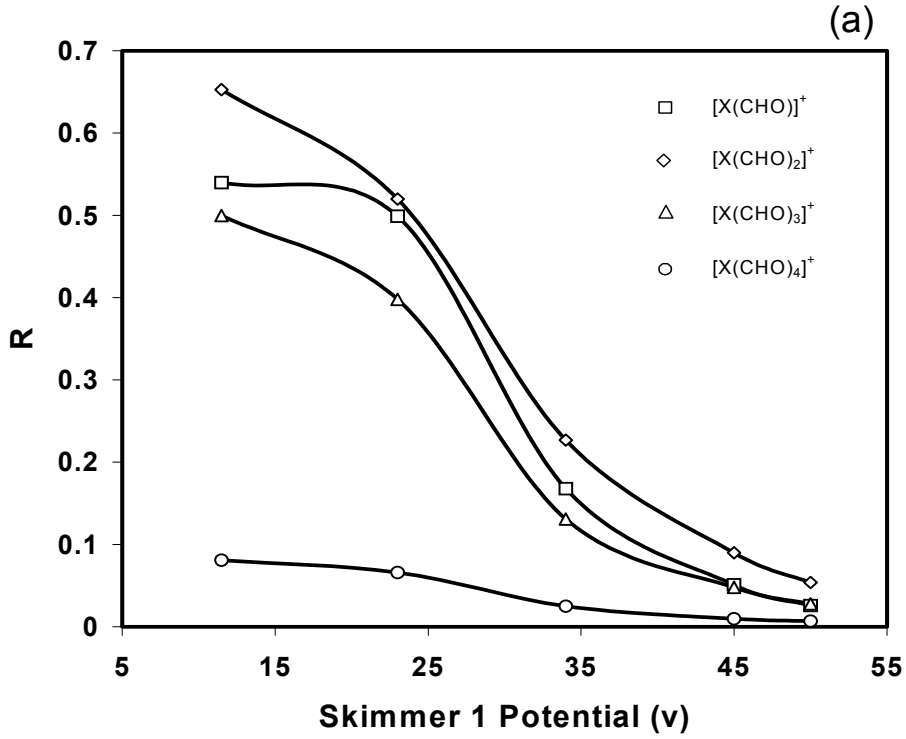
(a)
0.7
0.6
0.5
0.4
0.3
0.2
0.1
0
R
5
15
25
35
45
55
Skimmer 1 Potential (v)
[X(CHO)]+
[X(CHO)2]+
[X(CHO)3]+
[X(CHO)4]+

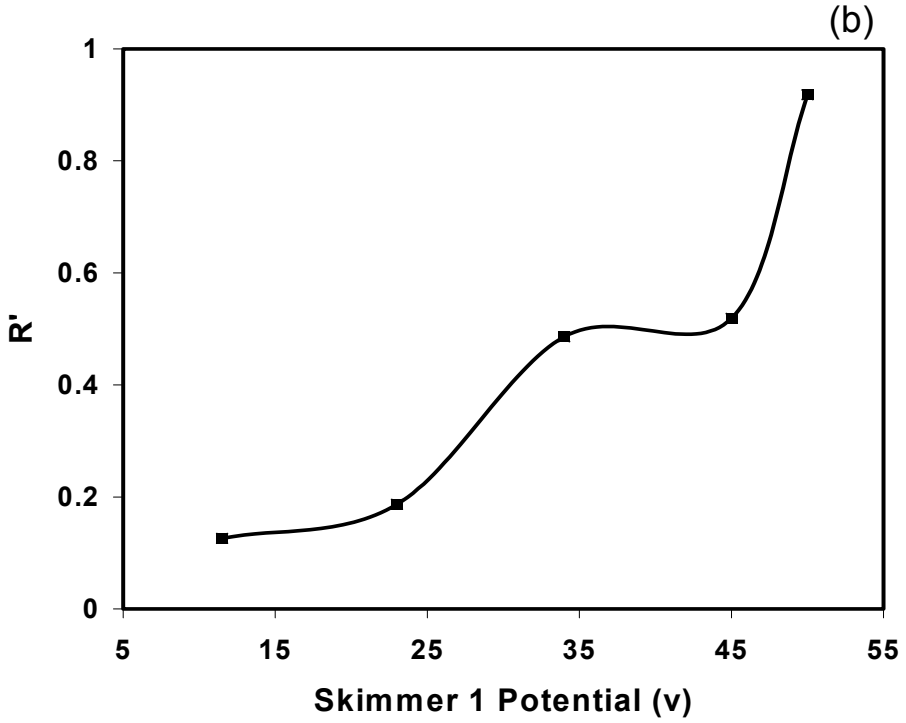
(b)
1
0.8
0.6
0.4
0.2
0
R'
5
15
25
35
45
55
Skimmer 1 Potential (v)

decreased, while $[X(CHO)]^+$, formed from the initiation step, was unchanged. Once the potential is higher than 23 V, no species of the $[X(CHO)_q]^+$ series with CHO units can survive from the fragmentation process. However, X^+, the assigned initiating species undergoes a steady increase in intensity as shown in Figure 45b, where its intensity is referred to the base peak from the precursor $[CpFebz]^+$ in the photoreaction. The initiating nature of X^+ can be established from its growing intensity at the expense of $[X(CHO)_{1-4}]^+$. The oligomer character of $[X(CHO)_q]^+$ species is proven by the dependence of their abundance on the flow rate in the on-line ESI-MS experiments. The flow rate will not change the detected counts of van der Waals cluster signals in the mass spectra at varied flow rates if they formed before the ESI spray. However, the signal intensities of oligomers formed by the propagation of the species, $[X(CHO)]^+$, in the solution within the ESI tip away from the irradiated zone is determined by the flow rate, because higher flow rate allows less time for the propagation process to take place in the tip. Figure 46 confirms the propagation process in the tip as the relative intensity of $[X(CHO)_{2-4}]^+$ decreases with increases of flow rate. The relative intensities are referred to $[X(CHO)]^+$ at each flow rate setting, since the high flow rate makes the sample solution absorb less photons at a constant laser intensity. This type of comparison eliminates the effect of absolute counts among the various species at each flow rate. Similar behavior is observed in the study of $[Fe(H_2O)(CHO)_{6-7}]^{2+}$ as shown in Figure 47. The increased flow rate, i.e., less propagation time, consistently reduces the ratio of $[Fe(H_2O)(CHO)_6]^{2+}$ to $[Fe(H_2O)(CHO)_5]^{2+}$. Here, $[Fe(H_2O)(CHO)_6]^{2+}$ is the first product in the

Figure 46

Relative intensity changes of $[X(CHO)_{2\text{-}4}]^+$ vs flow rate. RI represents the intensity ratios of $[X(CHO)_{2\text{-}4}]^+$ to $[X(CHO)]^+$. Mass spectra were acquired with 75 μM $[Cp(d_5)Febz]PF_6$ and 45 mM CHO in DCE at D = 6.7 mm.

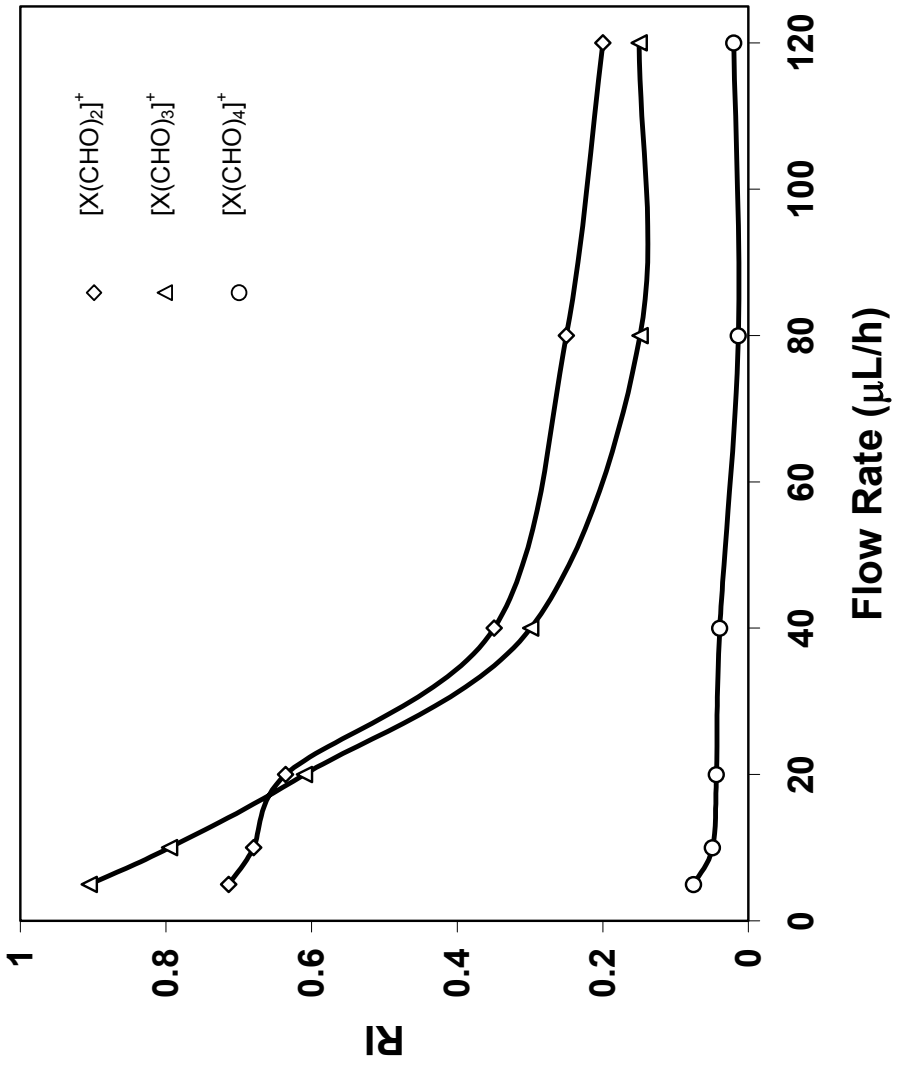
RI
1
0.8
0.6
0.4
0.2
0
0
20
40
60
80
100
120
Flow Rate (μL/h)
[X(CHO)2]+
[X(CHO)3]+
[X(CHO)4]+

Figure 47

Relative intensity changes of $[Fe(H_2O)(CHO)_{6\text{-}7}]^{2+}$ vs flow rate. RI is the intensity ratios of $[Fe(H_2O)(CHO)_{6\text{-}7}]^{2+}$ to $[Fe(H_2O)(CHO)_5]^{2+}$. Mass spectra were acquired with 50 μM $[CpFebz]PF_6$ and 40 mM CHO in DCE at D = 1 mm.

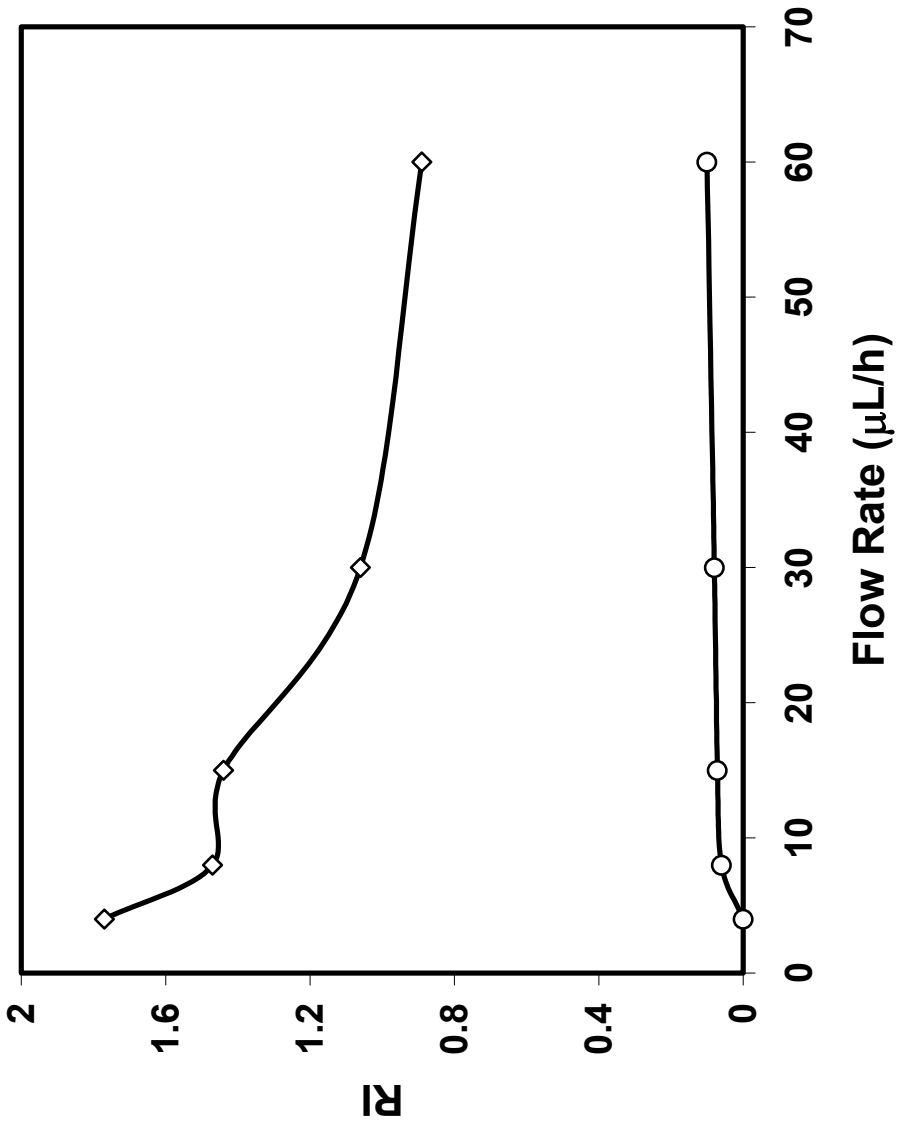
RI
2
1.6
1.2
0.8
0.4
0
0
10
20
30
40
50
60
70
Flow Rate (µL/h)

propagation of CHO from the initiating species, $[Fe(H_2O)(CHO)_5]^{2+}$, that is, the coordinatively saturated complex ion of Fe(II). The relative abundance of $[Fe(H_2O)(CHO)_7]^{2+}$ does not show a distinctive change with changed flow rate due to the low signal intensity at short thermal reaction times (9 – 140 ms).

The crown ether complex, characterized as bis(1,4,7,10-tetraoxacyclododecane)iron(II)-dihexafluorophosphate from the photoinitiated polymerization of ethylene oxide with initiators of the type $[CpFe(\eta^6\text{-arene})]PF_6$,[25] is ruled out for the oligomers of CHO in this study. As can be noticed from the structure in the crown ether complex, the number of its monomer units has to be "magic", like eight for the [12] crown-4 complex and ten for the [15] crown-5 complex. But the number of attached monomer molecules is in a successive integer pattern from one through ten for CHO units outside the Fe(II) coordinative shell for $[Fe(H_2O)(CHO)_j]^{2+}$ and from one through four for CHO units beyond the initiated species for $[X(CHO)_q]^+$.

The identity of the initiating species X^+ has been a puzzle even though considerable efforts were dedicated to solving it. The involvement of protons from the benzene or cyclopentadienyl in the initiator has been ruled out by using the deuterium-labeled initiators, which yielded the same X^+ and its oligomers $[X(CHO)_{1\text{-}5}]^+$, as well as the $[Fe(H_2O)(CHO)_j]^{2+}$ series, in the presence of CHO. The isotopic patterns of X^+ were not consistent with the presence of iron in the formulas, e.g., the absence of the isotopic peak at m/z = 138.1 for X^+. Replacing the PF_6^- anion with SbF_6^- still yielded products of the types $[X(CHO)_q]^+$ and $[Fe(H_2O)(CHO)_j]^{2+}$. At the same time, a new, albeit minor series of CHO-

containing species bearing a dipositive initiating site appeared in the spectrum. Using trifluoromethanesulfonate (Tf^-) counterion resulted in the same photolysis mechanism for $[CpFebz]^+$, but yielded no X^+, only the fully ring-deligated Fe(II) complex ions without CHO polymerization. The coordination of Tf^- into the iron(II) center stabilizes these complex ions in DCE, which reduces the reactivity of the ions with one or two CHO ligands for further reaction with free CHO molecules in the system. These findings imply the possibility of the participation of the anion or fluorine in the formation of X^+. One possible species in terms of close formula mass and the chemical pathway is $[CpFeF]^+$, containing a coordinated fluoride at an oxidized $[CpFe]^{2+}$ center. However, the calculated mass/charge of 139.9725 for $[CpFeF]^+$ does not agree with the mass of X^+ at 140.11±0.03 Da. This assignment can be eliminated, even if we ignore the absence of iron isotopic peaks in X^+, since the mass difference of 0.14 Da lies outside the error limits of the mass measurement of our TOF mass spectrometer.

In summary, our results support the conclusion that several products generated from the photolysis of $[CpFebz]]PF_6$ can serve as initiating species for the cationic polymerization of epoxides. A detailed mechanism that describes the key steps in this photoinitiated process is outlined in Scheme 7.

4.4 Photoreaction mechanism of 1,1'-dibenzoylferrocene

The photoreaction of 1,1'-dibenzoylferrocene (DBF) is evidenced by the simultaneous bleaching of its long-wavelength electronic absorption band and the enhancement of absorbance in the violet region upon continuous irradiation

Scheme 7

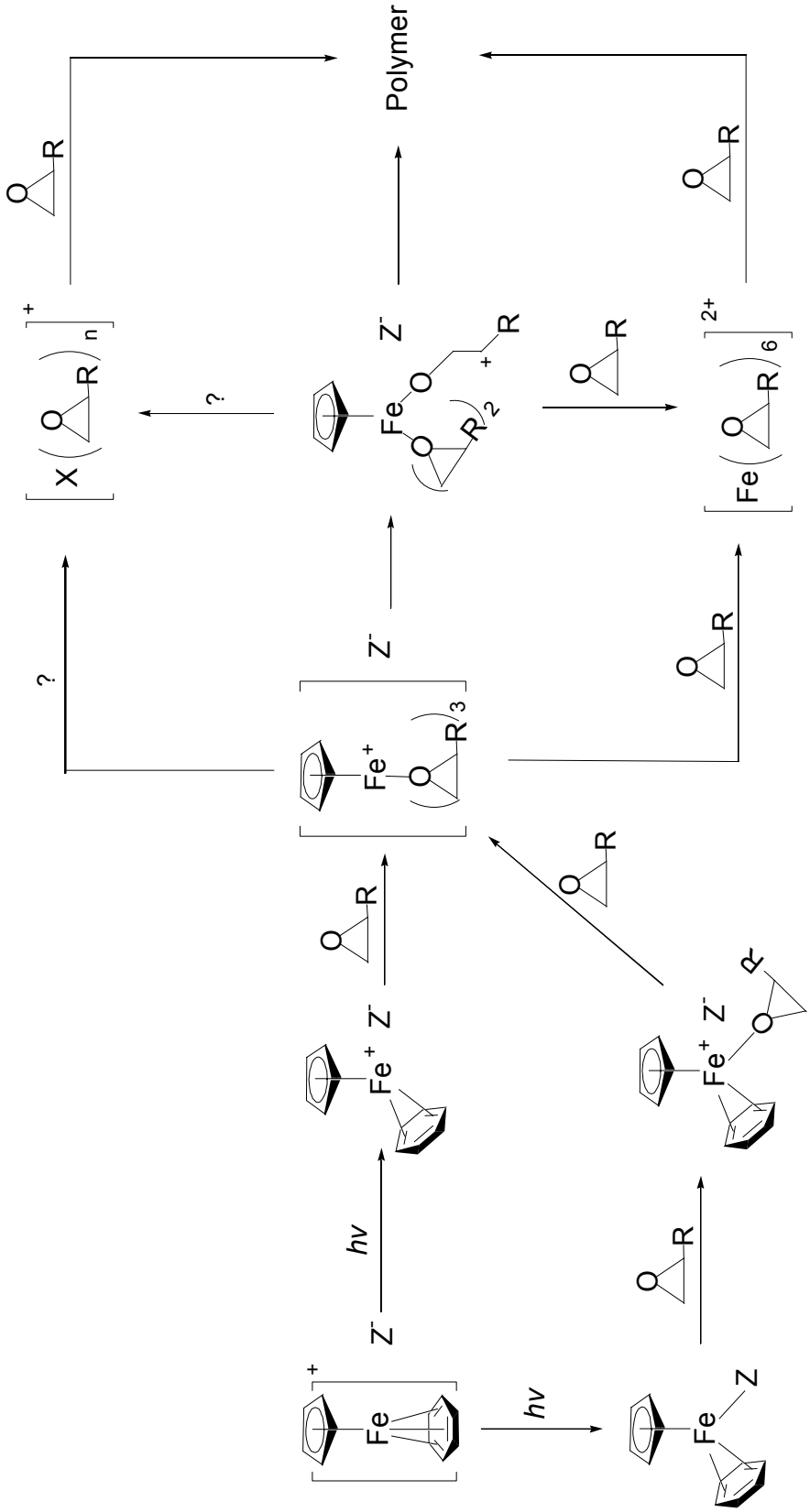

into the region of its ligand field band at 546 nm. Reported reaction systems and the photoproducts proposed or identified by different research groups[60-62] are summarized in Table 13, from which the discrepancies in the products and the reaction pathways can be recognized. In an attempt at identifying the photoreleased anion, a known anionic initiating species,[64,66,67] ^{1}H NMR and on-line mass spectrometric studies of the photolyte were conducted. Table 14 lists the ^{1}H NMR data obtained upon 546 nm photolysis of DBF in deuterated methanol, acetonitrile, and dimethyl sufoxide (DMSO). NMR data for the benzoylcyclopentadienide anion and the neutral acylcyclopentadienes[61,128] are also included in the table for comparison. It turned out that no bands characteristic of the benzoylcyclopentadienide, specifically for the $H_{2,5}$ and $H_{3,4}$ protons on the Cp ring, were found in these spectra from the three solvent systems, while new bands other than those from DBF were identified in spectra of the irradiated samples. It should be noticed that the NMR data[61] for the 1-benzoyl-1,3-cyclopentadiene were recorded with a sample produced by acidifying the benzoylcyclopentadienide anion with hydrochloric acid, not with the original product from the photoreaction. The difference in the identified product may arise from the shift of the equilibrium[129] between the 1-benzoyl-1,3-cyclopentadiene and its conjugate base, benzoylcyclopentadienide (Equation 26).

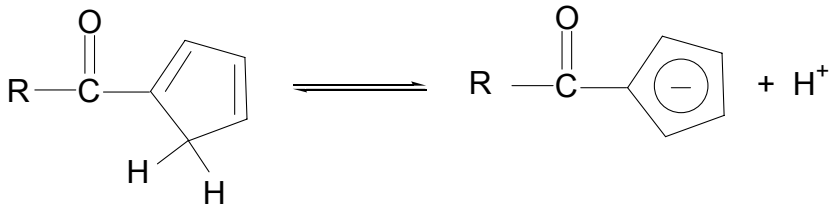

(26)

R = Me, Ph

Table 13 Summary of reaction conditions and products in the photolysis of DBF

Research Group	Reaction Conditions	Proposed/Identified Products
Ali[a]	$CpFe(\eta^5\text{-}C_5H_4C(O)Ph)$ and H_2O in solvent (S) (DMSO, etc.), *hv* (λ>280 nm)	$[CpFe(S)_3]^+$, $PhCO_2^-$, Cyclopentadiene
Che[b]	DBF and phen in deoxygened CH_3CN at 0°C, *hv* (visible)	$[Fe(phen)_3]^{2+}$, benzoylcyclopentadienide
Kutal[c]	DBF in solvent (S) (methanol, ect.), *hv* (λ=546 nm)	$[(\eta^5\text{-}C_5H_4C(O)Ph)Fe(S)_3]^+$, benzoylcyclopentadienide

Note: DMSO is dimethylsulfoxide; phen is 1,10-phenanthroline.

a. Ali, L.H. et al. *J. Chem. Soc., Dalton Trans.* **1973**, 1468-1475.

b. Che, D.J. et al. *Inorg. Chim. Acta* **1997**, *261*, 121-127.

c. Yamaguchi, Y.; Kutal,C. *Inorg. Chem.*, **1999**, *38*, 4861-4867.

Table 14 ^{1}H NMR data for irradiated DBF samples compared with acylcyclopentadienide and acylcyclopentadiene

Sample	Band (ppm) and Assignment[c]					
2.3 mM DBF in CD_3OD, *hv* for 400 seconds	3.4			6.7	6.9	
18 mM DBF in CD_3CN, *hv* for 586 seconds	3.5 (2H, $H_{E,E'}$)			6.6 (1H, H_C)	6.8 (1H, H_D)	7.2 (1H, H_B)
23mM DBF in DMSO (d_6), *hv* for 800 seconds	3.4 ($H_{E,E'}$)			6.6 (1H, H_C)	6.8 (1H, H_D)	Unresolved from Ph
Benzoylcyclopentadienide in CD_3CN		5.9 (2H, $H_{3,4}$)	6.4 (2H, $H_{2,5}$)			
Benzoylcyclopentadienide in DMSO (d_6)		5.7 (2H, $H_{3,4}$)	6.2 (2H, $H_{2,5}$)			
1-Benzoyl-1,3-cyclopentadiene in CCl_4[a]	3.53 (2H, $H_{E,E'}$)			6.65 (1H, H_C)	6.82 (1H, H_D)	7.2 (1H, H_B)
1-Acetyl-1,3-cyclopentadiene in CD_3Cl[b]	3.32 (2H, $H_{E,E'}$)			6.55-6.69 (1H, H_C)	6.72-6.85 (1H, H_D)	7.35 (1H, H_B)

a. From Che, D.J., ect. *Inorg. Chim. Acta* **1997**, *261*, 121-127.

b. From Grundke, G., etc. *J. Org. Chem.* **1981**, *46,* 5428-5431.

c. See the following structures and Cp proton labeling.

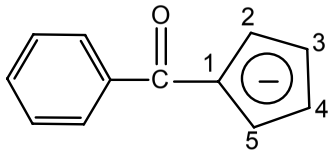

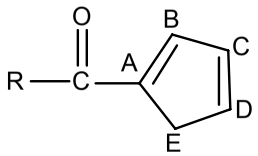

R = Me, Ph

In acetonitrile solution, the equilibrium favors the diene form that corresponds to the NMR bands observed.

Further study of the mechanism and product identities, including the confirmation of diene or anion and the characterization of other products from the photoreaction, involved the on-line irradiation at 488 nm and analysis by ESI-MS. As illustrated in Figure 36, the diene product, either bound to one cation carrier (H^+ or Na^+) or part of a two diene-one cation cluster, dominates the spectrum. From the mass spectrum, the proposed half-sandwich cation with an added proton also is identified, providing direct supporting evidence for the proposed mechanism.[62] Combining the findings from the NMR and ESI-MS studies, we can add a further step in the reaction mechanism (Scheme 8), in which the photogenerated anion, a strong nucleophile, abstracts a proton from the environment. In the presence of an anionically polymerizable monomer, the

Scheme 8

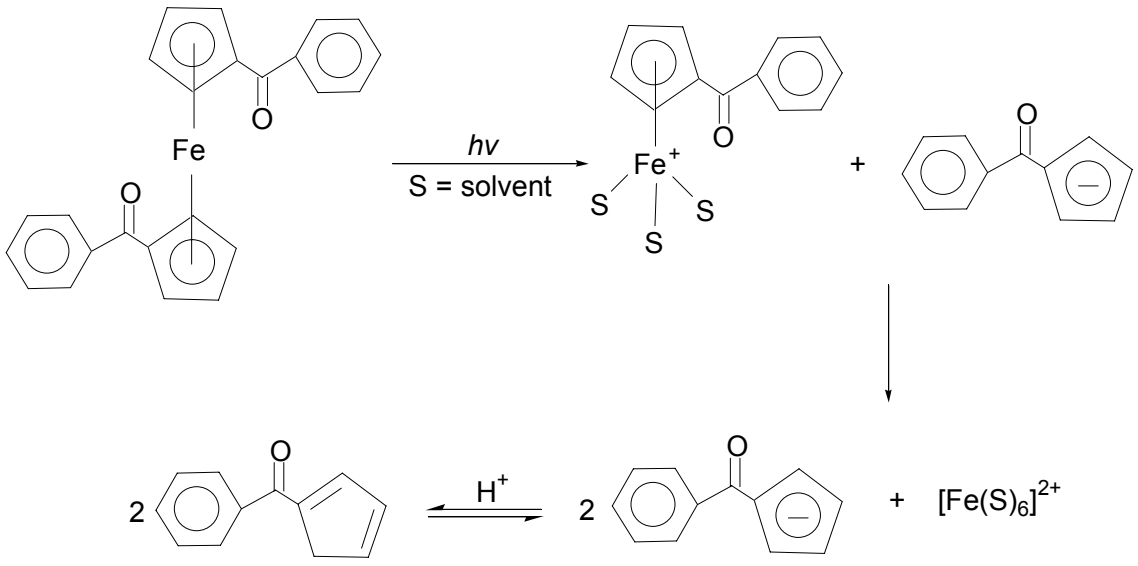

anion would attack the electrophilic site on the monomer and then start polymerization.

4.5 Comparison of the photochemical reactions of the iron(II) sandwich complexes

Photodeligation is the common feature in the photochemical processes of the three classes of iron(II) sandwich complexes, [CpFe(η^6-arene)]Z, dibenzoylferrocene, and [Fe(η^6-arene)$_2$]Z_2. The electronic transitions of these complexes in the visible region were assigned by reference to a qualitative molecular orbital diagram originally constructed for ferrocene.[56,62,41] Photoexcitation into these bands weakens the Fe-ring bonding, causing extremely rapid ring-slippage to produce a species with a reduced hapticity of the ligand. Different photochemical mechanisms have been proposed for the cleavage of Fe-ring bonds for each class. The type of ring determines the lifetimes of the ensuing intermediates toward substitution of the original ligand with suitable nucleophiles like solvent molecules. The intermediates or their decomposition products in the subsequent thermal reaction play essential roles in the polymerization reactions in which these complexes are employed as photoinitiators. Fully ring-deligated iron(II), complexed with solvent ligands or other nucleophiles, is proposed as the common product from the photolysis of the three iron(II) sandwich compounds, and indeed has been identified in this study. The Fe(II) complex ion, $[Fe(S)_6]^{2+}$, was detected and characterized by the on-line ESI-MS technique. It evolved from the intermediate $[CpFe(S)_3]^+$ in the

case of $[CpFebz]^+$ and from $[(\eta^5\text{-}C_5H_4C(O)Ph)Fe(S)_3]^+$ for DBF (S is the solvent and/or monomer molecule). No half-sandwich intermediate was found in the photolysis of $[Fe(\eta^6\text{-}mes)_2](PF_6)_2$, probably owing to the fast photodeligation reaction that was estimated to occur within a few microseconds,[62] far below the working time scale of the on-line ESI-MS technique.

The elucidation of the Fe(II)-initiated polymerization of CHO from the photolysis of $[CpFebz]PF_6$, as illustrated in this study, represents the first direct observation of products in each stage of the polymerization reaction, and provides mechanistic insight to the polymerization with other initiators that are able to generate the same initiating species photochemically. For example, since $[Fe(S)_6]^{2+}$ also is formed in the photolysis of $[Fe(\eta^6\text{-}mes)_2](PF_6)_2$ in acetonitrile solution, the ready solidification of thin films formulated with a pendant epoxide and $[Fe(\eta^6\text{-}mes)_2](PF_6)_2$ under relatively mild processing conditions implies the initiating role of Fe(II) that could result from the thermal decomposition of the parent complex. Efforts to develop and design new cationic initiators of Fe-containing types should focus on exploring a wide range of compounds aimed at better application and formulation properties as long as they release Fe(II) upon light excitation.

A complete picture of the photochemical reaction route for DBF is visualized by combining information obtained from both the on-line ESI-MS and NMR experiments. Upon irradiation with 488-nm light, the half-sandwich complex ion, the fully ring-deligated Fe(II) complex, and the photoreleased ligand in the form of 1-benzoyl-1,3-cyclopentadiene were characterized at a post-irradiation

thermal reaction time of ca. 6 milliseconds in the ESI-MS experiment. NMR band assignments and the corresponding ratios of protons on the Cp ring confirmed the structure of the diene deduced from mass spectrometry. The shift toward forming the diene in the equilibrium between benzoylcyclopentadienide and 1-benzoyl-1,3-cyclopentadiene in pure acetonitrile reflects the highly nucleophilic nature of the photoreleased anion, which is the key character of a good initiating species for anionic polymerization. At the same time, the formation of cationic Fe(II) complexes from the photolysis reaction, as seen from the other two classes of sandwich complexes, suggests the potential application of DBF as a cationic photoinitiator for polymerization.

CHAPTER 5

CONCLUSIONS

This study has demonstrated that electrospray ionization mass spectrometry can be a powerful technique for probing the mechanisms of photoinitiated reactions in solution. Direct laser irradiation at the nanospray tip of the electrospray ionization source allows the probing of reaction intermediates with lifetimes in the range of 4 – 400 ms, which facilitates the recognition of decay pathways of intermediates in the reaction course by monitoring the distribution changes of intermediates and their products in the ensuing thermal reactions at various time scales. A complete elucidation of the photolysis mechanism of [CpFebz]PF_6 in acetonitrile (AN) at room temperature has been achieved by the identification of intermediate $[CpFe(AN)_3]^+$ with lifetime of ca. 50 ms and the parent-offspring relationship of this species and $[Fe(AN)_6]^{2+}$. The mixed-sandwich complex has been shown incapable of photochemically initiating the polymerization of cyclohexene oxide (CHO) in acetonitrile, since the monomer does not compete effectively with solvent for coordination sites on the metal center. With the same photoinitiator and monomer system but conducting the reaction in 1,2-dichloroethane, a coordinatively weaker solvent, initiation and monomer propagation processes have been identified. Demonstrated in the photoinitiation of CHO by [CpFebz]PF_6 is the intermediate nature of the half-sandwich species of the type $[CpFe(H_2O)(CHO)_{0-4}]^+$ with a lifetime of ca. 20 ms, as well as the reaction sequence of producing the offspring species $[Fe(H_2O)(CHO)_{4-15}]^{2+}$ from the intermediate, constituting the first direct support for the earlier proposals that photogenerated $[CpFe(epoxide)_3]^+$ is involved in initiating polymerization. Moreover, we have provided evidence for the

involvement of at least two other initiating species: fully ring-deligated Fe(II) complexes and a non-iron containing species X^+. The establishment of the three initiating species, the recognition of the first few steps of propagation with these initiating species, and the identification of intermediate species in the reaction course allow for the proposal of an updated mechanism to describe the photoinitiation and polymerization reactions.

New insight into the photolysis of 1,1'-dibenzoylferrocene (DBF) has also been provided in the investigation using on-line ESI-MS and ^{1}H NMR to characterize products in the reaction. The half-sandwich species, $[(\eta^5\text{-}C_5H_4C(O)Ph)Fe(CH_3CN)_3]^+$, has been identified directly by mass spectrometry from the photolyzed DBF solution in acetonitrile along with the Fe(II) complex ions, $[Fe(AN)_{3\text{-}5}]^{2+}$, the product resulting from the thermal decomposition of the half-sandwich species. The chemical structure of a major species corresponding to the formula of 1-benzyol-1,3-cyclopentadiene identified by mass spectrometry has been verified by the appropriate ^{1}H NMR band assignments. These characterized products lead to a detailed mechanism of the photodeligation of DBF, depicting the loss of the first ring-ligand to form a benzoylcyclopentadienide anion and the half-sandwich intermediate that quickly decomposes into $[Fe(AN)_6]^{2+}$ with release of the second anion. The strong nucleophilic feature of the anion is reflected by its fast abstraction of a proton in the acetonitrile medium, which is consistent with its being a good anionic initiating species. We are not been able to observe the half-sandwich intermediate from the photolysis of

$[Fe(\eta^6\text{-mes})_2](PF_6)_2$ in a preliminary experiment with on-line ESI-MS, which is supportive of the reported estimation of a microsecond lifetime for the compound.

Future work is needed in three directions. (i) In order to obtain a complete and detailed mechanism of initiation for the $[CpFe(\eta^6\text{-arene})]^+$ photoinitiators, the identity of X^+ at m/z = 140.1 has to be determined. Conducting the photoreaction in other solvents may provide new insight into its character and the use of tandem mass spectrometry will be helpful in elucidating its structure. Preparative photolysis is another option for characterizing the species with other measures like NMR, but its stability needs to be considered for the synthesis and the isolation processes. (ii) Complexes similar to those studied in this project or other Fe-containing photoinitiator systems can be developed. Research on these developments may address application issues such as the excitation light wavelength and compatibility with various monomers, as long as the target active initiating species, cationic Fe(II) complexes, can be photoreleased from them. (iii) The application of the on-line ESI-MS technique can be extended to other photoreactions that require the probing of short-lived active species important to the elucidation of reaction mechanisms. The time limit for allowed thermal reaction time can be further lowered to a few hundred microseconds by trying tips of smaller inner diameter, e.g., 4 μm.

REFERENCES

(1) Decker, C. *Prog. Polym. Sci.* **1996**, *21*, 593-650.

(2) Decker, C. *Polym. Int.* **1998**, *45*, 133-141.

(3) Buhler, N.; Bellus, D. *Pure Appl. Chem.* **1995**, *67*, 25-31.

(4) Andrzejewska, E. *Prog. Polym. Sci.* **2001**, *26*, 605-665.

(5) Ohkawa, K.; Tachikawa, H.; Chikaoka, S. In *PCT Int. Appl.* (1999), 50 pp., WO 9928295, A1 19990610.

(6) Cumpston, B. H.; Ananthavel, S. P.; Barlow, S.; Dyer, D. L.; Ehrlich, J. E.; Erskine, L. L.; Heikal, A. A.; Kuebler, S. M.; Lee, I. Y. S.; McCord-Maughont, D.; Qin, J.; Rockel, H.; Rumi, M.; Wu, X.-L.; Marder, S. R.; Perry, J. W. *Nature (London)* **1999**, *398*, 51-54.

(7) Crivello, J. V. *Radiat. Phys. Chem.* **2002**, *63*, 21-27.

(8) Szwarc, M.; Van Beylen, M. *Ionic Polymerization and Living Polymers*; Chapman & Hall: New York, 1993.

(9) Stevens, M. P. *Polym. Chem.: An Introduction*; 3rd ed.; Oxford University Press: New York, 1999.

(10) Moad, G.; Solomon, D. H. *The Chemistry of Free Radical Polymerization*; First ed.; Elsevier Science Ltd: Oxford, 1995.

(11) Pu, Z. *Overview of Polymerization Kinetics*; Marcel Dekker. Inc.: New York, 1989.

(12) Schnabel, W. *Macromol. Rapid Comm.* **2000**, *21*, 628-642.

(13) Crivello J. V.; Dietliker, K. *Chemistry & Technology of UV & EB Formulation for Coatings, Inks, & Paints*; 2nd ed.; John Wiley and Sons: Chichester; New York, 1998.

(14) Ravve, A. *Principles of Polymer Chemistry*; Plenum Press: New York, 1995.

(15) Crivello, J. V.; Sangermano, M. *J. Polym. Sci. A* **2001**, *39*, 343-356.

(16) Dossow, D.; Zhu, Q. Q.; Hizal, G.; Yagci, Y.; Schnabel, W. *Polymer* **1996**, *37*, 2821-2826.

(17) Yagci, Y.; Hepuzer, Y. *Macromolecules* **1999**, *32*, 6367-6370.

(18) Denizligil, S.; Yagci, Y.; McArdle, C. *Polymer* **1995**, *36*, 3093-3098.

(19) Hepuzer, Y.; Kucuktonbekici, U.; Yagci, Y. *J. Photoch. Photobio. A* **2000**, *130*, 71-74.

(20) Onen, A.; Yagci, Y. *Polymer* **2001**, *42*, 6681-6685.

(21) Yagci, Y.; Endo, T. *Adv. Polym. Sci.* **1997**, *127*, 59-86.

(22) Redakcji, O.; Jakubiak, J.; Rabek, J. F. *Polymery* **1999**, *44*, 447-570.

(23) Roloff, A.; Meier, K.; Riediker, M. *Pure Appl. Chem.* **1986**, *58*, 1267-1272.

(24) Meier, K.; Zweifel, H. *J. Imag. Sci.* **1986**, *30*, 174-177.

(25) Meier, K.; Zweifel, H. *J. Radiat. Curing* **1986**, 26-32.

(26) Lohse, F.; Zweifel, H. *Adv. Polym. Sci.* **1986**, *78*, 61-81.

(27) Hendrickson, W. A.; Palazzotto, M. C. In *Advances in Chemistry*; Kutal, C., Ed.; American Chemical Society Symposium series 238; American Chemical Society: Washington, DC, 1993, pp 411-430.

(28) Gill, T. P.; Mann, K. R. *J. Organomet. Chem.* **1981**, *216*, 65-71.

(29) Lee, C. C.; Iqbal, M.; Gill, U. S.; Sutherland, R. G. *J. Organomet. Chem.* **1985**, *288*, 89-96.

(30) Gill, T. P.; Mann, K. R. *Organometallics* **1982**, *1*, 485-488.

(31) Nesmeyanov, A. N.; Vol'kenau, N. A.; Shilovtseva, L. S. *Dokl. Akad. Nauk SSSR* **1970**, *190*, 857-9 [Chem].

(32) Gill, T. P.; Mann, K. R. *Inorg. Chem.* **1983**, *22*, 1986-1991.

(33) Boyd, D. C.; Bohling, D. A.; Mann, K. R. *J. Am. Chem. Soc.* **1985**, *107*, 1641-4.

(34) Schrenk, J. L.; Palazzotto, M. C.; Mann, K. R. *Inorg. Chem.* **1983**, *22*, 4047-9.

(35) Schrenk, J. L.; McNair, A. M.; McCormick, F. B.; Mann, K. R. *Inorg. Chem.* **1986**, *25*, 3501-3504.

(36) Mann, K. R.; Blough, A. M.; Schrenk, J. L.; Koefod, R. S.; Freedman, D. A.;Matachek, J. R. *Pure Appl. Chem.* **1995**, *67*, 95-101.

(37) McNair, A. M.; Schrenk, J. L.; Mann, K. R. *Inorg. Chem.* **1984**, *23*, 2633-2640.

(38) Chrisope, D. R.; Park, K. M.; Schuster, G. B. *J. Am. Chem. Soc.* **1989**, *111*, 6195-6201.

(39) Roman, E.; Barrera, M.; Hernandez, S.; Lissi, E. *J. Chem. Soc. Perk. T. 2* **1988**, 939-942.

(40) Jakubek, V.; Lees, A. J. *Chem. Comm.* **1999**, 1631-1632.

(41) Jakubek, V.; Lees, A. J. *Inorg. Chem.* **2000**, *39*, 5779-5786.

(42) Klingert, B.; Riediker, M.; Roloff, A. *Comment. Inorg. Chem.* **1988**, *7*, 109-38.

(43) Bowser, R.; Davidson, R. S. *J. Photoch. Photobio. A* **1994**, *77*, 269-276.

(44) Chen, X. D.; Li, K. Y.; Chen, Y. L. *Chinese Sci. Bull.* **1995**, *40*, 527-528.

(45) Chen, X. D.; Chen, Y. L. *J. Appl. Polym. Sci.* **1997**, *66*, 2551-2554.

(46) Park, K. M.; Schuster, G. B. *J. Organomet. Chem.* **1991**, *402*, 355-362.

(47) Kotch, T. G.; Lees, A. J.; Fuerniss, S. J.; Papathomas, K. I. *Chem. Mater.* **1995**, *7*, 801-805.

(48) Rabek, J. F.; Lucki, J.; Zuber, M.; Qu, B. J.; Shi, W. F. *J. Macromol. Sci. Pure* **1992**, *29*, 297-310.

(49) Rabek, J. F.; Lucki, J.; Zuber, M.; Qu, B. J.; Shi, W. F. *Polymer* **1992**, *33*, 4838-4844.

(50) Allen, N. S.; Edge, M.; Jasso, A. R.; Corrales, T.; TellezRosas, M. *J. Photoch. Photobio. A* **1997**, *102*, 253-258.

(51) Wang, P. F.; Shen, Y. Q.; Wu, S. K.; Adamczak, E.; Linden, L. A.; Rabek, J. F. *J. Macromol. Sci. Pure* **1995**, *A32*, 1973-1983.

(52) Bolln, C.; Frey, H.; Mulhaupt, R. *J. Macromol. Sci. Pure* **1995**, *33*, 587-592.

(53) Saegusa, T.; Matsumot. S. I. *J. Macromol. Sci. Pure* **1968**, *6*, 1559-&.

(54) Houlton, A.; Miller, J. R.; Roberts, R. M. G.; Silver, J. *J. Chem. Soc., Dalton Trans.* **1990**, 2181-4.

(55) Houlton, A.; Miller, J. R.; Roberts, R. M. G.; Silver, J. *J. Chem. Soc., Dalton Trans.* **1991**, 467-70.

(56) Morrison, W. H.; Ho, E. Y.; Hendrickson, D. N. *Inorg. Chem.* **1975**, *14*, 500-506.

(57) Gamble, G.; Grutsch, P. A.; Ferraudi, G.; Kutal, C. *Inorg. Chim. Acta* **1996**, *247*, 5-10.

(58) Lehmann, R. E.; Kochi, J. K. *J. Am. Chem. Soc.* **1991**, *113*, 501-512.

(59) Bergamini, P.; Dimartino, S.; Maldotti, A.; Sostero, S.; Traverso, O. *J. Organomet. Chem.* **1989**, *365*, 341-346.

(60) Ali, L. H.; Cox, A.; Kemp, T. J. *J. Chem. Soc., Dalton Trans.* **1973**, 1468-75.

(61) Che, D.-J.; Li, G.; Du, B.-S.; Zhang, Z.; Li, Y. H. *Inorg. Chim. Acta* **1997**, *261*, 121-127.

(62) Yamaguchi, Y.; Kutal, C. *Inorg. Chem.* **1999**, *38*, 4861-4867.

(63) Tarr, A. M.; Wiles, D. M. *Can. J. Chem.* **1968**, *46*, 2725-2731.

(64) Yamaguchi, Y.; Palmer, B. J.; Wakamatsu, T.; Yang, D. B.; Kutal, C. *Polym. Mater. Sci. Eng.* **1998**, *79*, 1-2.

(65) Yamaguchi, Y.; Palmer, B. J.; Kutal, C.; Wakamatsu, T.; Yang, D. B. *Macromolecules* **1998**, *31*, 5155-5157.

(66) Yamaguchi, Y.; Kutal, C. In *Coordination Chemistry at the Turn of the Century*; Ondrejovic, G, Sirota, A., Eds.; Slovak Technical University Press: Bratislava, 1999; pp 209-214.

(67) Yamaguchi, Y.; Kutal, C. *Macromolecules* **2000**, *33*, 1152-1156.

(68) Karpinski, Z. J.; Kochi, J. K. *Inorg. Chem.* **1992**, *31*, 2762-2767.

(69) Kochi, J. K.; Wei, C. H. *J. Organomet. Chem.* **1993**, *451*, 111-121.

(70) Gamble, G.; Kutal, C. *Polym. Adv. Technol.* **1994**, *5*, 63-9.

(71) Hanton, S. D. *Chem. Rev.* **2001**, *101*, 527-569.

(72) Jackson, A. T.; Yates, H. T.; Lindsay, C. I.; Didier, Y.; Segal, J. A.; Scrivens, J. H.; Critchley, G.; Brown, J. *Rapid Comm. Mass Spectrom.* **1997**, *11*, 520-526.

(73) Easterling, M. L.; Mize, T. H.; Amster, I. J. *Int. J. Mass Spectrom.* **1997**, *169*, 387-400.

(74) Montaudo, G.; Montaudo, M. S.; Puglisi, C.; Samperi, F. *J. Polym. Sci. A* **1996**, *34*, 439-447.

(75) Maloney, D. R.; Hunt, K. H.; Lloyd, P. M.; Muir, A. V. G.; Richards, S. N.; Derrick, P. J.; Haddleton, D. M. *J. Chem. Soc., Chem. Comm.* **1995**, 561-2.

(76) Jackson, A. T.; Yates, H. T.; Scrivens, J. H.; Green, M. R.; Bateman, R. H. *J. Am. Soc. Mass Spectrom.* **1997**, *8*, 1206-1213.

(77) Bottrill, A. R.; Giannakopulos, A. E.; Waterson, C.; Haddleton, D. M.; Lee, K. S.; Derrick, P. J. *Anal. Chem.* **1999**, *71*, 3637-3641.

(78) Jackson, A. T.; Yates, H. T.; Scrivens, J. H.; Green, M. R.; Bateman, R. H. *J. Am. Soc. Mass Spectrom.* **1998**, *9*, 269-274.

(79) Scrivens, J. H.; Jackson, A. T.; Yates, H. T.; Green, M. R.; Critchley, G.; Brown, J.; Bateman, R. H.; Bowers, M. T.; Gidden, J. *Int. J. Mass Spectrom.* **1997**, *165*, 363-375.

(80) Pastor, S. J.; Wilkins, C. L. *Int. J. Mass Spectrom.* **1998**, *175*, 81-92.

(81) Wang, J. R.; Javahery, G.; Petrie, S.; Bohme, D. K. *J. Am. Chem. Soc.* **1992**, *114*, 9665-9666.

(82) Brodbelt, J. S.; Liou, C. C.; Maleknia, S.; Lin, T. Y.; Lagow, R. J. *J. Am. Chem. Soc.* **1993**, *115*, 11069-11073.

(83) Richardson, D. E.; Alameddin, N. G.; Ryan, M. F.; Hayes, T.; Eyler, J. R.; Siedle, A. R. *J. Am. Chem. Soc.* **1996**, *118*, 11244-11253.

(84) Feichtinger, D.; Plattner, D. A.; Chen, P. *J. Am. Chem. Soc.* **1998**, *120*, 7125-7126.

(85) Hinderling, C.; Feichtinger, D.; Plattner, D. A.; Chen, P. *J. Am. Chem. Soc.* **1997**, *119*, 10793-10804.

(86) Griffiths, W. J.; Jonsson, A. P.; Liu, S. Y.; Rai, D. K.; Wang, Y. Q. *Biochem. J.* **2001**, *355*, 545-561.

(87) Maziarz, E. P.; Baker, G. A.; Mure, J. V.; Wood, T. D. *Int. J. Mass Spectrom.* **2000**, *202*, 241-250.

(88) McEwen, C. N.; Simonsick Jr., W. J.; Larsen, B. S.; Ute, K.; Hatada, K. *J. Am. Soc. Mass Spectrom.* **1995**, *6*, 906-911.

(89) Koster, S.; Duursma, M. C.; Boon, J. J.; Heeren, R. M. A. *J. Am. Soc. Mass Spectrom.* **2000**, *11*, 536-543.

(90) Shan, L.; Murgasova, R.; Hercules, D. M.; Houalla, M. *J. Mass Spectrom.* **2001**, *36*, 140-144.

(91) Lover, T.; Henderson, W.; Bowmaker, G. A.; Seakins, J. M.; Cooney, R. P. *J. Mater. Chem.* **1997**, *7*, 1553-1558.

(92) Kane-Maguire, L. A. P.; Kanitz, R.; Sheil, M. M. *J. Organomet. Chem.* **1995**, *486*, 243-248.

(93) Traeger, J. C. *Int. J. Mass Spectrom.* **2000**, *200*, 387-401.

(94) Henderson, W.; Nicholson, B. K.; McCaffrey, L. J. *Polyhedron* **1998**, *17*, 4291-4313.

(95) Arakawa, R.; Lu, J.; Mizuno, K.; Inoue, H.; Doe, H.; Matsuo, T. *Int. J. Mass Spectrom.* **1997**, *160*, 371-376.

(96) Espenson, J. H.; Tan, H. S.; Mollah, S.; Houk, R. S.; Eager, M. D. *Inorg. Chem.* **1998**, *37*, 4621-4624.

(97) Bakhtiar, R.; Hop, C. *J. Phys. Org. Chem.* **1999**, *12*, 511-527.

(98) Aliprantis, A. O.; Canary, J. W. *J. Am. Chem. Soc.* **1994**, *116*, 6985-6986.

(99) Brum, J.; Dell'Orco, P.; Lapka, S.; Muske, K.; Sisko, J. *Rapid Commun. Mass Spectrom.* **2001**, *15*, 1548-1553.

(100) Zechel, D. L.; Konermann, L.; Withers, S. G.; Douglas, D. J. *Biochem.* **1998***, 37,* 7664-7669.

(101) Xu, X. M.; Lu, W. Z.; Cole, R. B. *Anal. Chem.* **1996**, *68*, 4244-4253.

(102) Arakawa, R.; Matsuda, F.; Matsubayashi, G. E.; Matsuo, T. *J. Am. Soc. Mass Spectrom.* **1997**, *8*, 713-717.

(103) Arakawa, R.; Mimura, S.; Matsubayashi, G.; Matsuo, T. *Inorg. Chem.* **1996**, *35*, 5725-5729.

(104) Arakawa, R.; Tachiyashiki, S.; Matsuo, T. *Anal. Chem.* **1995**, *67*, 4133-4138.

(105) Arakawa, R.; Jian, L.; Yoshimura, A.; Nozaki, K.; Ohno, T.; Doe, H.; Matsuo, T. *Inorg. Chem.* **1995**, *34*, 3874-3878.

(106) Brum, J.; Dell'Orco, P. *Rapid Commun. Mass Spectrom.* **1998**, *12*, 741-745.

(107) Volmer, D. A. *J. Chromatogr. A* **1998**, *794*, 129-146.

(108) Ronco, S.; Ferraudi, G.; Roman, E.; Hernandez, S. *Inorg. Chim. Acta* **1989**, *161*, 183-186.

(109) Armarego, W. L. F.; Perrin, D. D. *Purification of Laboratory Chemicals*; Butterworth-Heinemann: Oxford, 1996.

(110) Nesmeyanov, A. N.; Vol'kenau, N. A.; Bolesova, I. N. *Dokl. Akad. Nauk SSSR* **1963**, *149*, 615-18.

(111) Dabirmanesh, Q.; Roberts, R. M. G. *J. Organomet. Chem.* **1993**, *460*, C28-C29.

(112) Dabirmanesh, Q.; Fernando, S. I. S.; Roberts, R. M. G. *J. Chem. Soc. Perk. T. 1* **1995**, 743-749.

(113) King, R. B. *Transition-Metal Chemistry*; Academic Press: New York, 1965.

(114) Hamon, J. R.; Hamon, P.; Sinbandhit, S.; Guenot, P.; Astruc, D. *J. Organomet. Chem.* **1991**, *413*, 243-55.

(115) Shabanova, E.; Schaumburg, K.; Kamounah, F. S. *J. Chem. Res. (S)* **1999**, 364-365.

(116) Burger, P.; Brintzinger, H. H. *J. Organomet. Chem.* **1991**, *407*, 207-213.

(117) Lavallee, R. J. Ph. D. Dissertation, University of Georgia, 1997.

(118) Wegner, E. E.; Adamson, A. W. *J. Am. Chem. Soc.* **1966**, *88*, 394-404.

(119) Kutal, C.; Yamaguchi, Y.; Ding, W.; Sanderson, C. T.; Li, X.; Gary, G.; Amster, I. J. Crivello, Eds., ACS Symposium, 2002 (in press).

(120) Kane-Maguire, L. A. P.; Kanitz, R.; Sheil, M. M. *Inorg. Chim. Acta* **1996**, *245*, 209-214.

(121) Berkel, G. J. V.; Giles, G. E.; Bullock, J. S.; Gray, L. J. *Anal. Chem.* **1999**, *71*, 5288-5296.

(122) Van Berkel, G. J.; Zhou, F. *Anal. Chem.* **1995**, *67*, 2916-23.

(123) Purcell, K. F.; Kotz, J. C. *Inorganic Chemistry*; W.B. Saunsers: Philadelphia, 1977.

(124) Duncan, M. A. *Ann. Rev. Phys. Chem.* **1997**, *48*, 69-93.

(125) *CRC Handbook of Chemistry and Physics*; 76th ed.; Lide, D. R.; Frederikse, H. P. R., Eds.; CRC Press: Boca Raton, FL, 1995.

(126) Vereshchagin, A. N.; Anastaseva, A. P.; Vulfson, S. G. *Bull. Acad. Sci. USSR, Div. Chem. Sci.* **1969**, 499-503.

(127) Odian, G. *Principles of Polymerization*; 2nd ed.; Wiley-Interscience: New York, 1981.

(128) Grundke, G.; Hoffmann, H. M. R. *J. Org. Chem.* **1981**, *46*, 5428-5431.

(129) Okuyama, T.; Ikenouchi, Y.; Fueno, T. *J. Am. Chem. Soc.* **1978**, *100*, 6162-6166.